CDT

Centre de
Développement
Technologique

FINAL REPORT

A STUDY OF SULFUR SOLUBILITY AND DIFFUSIVITY IN Cr_2O_3 AND ITS ROLE IN MATERIALS DEGRADATION IN COAL COMBUSTION SYSTEMS

prepared for:

Department of Energy, Mines & Resources
(CANMET)
568 Booth Street
Ottawa (Ontario) K1A 0G1

April 1986 CDT PROJECT P859

CONTRACT REPORT NUMBER: OST83-00227
REQUISITION NUMBER: 23440-3-9109
CONTRACTOR: Ecole Polytechnique de Montreal

AUG 19 1988

MICROMEDIA

3-9109

CDT
Centre de Développement Technologique
École Polytechnique de Montréal

CDT-PROJECT P859

FINAL REPORT

A STUDY OF SULFUR SOLUBILITY AND DIFFUSIVITY IN Cr_2O_3 AND ITS ROLE IN MATERIALS DEGRADATION IN COAL COMBUSION SYSTEMS

prepared for:

Department of Energy, Mines & Resources
(CANMET)
Physical Metallurgy Research Labs
568 Booth Street
Ottawa (Ontario) K1A OG1

by:

Frank Ajersch, Eng.
Mohamed Benlyamani
Department of Metallurgical Engineering

submitted by:

LE CENTRE DE DÉVELOPPEMENT TECHNOLOGIQUE
DE L'ECOLE POLYTECHNIQUE DE MONTREAL
Campus de l'Université de Montréal
Case postale 6079, Succursale A
Montréal, Québec H3C 3A7

113AP
April 1986

Frank Ajersch, Eng.
Project Director

CDT
Centre de
Développement
Technologique
École Polytechnique
de Montréal

A STUDY OF SULFUR SOLUBILITY AND DIFFUSIVITY IN Cr_2O_3 AND ITS ROLE IN MATERIALS DEGRADATION IN COAL COMBUSTION SYSTEMS

ABSTRACT

An experimental technique was developed for the equilibration of ultra pure Cr_2O_3 powder in a controlled reaction gas atmosphere of P_{O_2} from 10^{-6} to 10^{-12} atm and P_{S_2} from 10^{-2} to 10^{-16} atm at 1273°K. Due to the low solubility of sulfur, the number of analytical methods is limited and a neutron activation method was finally adopted. The limiting solubility varies between 16 ppm to 93 ppm for the range of atmospheres in this study and was found to vary with the sulfur partial pressure.

An analysis of the different modes of incorporting sulfur is presented by considering anionic, interstitial and cationic lattice sites. Equations are developed relating the equilibrium sulfur to each type of mechanism.

In a second part of this study, polycrystalline samples of Cr_2O_3 for the determination of sulfur diffusivity were prepared by sintering at 1823°K for 2 hrs at $P_{O_2} = 10^{-6}$ atm. Small polished parallelpipeds of Cr_2O_3 were exposed to an atmosphere containing ^{35}S and diffusion profiles were obtained by abrasion polishing of the sample and measuring the residual sulfur activity in the samples.

CDT
Centre de Développement Technologique
École Polytechnique de Montréal

ÉTUDE DE LA SOLUBILITÉ ET DE LA DIFFUSIVITÉ DU SOUFRE DANS Cr_2O_3 ET SON RÔLE DANS LA DÉGRADATION DES MATÉRIAUX UTILISÉS AU COURS DE LA COMBUSTION DE CHARBON

RÉSUMÉ

Une méthode expérimentale a été développée pour équilibrer le Cr_2O_3 de haute pureté dans une gamme de pression de soufre et d'oxygène de 10^{-2} à 10^{-16} atm et 10^{-6} à 10^{-12} atm respectivement.

Pour quantifier le soufre dissout dans Cr_2O_3 un certain nombre de techniques instrumentales a été testé et nous avons trouvé que la méthode d'analyse par activation neutronique pemet de déterminer avec succès les quantités dissoutes. Nous avons trouvé que la solubilité limite varie entre 16 et 93 ppm et dépend de la pression partielle du soufre utilisé.

L'analyse des différents modes d'incorporation du soufre dans le réseau cristallin de Cr_2O_3 est aussi présenté et les relations entre la solubilité et les pressions partielles de soufre et de l'oxygène sont développées pour chaque mode d'incorporation.

La deuxième partie de cette étude consiste en la détermination de la diffusivité du soufre dans Cr_2O_3 dans une gamme de température entre 1173°K et 1373°K. L'obtention d'échantillons polycristallin a été réalisé par le frittage de pastilles à 1873°K à $P_{O_2} = 10^{-6}$ atm. Les échantillons en forme de parallélipède sont polies à l'aide d'abrasifs jusqu'à 1 μm. Le soufre radioactif ^{35}S a été utilisé comme radiotraceur et la détermination des coefficients de diffusion a été atteinte par la mesure de l'activité résiduelle de l'échantillon en enlevant des couches successives de l'oxyde par abrasion.

TABLE OF CONTENTS

		Page
INTRODUCTION		1
I.	LITERATURE REVIEW	4
I.1	DEFECT STRUCTURE	4
I.2	ELECTRICAL CONDUCTIVITY	5
I.3	OXIDATION OF CHROMIUM	10
I.4	SULFUR SOLUBILITY IN CHROMIUM OXIDE	13
1.5	MECHANISM AND KINETICS OF SULFUR DISSOLUTION	15
II.	EXPERIMENTAL	18
II.1	EQUILIBRATION SYSTEM APPARATUS	18
II.2	EXPERIMENTAL PROCEDURE	21
II.3	OXYGEN PROBE	22
II.4	METHODS OF SULFUR ANALYSIS	28
II.4.1	LECO infrared analysis	31
II.4.2	Analysis by proton induced X-ray emission (PIXE)	32
II.4.3	Analysis of sulfur by neutron activation	34
III.	RESULTS AND DISCUSSION	36
III.1	CALCULATION OF CHEMICAL EQUILIBRIUM OF THE REACTION GASES	36
III.2	DETERMINATION OF SULFUR SOLUBILITY IN Cr_2O_3	60
III.2.1	Solubility of sulfur using LECO infrared analysis	60
III.2.2	Sulfur analysis using the PIXE method	62
III.2.3	Results of sulfur analysis by neutron activation	68

(Cont'd) - TABLE OF CONTENTS

		Page
IV.	DISCUSSION	72
	IV.1 INTRODUCTION	72
	IV.2 SUBSTITUTION ON AN ANIONIC SITE	74
	IV.2.1 Sulfur in the form of S^{-2}	74
	IV.2.2 Sulfur in the form of S^{-}	74
	IV.2.3 Sulfur in the form S°	76
	IV.3 SUBSTITUTION ON AN INTERSTITIAL SITE	79
	IV.3.1 Sulfur in the form S_i°	79
	IV.3.2 Sulfur in the form S_i^{+}	79
	IV.3.3 Sulfur in the form S^{+2}	81
	IV.4 SUBSTITUTION IN A CATIONIC VACANCY	82
	IV.4.1 Sulfur in the form of S^{+2}	82
	IV.4.2 Sulfur in the form S^{+}	84
	IV.5 CHOICE OF THE MECHANISM OF SULFUR DISSOLUTION	86
V.	STUDIES UNDER INVESTIGATION	90
	V.1 EXPERIMENTAL PROCEDURE	92
CONCLUSIONS		96
REFERENCES		98
APPENDIX A		102
APPENDIX B		105

CDT
Centre de
Développement
Technologique
École Polytechnique
de Montréal

INTRODUCTION

Stainless alloys containing Fe, Ni and Cr which generally show corrosion resistance and good mechanical strength at high temperatures in air or oxydizing atmospheres, present much larger corrosion risks when exposed to atmospheres containing several gases, particularly oxygen, nitrogen, sulfur and carbon. Atmospheres containing oxygen and sulfur found in fluidized-bed reactors used for coal combustion (1,2), are particularly aggressive to the alloys used in the heat exchanger tubes.

From thermodynamic considerations, only Cr_2O_3 should form on the exposed surfaces for the oxygen and sulfur pressures that are encountered at the reaction temperatures. Inspection of the tubes in a coal combustion systems has, however shown fissures or detachments of the oxide layer presumally caused by sulfide phases at the metal/ oxide interface. The formation and growth of these sulfide phases can only occur by the transport of sulfur from the gas-oxide surface through the oxide layer.

Initially, the non oxidized alloy forms a protective Cr_2O_3 layer. The dissolution of sulfur in this oxide layer has not been quantified based on the existing literature and diffusion coefficients of sulfur in this system are even less documented. As the oxide layer grows, cracks and surface defects of the oxide permit gaseous sulfur to penetrate trough the oxide and accelerate the degradation process.

As part of an overall investigation on the degradation of these types of alloys by CANMET, this study focuses only on the solubility and transport of sulfur through chromic oxide Cr_2O_3.

The first part of this study deals with the determination of the solubility of sulfur in pure Cr_2O_3 for controlled oxygen and sulfur pressures from $P_{O_2} = 10^{-6}$ to 10^{-12} and $P_{S_2} = 10^{-2}$ to 10^{-16} atm at a temperature of 1273K.

The second part of this study focuses on the determination of the diffusion coefficient of sulfur in polycrystalline and monocrystalline Cr_2O_3 in the temperature range from 1173 to 1373K. These measurements are still to be completed.

An outline of the work carried out in this study is summarized below.

The first chapter consists of a critical evaluation of the literature on the solubility and the various interpretations of the defect structure of Cr_2O_3 as a function of oxygen pressure and temperature.

The second chapter deals with the experimental method used for the equilibration experiments with the desired reaction gas atmosphere, followed by the determination of the most reliable method of sulfur analysis in Cr_2O_3. Due to the low level of sulfur that were encountered (<100 ppm), conventional methods proved to be inadequate and new innovative methods had to be explored. This was a critical factor in the execution of this study and also proved to be very time consuming. After attempting a thermogravimetric method, LECO-infrared analysis, proton induced X-ray emission, only the neutron activation technique resulted in reliable and reproducible results.

The chapter on results first presents the thermodynamic calculations for the oxygen and sulfur partial pressures produced from introducing afferent combinations of gas mixtures into the reaction chamber.

It was found that the choice of the gas mixture is extremely important in obtaining thermodynamically buffered mixtures in order to maintain a constant specified reaction gas atmosphere over long periods of time. A comparison of results of sulfur analysis is then presented showing the reliability of the neutron activation method eventually adopted.

The effects of sulfur and oxygen pressure on the solubility of sulfur in Cr_2O_3 are then discussed in terms of the various possible forms of sulfur dissolution within the oxide lattice. Analytic equation are developed for different ionic forms of sulfur on different lattice sites, as a function of oxygen and sulfur partial pressure. A numerical method of the solution of this equation is also proposed.

In the final section of this report, the experimental methods of obtaining dense polycrystalline Cr_2O_3 sample are first described. These samples will be used for the measurement of the diffusion coefficients in the temperature range from 1173 to 1373K. Due to the low sulfur contents that were found in the solubility section of this study, the only reliable method of determining the sulfur profile is judged to be a radiotracer technique using ^{35}S. An analytical method for obtaining the diffusion coefficients from this type of data has been proposed.

CDT
Centre de
Développement
Technologique
École Polytechnique
de Montréal

I. LITERATURE REVIEW

I.1 DEFECT STRUCTURE

The oxidation of chromium has been the object of numerous studies (3,4,5) because of its strategic use in alloys used for corrosion resistance. The nature and the rate of formation of an oxide layer are complex and depend on alloy composition, temperature, and oxygen partial pressure to which the alloy is exposed. Various oxides with O/Cr ratios from 1.5 to 3 have been described (6) and some of the oxides have not been well characterized. At low temperature (up to 773K) it is generally accepted that CrO_2 and CrO_3 are stable solid compounds, but at high temperature (>1273K) it has been accepted that the only stable solid compound oxide is Cr_2O_3.

This oxide crystallizes in a hexagonal rhombohedric form and the oxygen atoms occupy the hexagonal-close packed sites, whereas the chromium atoms occupy 2/3 of the octahedral sites. Cr_2O_3 has the corundum structure and can be grouped with Ti_2O_3, αFe_2O_3, αAl_2O_3 and easily forms mixed crystals (spinels) with these oxides. Using X-ray methods, Dicerbo and Seybolt (7) reported lattice parameter values of a_o = 4.9591Å and c_o = 1.599Å at 293K.

Chemical analyses have also generally shown that the chromium content is slightly lower than the value found for the stoichiometric compound of 68.4 wt% (8).

According to Monty (9), the deviation from stoichiometry of Cr_2O_3 is very small and the concentration of defects, to a large degree, depends on the impurity of the oxide, the oxygen partial pres-

sure, especially at low temperatures, where the number of intrinsic defects is very small. Hay et al. (10) have attempted to determine the degree of non-stoichiometry between 1223K and 1473K, by measuring the weight change of a Cr_2O_3 sample under varying oxygen partial pressures. They observed a slight weight decrease as the P_{O_2} decreases, but their results are not sufficiently accurate to derive a relationship between the weight change and the oxygen pressure, and consequently could not formulate any conclusions as to the major contributions of the defect structure of Cr_2O_3. One can however assume from thermodynamic considerations (11) that, regardless of the type of defect structure, a weight loss will always occur in these type of experiments due to the volatility of CrO_3, especially when the oxygen partial pressure is high ($P_{O_2} > 10^{-2}$ atm).

Cojocaru (12), on the other hand found that the oxide formed by heating CrO_3 between 673 and 1273K over a period of 4 hours presents a large deviation from stoichiometry with an O/Cr ratio equal to 1.6 which represents x = 0.12 in the form $Cr_{2-x}O_3$. This surprising result can only be assumed to be attributed to incomplete reducton of the CrO_3 and is contrary to the generally accepted values in the literature. Hagel and Seybolt (13) explain the difficulty of measuring the concentration of defects at low temperatures by describing them as "frozen-in" and that their mobility increases only when the temperature is increased.

I.2 ELECTRICAL CONDUCTIVITY

Even though there seem to be numerous studies in the literature, the results of the different authors have not led to definite conclusion as to the variation of the electrical conductivity of Cr_2O_3 as a function of temperature and, to a lesser extent, as a function of the oxygen partial pressure is seen in Figure 1.

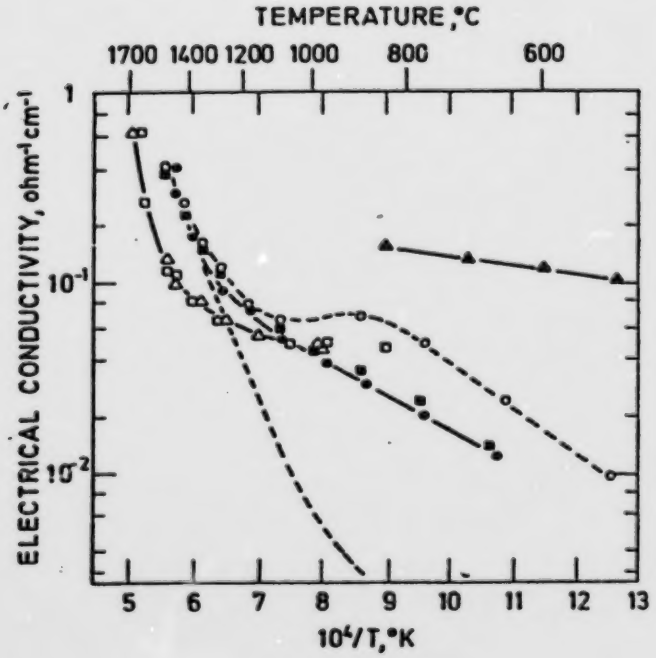

FIGURE 1: Electrical conductivity of Cr_2O_3 as a function of temperature. Results of Hauffe and Block[14] (Δ, air), Fischer and Lorenz[19] (Δ, air; □, argon), Hagel and Seybolt[13] (□, air; •, nitrogen; o, argon), Grawford and Vest[16] (---).

This diversity of results cannot clearly identify the mobile species in the oxide but generally, it is possible to distinguish between the conductivity behavior for two temperature regions.

At high temperatures (from 1273K to 1473K) the electrical conductivity does not vary with oxygen partial pressure, whereas at low temperatures a definite influence has been observed. The temperature demarcation between the two region depends on the crystal structure of the Cr_2O_3 (monocrystal or polycrystal) as well as on the concentration of impurities (doping). In all cases, the conductivities measured are essentially electronic (13) and that the ionic contribution is generally negligeable ($\sigma_i/\sigma_e \approx 10^{-3} - 10^{-5}$).

Cr_2O_3 is considered to be an intrinsic p-type semi conductor at high temperatures (14). Hagel and Seybolt (13) found that at high temperatures, the oxide exhibits an ionic disorder, based on their study of the auto-diffusion of chromium (^{51}Cr) in Cr_2O_3, and on their conductivity measurements. They have proposed a model for the defect structure according to the equation

$$Cr_{cr} \rightleftharpoons V_{cr}''' + Cr_i^{\cdot\cdot\cdot} + h^{\cdot} \qquad (I.3)$$

where: Cr_{cr} = chromium atom on iits normal site
V_{cr}''' = chromium vacancy, negativety charged (-3)
$Cr_i^{\cdot\cdot\cdot}$ = chromium interstitial, positively charged (+2)
$h^{\cdot}$ = electron hole (+1).

This model previously described by Hauffe and Block (14) can qualitatively explain the fact that the conductivity is independent of oxygen pressure at high temperature, but does not explain the results obtained at low temperature which shows a decrease of conductivity with decreasing oxygen partial pressure.

Hicks et al. (15) have studied the combined effects of oxygen pressure and temperature on sintered Cr_2O_3 samples and suggest that the oxide is cation deficient in air and in pure oxygen between 500 and 1600K. They do not explain the effect of oxygen pressure and they assume that other types of defects must contribute, especially when P_{O_2} is very small. The results of Hicks et al. (15) are shown in Figure 2 who also show a distinct demarcation between the high temperature and the low temperature regions.

Crawford and Vest (16) have produced a detailed but concise study of the variation of the conductivity of monocrystalline samples as a function of temperature and oxygen partial pressure. They show conclusively that the monocrystal is an intrinsic electronic conductor at high temperature, which seems to confirm the results on polycrystalline samples of the previous studies. At low temperature, they also find that the conductivity depends on the oxygen partial pressure which they represent by the following equation

$$3/2\ O_2 \rightleftarrows 2V_{Cr}^{'''}\ 6h^{\cdot} + 3\ O_O \qquad (I.1)$$

where: O_2 = gaseous oxygen

O_O = oxygen ion on its normal site.

Equation (I.2) relates the conductivity to the electron hole density and the oxygen partial pressure, by using the mass conservation and charge balance equations, so that

$$\sigma_e \propto [h^{\cdot}]$$

$$\propto P_{O_2}^{3/16} \qquad (I.2)$$

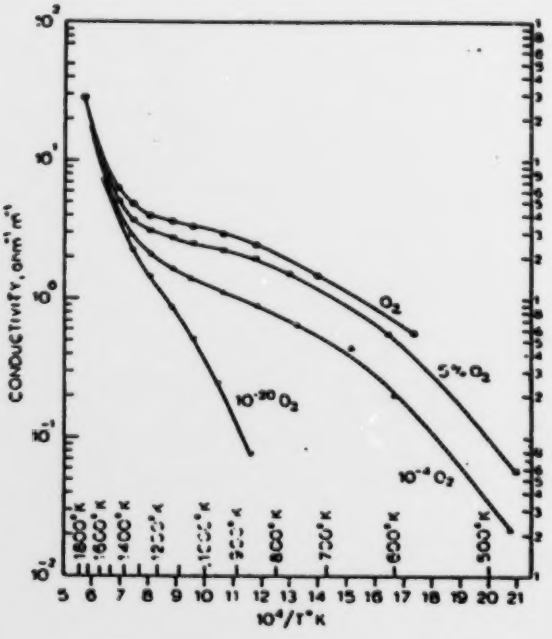

FIGURE 2: Variation of electrical conductivity of Cr_2O_3 with oxygen partial pressure [15].

This equation has not been experimentally proved by Crawford and Vest (16) but other studies (17) on the auto-diffusion of (^{51}Cr) in mono-crystals of Cr_2O_3 equilibrated in different atmospheres at 1300°C, have shown the validity of this relation, which leads one to believe that the defect model proposed by (16) best describes the conductivity behavior with varying P_{O_2} at low temperatures. They stress that the validity of their model strongly depends on the purity of the products used. It is highly probable that the differences which they observe are greatly influenced by their appreciable Al content (≈0.1%) in the oxide.

In summary, this literature review brings out the complexity of the defect structure of Cr_2O_3 and the difficulty of experimental determination of their characteristics. The uncertainty of the results is also due to the difficulty in analytically formulating a defect model which fits the experimental results of the various studies.

It is generally accepted that the oxide is an intrinsic p-type conductor at high temperatures, and that the concentration of defects depends to a large degree on the purity, and oxygen partial pressure at low temperatures. The model proposed by Hauffe and Block (14) and by Hagel and Seybolt (13) are the only ones that justify the behavior at high temperatures, both referring to the defect structure proposed by Crawford and Vest (16) at low temperature.

I.3 OXIDATION OF CHROMIUM

Chromium exhibits a complex behavior when exposed to oxidizing atmospheres at high temperatures. A large number of parameters must be taken into consideration to represent the phenomenon. For example, transport of reactive species through the oxide can occur by

volume diffusion, along grain boundaries and other easy diffusion paths, such as through microfissures. Intergranular stresses in the oxide layer are also produced during oxidation, causing fissurisation, and deformation of this layer with possible detachment from the metal interface. It is not surprising therefore, that the kinetics and mechanism of chromium oxidation are largely influenced by the experimental conditions resulting in discrepancies in the literature.

The formulation of a Cr_2O_3 layer on chromium metal is generally considered to proceed according to a parabolic rate law (20) at least for a certain stage of the reaction. According to the literature, the values of the parabolic rate constant however can vary by a factor of about 100 (21,22) for temperatures below 1473K at atmospheric pressure. The major differences can be attributed to impurities in the oxide layer. Fischer and Lorenz (19) found that Cr_2O_3 is an intrinsic conductor above 1473K and that doping with other elements greatly affects the rate of oxidation.

The oxidation mechanism is still not clearly understood. It has been reported in some studies that the rate of oxidation of chrome metal is independent of oxygen pressure. Hagel (22) studied the oxidation of chromium between 1023K and 1373K and found that the reaction rate decreases slightly when the oxygen pressure is reduced, but he considers that this variation is negligeable, and that the transport of chromium through the oxide does not involve anionic defects.

In a more detailed investigation, Kassner et al. (23) studied the oxidation of chromium and as well as the diffusion fo ^{51}Cr in Cr_2O_3 at low oxygen partial pressures generated by H_2-H_2O (23) gas mixtures between 973K and 1273K. They found that the oxidation rate, as well as the diffusion of the tracer is directly related to the oxygen partial

pressure. Their parabolic rate constant was found to be related to the oxygen pressure according to the following equation

$$K_p \propto P_{O_2}^{3/16} \qquad (I.4)$$

This result is in agreement with the defect equation of Crawford and Vest (16) described previously.

The more recent study of Kofstad and Lillerud (18) has also shown that oxygen partial pressure does influence the oxidation rate. In interpreting their results, they propose a new defect structure model where the major defects of the oxide are chromium interstitials for oxygen pressures in the range corresponding to the decomposition of Cr_2O_3, and they conclude that the oxide becomes an intrinsic electronic conductor at near atmospheric pressures. Hindam and Whittle (5) also support this model in their study of the growth of Cr_2O_3 at low temperatures by applying the model to their results, and have found a reasonable agreement between the experimental results and the model. Kofstad and Lillerud (18) however advise caution in the use of this model and suggest that conductivity measurements are necessary to ascertain its validity.

Kröger (24), in a detailed study of the conductivity of Cr_2O_3, was not able to ascertain whether, interstitials or vacancies were the major contributes.

Considering previous thermogravimetric studies (10), a weight-loss behavior is inconsistent with the model proposed by Kofstad and Lillerud (18) which predicts a weight gain. It was also shown (8) in studies using chemical analysis that the non-stoichiometry of Cr_2O_3 is due to cationic vacancies.

In conclusion, the most thorough of the studies (5,18,25) on chromium oxidation and growth of a Cr_2O_3 layer show that the phenomena are far from simple.

I.4 SULFUR SOLUBILITY IN CHROMIUM OXIDE

Complex gas atmospheres consisting of the elemental constituents (C-O-S-N) are commonly encountered in combustion of hydrocarbon fuel (containing sulfur) with air. The reaction products of the oxidation of metals and alloys can either be oxides but can also be sulfides or oxysulfides in certain cases, depending on P_{O_2} and P_{S_2}. The formation of an oxide also does not exclude the penetration of sulfur or even the formation of sulfides at the metal-oxide interface, as has been reported for oxide layers of NiO, and Fe_2O_3 (26,27,28,29). It is often proposed that the sulfur diffuses via macroscopic defects such as fissures, pores, along grain boundaries as well as along dislocation boundaries. Volume diffusion across a grain is also significant especially at high temperatures and is based on the migration of sulfur within oxide crystal lattice.

A thorough literature review showed that the experimental results on the solubility of sulfur in oxides is still not well defined, and in some cases it is not known at all, such as for Cr_2O_3 and Al_2O_3. In CaO, for example, St. Pierre and Chipman (31) estimate that the sulfur solubility reaches 0.8% at 1823K. Sharma and Richardson (32) on the other hand found that only 0.036% S dissolves at 1923K. According to Kor and Richardson (33) the solubility limits are 0.003% at 1773K and 0.011% at 1923K. In wustite, Kor and Turkdogan (34) found that the sulfur solubility limit is 0.014% at 1523K using an Ar, H_2-SO_2-CO_2 gas mixture. Other studies show 0.011% (35) and 0.03% (36) for similar conditions.

Additional results on sulfur solubility in metallic oxides come from corrosion studies in oxidizing and sulfurizing atmospheres. Flatley and Birks (37) report a solubility of 0.03% in magnetite, and varies between 0.03 to 0.4% in wustite. Other studies by Birks and Tottam (59) show a value of 0.8% in Cu_2O at 1273K and 0.5% in CuO at 1073K. Even though the solubility of sulfur has been the object of numerous investigations, the values reported by different authors are quite inconsistent. In an earlier study, Birks (38) reported that the solubility can reach 5 at.% in NiO whereas Chang (39) estimates that it is only 100 ppm at 1273K. In a more recent study by Pope and Birks (40), dissolved sulfur was found to be between 100 and 200 ppm at temperatures between 1173K and 1273K. These differences are in part due to the long equilibration time necessary for reaching solubility limits which are very low, and the analytical techniques that were used to quantify the sulfur content.

Experimental results on the solubility of sulfur in Cr_2O_3 are virtually inexistent. Most studies (41,43) show oxidation rates of chromium or chromium alloys in sulfurizing atmospheres such as (C-O-S or H_2S/H_2). In a study on the corrosion of pure chromium, Asmundis et al. (41) found that the concentration of sulfur varies between 0.1 to 0.25 wt% in pure SO_2 atmospheres between 973K and 1273K, whereas Korev et al. (42) found values up to 9.43%, clearly indicating that a chromium sulfide must be formed. More recently, Romeo and Spacil (43) have shown that pre-oxidized samples of chromium can dissolve up to 0.5% S in the oxide.

In all of the corrosion studies, the sulfur content was determined by the use of a microprobe and the authors admit to the difficulty of identifying whether the detected sulfur is actually in solution on whether small local concentrations of chromium sulfide phase are present.

Microscopic sulphide inclusions in the oxide phase will result in an uneven sulfur distribution, and can explain the large variation of sulfur content reported in the corrosion studies.

The dissolution of sulfur in oxides implies transport via a certain defect structure. One can readily see that any small impurity (doping) plays a significant role, and can change the values of the solubilities considerably. This is probably the major reason for the discrepancies of sulfur solubility values in the literature. The choice of a reliable method of analysis is also of prime importance especially in cases where the solubilities are very small.

1.5 MECHANISM AND KINETICS OF SULFUR DISSOLUTION

All studies on sulfur diffusion in oxides have shown that sulfur diffuses much more rapidly than oxygen but that the diffusion mechanism is much more difficult to explain. This difficulty of formulating a mechanism is due to complex behavior that sulfur exhibits in different oxide structures. Sulfur can be present in many different valence states ($S^{=}$, S^{-}, S°, S^{+}, S^{++}) and the ionic radii can vary from 1.8 to 0.6Å which is either smaller or layer than the oxygen in the oxide lattice.

The literature reports sulfur in all of the possible valence states. In a study of sulfur (^{35}S) diffusion in NiO, Chang (39) found that the electrical conductivity decreases with increasing sulfur content. He claims that the reduction in conductivity is due to sulfur penetration via anionic vacancies in the form of S^{-} or S°. According to Howng and Wagner (45) however, the decrease in conductivity may be due to the presence of S^{3+} substituted on the nickel sites ($S^{\bullet}_{Ni}$). On

the other hand, Pope and Briks (40) observe no variation at all in electrical conductivity which would indicate that sulfur enters the NiO lattice in the form of S^{2+} (S_O°) substituted on the oxygen sites, or in the form of S_i° on the interstitial sites.

More recently, Howng (47) claims that sulfur can enter the NiO lattice, simultaneously according to two mechanisms. One is a fast migration of S^{2+} via the cationic vacancies, and the other is a slow migration of S^{2-} via the anionic vacancies.

Sulfur penetration in the form of S^{-} via the anionic sites has been proposed by Romeo et al. (48) for the case of chromium oxide. They show that as an electron donor, sulfur enhances the diffusivity of chromium by reducing the number of electron holes and increasing the concentration of chromium defects. This interpretation justifies the observation that the oxidation rate of chromium is much higher in a sulfurizing atmosphere than in an oxidizing atmosphere. The defect equation for Cr_2O_3 proposed by Romeo et al. (48) corresponds to equation (2) and the sulfur subtitution mechanism can be written as:

$$\tfrac{1}{2} S_2 + O_O + h^{\cdot} \rightleftharpoons S_O^{\circ} + \tfrac{1}{2} O_2 \qquad (I.5)$$

In a detailed study on the corrosion of pre-oxidized alloys of composition $Ni_{77}\ Cr_{16}\ Fe_7$, Moulin (49) found that the change of the parabolic reaction rate constant Kp as a function of sulfur pressure corresponds to the presence of S^{2+} on the cationic sites in the layer of chromium oxide. This result is based on an oversimplified hypotheses, which leads to a negligible effect of the oxygen partial pressure on the value of Kp. Based on results of other oxides, this result is most unlikely.

The problem is thus far from being completely solved. It seem that the validity of the equations for the sulfur solubility as a fraction of sulfur and oxygen pressure, as given in Table V.2 would eventually lead to identifying the form that sulfur occupies in the chromium oxide lattice.

The only study that reports the diffusivity of sulfur in chromium oxide as a function of temperature is by Chang (39) who finds that the values are very high, given by:

$$D_S \text{ in polycrystalline } \alpha\text{-}Cr_2O_3 = 4.2\times10^{-7} \text{ (-17800/RT) } cm^2 \cdot s^{-1} \quad (I.6)$$

It should be noted that the oxide used in this study was not pure (only 99.9%). This can greatly alter the diffusion mechanism, as was reported in the literature (16,19,20). In addition, the sintering conditions for the polycrystalline material were not clearly specified. The temperature and oxygen partial pressure of sintering are known to have an effect on the type of defect structure that is obtained since sintering kinetics are controlled by the volume diffusion of oxygen (50,51). These studies also show that the crystal defects of the product depend on the sintering conditions. For example, Chang (39) sintered his samples in air at 1773K, and at this temperature CrO_3 is easily volatilized especially under high oxygen partial pressures such as in air. This factor could easily change the stoichiometry of the samples used as the starting material for their diffusion studies.

II. EXPERIMENTAL

II.1 EQUILIBRATION SYSTEM APPARATUS

Since there was no reliable data for sulfur solubility in the literature, a few preliminary experiments were carried out using a SETARAM thermobalance to measure the weight change of a sample of sintered Cr_2O_3 in a controlled gas atmosphere. A mixture of CO/CO_2 = 10^{-2} and SO_2/N_2 = 10^{-1} at 1273K was passed over the sample suspended in a platinum were basket representing oxygen partial pressures of 10^{-11} atm and sulfur partial pressures of $10^{-2.30}$ atm. No significant weight change was observed even at be highest sensitivity of the balance (10 mg full scale) for repeated tests. A maximum weight gain of 0.1 mg was obtained after 70 hours of reaction time for the experimental conditions indicated above. This is only slightly above the limiting sensitivity of the thermobalance and led to the conclusion that a thermogravimetric technique was not suitable. The evaporation of certain compounds such as CrO_3 and CrO_2 present as minor constituents at these temperatures based on thermodynamic considerations, can also contribute to a weight change (loss) over the long duration experiments and thus lead to erroneous results.

An apparatus was therefore designed specifically for the equilibration of Cr_2O_3 samples and is shown in Figure 3. The entire system is made of quartz, consisting of a main reactor tube 4.2 cm in diameter and 60 cm long fitted with a ground glass joint for introducing the samples. The reaction tube was heated by means of a split shell Lindberg Hevy-duty (type MK-2018) furnace with a constant temperature zone of about 10 cm, and controlled by a Lindberg proportional temperature controlled (model no. 59344).

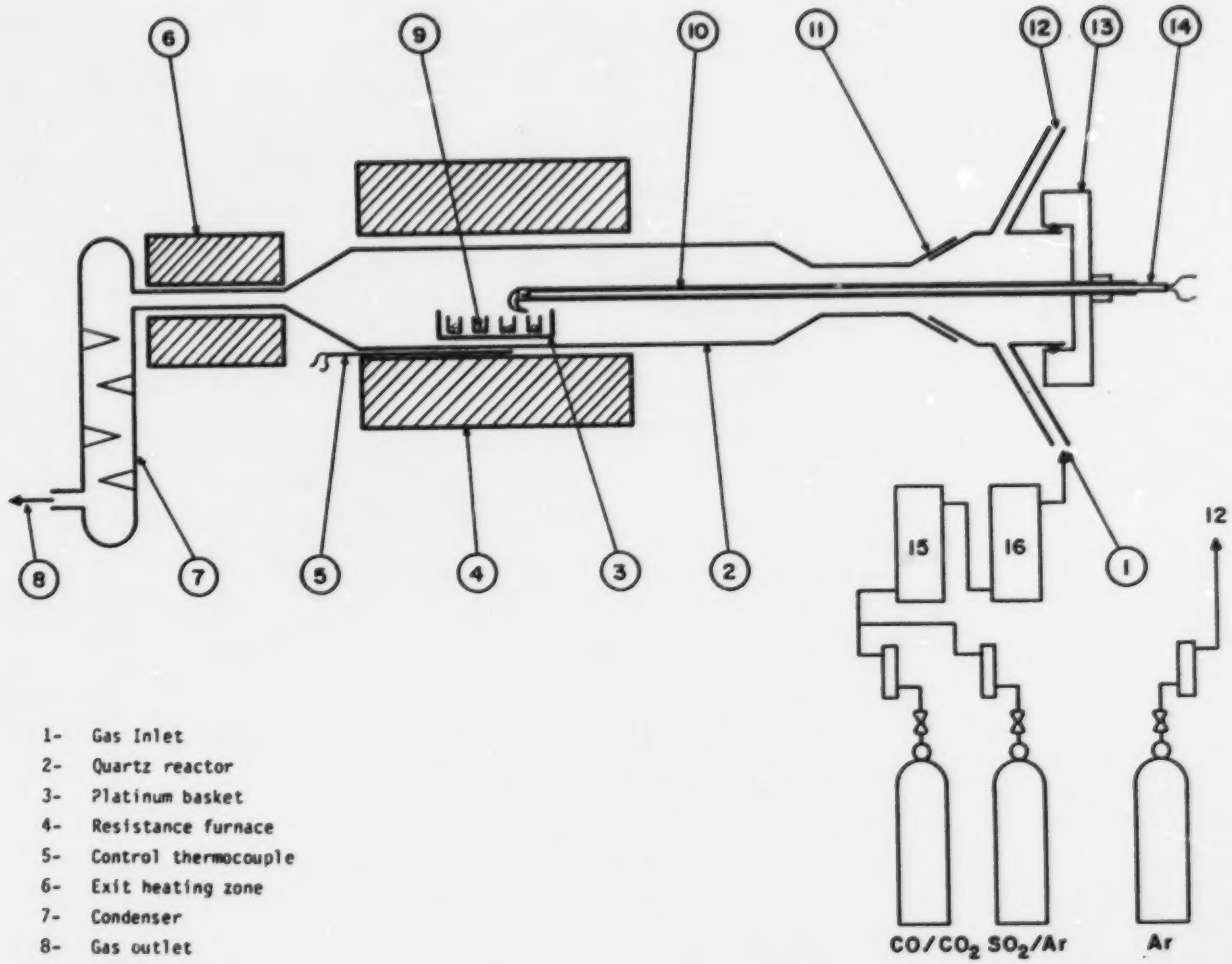

1- Gas Inlet
2- Quartz reactor
3- Platinum basket
4- Resistance furnace
5- Control thermocouple
6- Exit heating zone
7- Condenser
8- Gas outlet
9- Sample
10- Sliding quartz rod
11- Ground glass joints
12- Flushing gas
13- O-ring seal
14- Pt/Rh-Pt measuring thermocouple
15- Gas mixing chamber
16- $CaSO_4$ desicccant

FIGURE 3: Experimental apparatus.

Spec-pure α-Cr_2O_3 (Johnson-Matthey) in the form of 5-10 μm powder was used as the starting material. The total impurity content of their product was certified to be less than 10 ppm. About one gram of sample was placed in powdered form into each of the fine mesh platinum crucibles supported on a platinum plate and contained in a platinum wire mesh boat as shown in the figure. The loose powdered form of Cr_2O_3 was used in order to facilitate saturation of the oxide with sulfur by minimizing diffusion of reaction gases through the particulate solids.

Pure platinum containers were used specifically for two reasons.

(1) good corrosion resistance in the atmospheres used, with no chemical interaction with the chromium oxide powder;
(2) catalytic effect of the large platinum surface provided by the mesh in order to achieve the desired oxygen and sulfur partial pressures from the mixture of inlet gases.

Constant head capillary flow meters were used to introduce the gas mixture into the furnace. The values of the flow rates of CO/CO_2 and SO_2/Ar gas mixtures required at ambient temperature producing the desired oxygen and sulfur pressures at the equilibration temperature were calculated using the F*A*C*T system of thermochemical computation. The details of the computational method and the results for specific mixtures are given in the section on "RESULTS". It was found that 50 cm^3 min^{-1} of each reaction gas was suitable for the reaction volume of the apparatus. Prior to introduction into the reaction chamber, the gases are mixed in a column of glass beads (0.5 cm dia.) followed by a copper sulfate column in order to dry the reaction gas.

The gaseous species produced at the reaction temperature are numerous, some of which can condense at the reactor exit. If the reaction exit tube is too small in diameter, or if it is not heated, sulfur and CS_2 can condense and eventually block the tube. To avoid this problem a condenser was designed consisting of a series of baffles in a pyrex tube 70 cm high and 5.5 cm in diameter. Heating tape was applied at the exit of the reaction tube and maintained at 623K in order to prevent condensation in this narrow section of the apparatus.

The temperature was measured with a Pt-Pt10%Ph thermocouple contained in a quartz sheath shaped with a hook at the hot end which was used to place the crucible in the desired position, as well as to remove the samples. A Keithley (model 191) digital voltmeter was used to measure the temperature continuously, and was found to vary ±2K with respect to the control temperature of 1273K.

II.2 EXPERIMENTAL PROCEDURE

The sequence of operations of a typical run is follow:

- About 1g of Cr_2O_3 powder was placed in each of the four crucibles, placed in the platinum wire mesh boat and pushed into the constant temperature zone of the furnace.
- The furnace was sealed using the ground glass joint.
- The temperature was raised to the desired value under a specific CO/CO_2 atmosphere.
- The SO_2/Ar gas mixture was introduced when the reaction temperature reacted 1273K.
- After 24 hours of reaction, two crucibles were removed by quenching under argon.

- Two new samples were then introduced into the platinum boat and placed into the constant temperature zone using identical CO/CO_2 and SO_2/Ar mixtures as before.
- After 48 hours of reaction time, all four samples were removed from the furnace.

This method provided two samples each with 24 h, 48 h and 72 h reaction time at controlled oxygen and sulfur partial pressure. The procedure was repeated for each new set of atmospheric conditions.

II.3 OXYGEN PROBE

In order to measure the oxygen potential within the reaction tube an oxygen probe was used to verify that the correct oxygen potential was generated with the reaction gas mixture that is introduced. At first a calcia stabilized zirconia tube 60 cm long using air as the reference was employed but proved to be unsuccessful. Fissures appeared in the zone between the reaction temperature and the cold end. The design of the reaction tube and furnace assembly could not prevent this large thermal gradient and fissuration occurred on repeated replacement of this type of probe.

A mini-probe was consequently built on the design patented by Deportes et al. (52). This type of probe has a sealed-in internal reference, usually consisting of a mixture of a metal and its oxide such as Ni/NiO, Cu/Cu_2O or Co/CoO. Its small size, of the order of 0.3 cm in diameter and 4 cm long, avoids the problem of thermal shock (52,53) since the entire probe can be placed in the hot zone of the furnace. Recent techniques of Gantès (54) and the slip casting technique of Rivier and Pelton (55) were used for fabricating the zirconia tubes and the tube were sintered at 1923K. A schematic diagram of the assembly is shown in Figure 4.

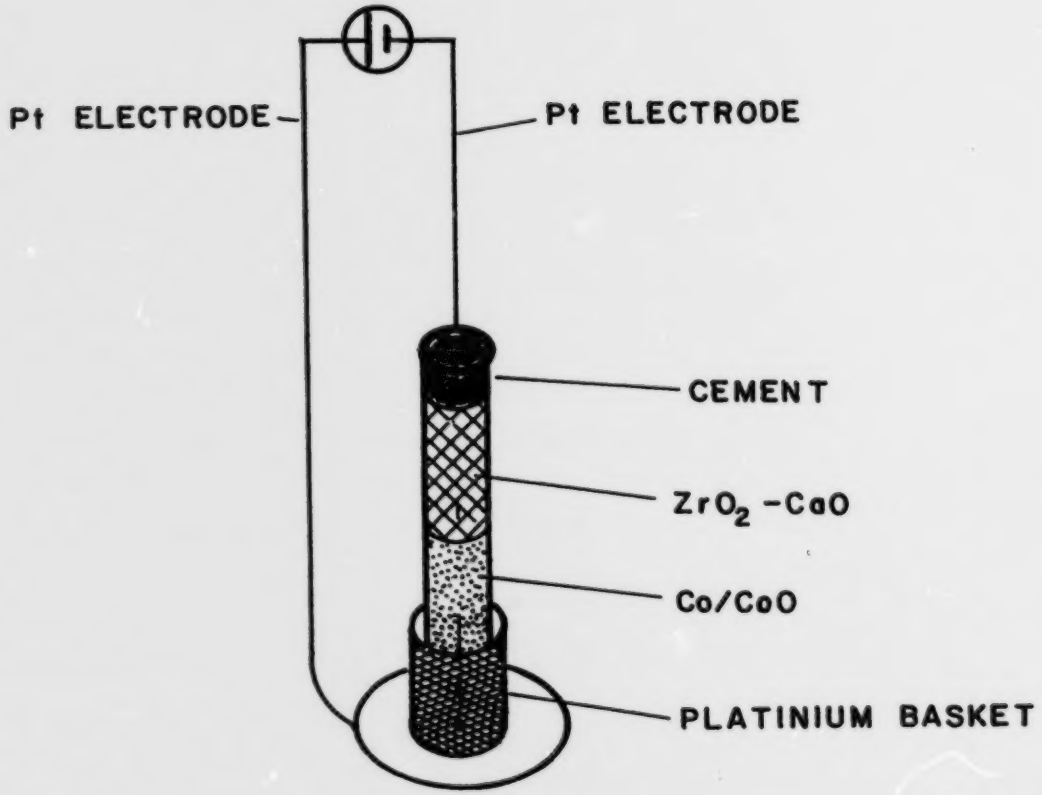

FIGURE 4: Design of the oxygen miniprobe.

A mixture of cobalt/cobalt oxide was used as the internal reference with platinum wire electrodes. The electrochemical cell reaction can be simply written as

$$(Po_2^{ext}) \;\Big|\; (ZrO_2)_{0.95}\,(CaO)_{0.05} \;\Big|\; \begin{matrix} CO/CoO \\ (Po_2^{int}) \end{matrix}$$

The cobalt oxide (CoO) was prepared from pure cobalt powder according to the method described by Pascal (56) by reaction with oxygen at 1373K since Co_3O_4 is stable up to a temperature of 1300K. X ray diffractometry of the product identified only the divalent oxide form.

The reference mixture was sealed into the zirconia tube using a high temperature ceramic cement. The choice of the composition of this cement is based on studies of Gantès (54) who experimented with several compositions. Properties of low electrical conductivity, high fusion temperature (1600K) low thermal expansion coefficient (close to that of ZrO_2) and corrosion resistance are necessary in order to obtain a perfect seal.

This cement was prepared synthetically from the primary compounds with compositions listed in Table II.1.

TABLE II.1: COMPOSITION OF REFRACTORY CEMENT USED FOR THE MINIPROBE

Compound	SiO_2	Al_2O_3	K_2O	Na_2O	CaO	ZnO	ZrO_2
wt%	61.81	10.4	1.91	1.27	16.27	2.06	6.27
Thermal expansion coefficient $\sim 9\times10^{-6}K^{-1}$				Curing temp. 1600K			

CDT
Centre de
Développement
Technologique
École Polytechnique
de Montréal

The probe was first tested in air to verify its proper operation. Figure 5 shows a good agreement with the measured e.m.f. and that calculated from the thermodynamic data of Kubaschewski and Alcock (57) for the Co/CoO system. An incertitude of ±2Kcal for $\Delta G°$ represents a difference of ±22 mV. The values in Figure 5 show a maximum difference of only 15 mV between our experimental results and those of Kubaschewski and Alcock (57), which confirms the proper functioning of the probe.

When this mini-probe was used in an atmosphere containing sulfur (CO/CO_2 and SO_2-Ar mixtures) the probe characteristics deteriorated with prolonged exposure. Fluctuation in e.m.f. were first observed followed by a progressive decrease of e.m.f. in all cases. After many repeated tests, no stable values could be obtained. All attempts of improving electrode contact and improving cement properties failed.

Figures 6a, 6b and 6c show the cement electrode contact before and after exposure to the reaction gas atmosphere. It can be seen that the cement has reacted, producing pores, thus leading to probable gas leaks to the internal reference. Since the internal oxygen pressure (reference) is of the order of 10^{-12} atm and the reaction gas is only 10^{-5}-10^{-10} atm. The e.m.f. produced would naturally decrease according to the Nernst equation:

$$\Delta E = \frac{RT}{nF} \ln \frac{P_{O_2}^{ext}}{Po_2^{int}} \qquad \text{(II.1)}$$

where:
- ΔE = e.m.f.
- R = gas constant
- T = temperature in Kelvin
- F = Faraday constant
- $P_{O_2}^{ext}$ = oxygen pressure in the gas
- $P_{O_2}^{int}$ = oxygen pressure in the probe.

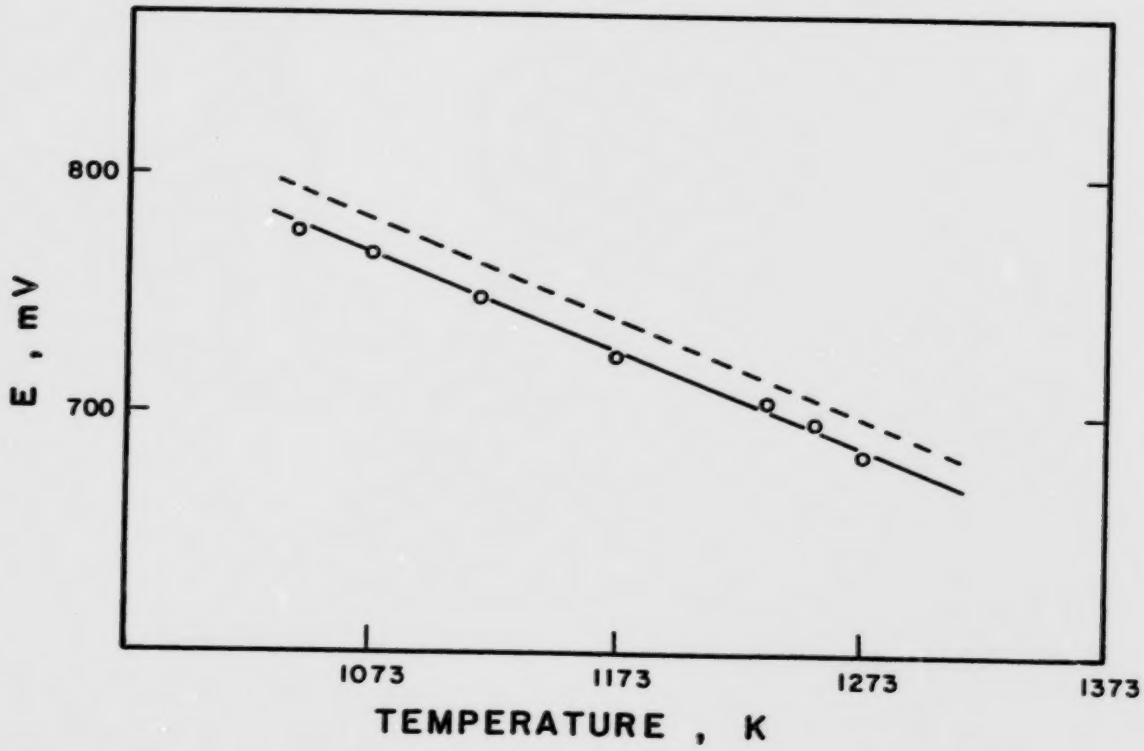

FIGURE 5: Results of E.M.F. measurements using the oxygen miniprobe vs. temperature (—) and calculated E.M.F. from thermodynamic data of (57) (---).

FIGURE 6a: General aspect of the miniprobe before use (X6).

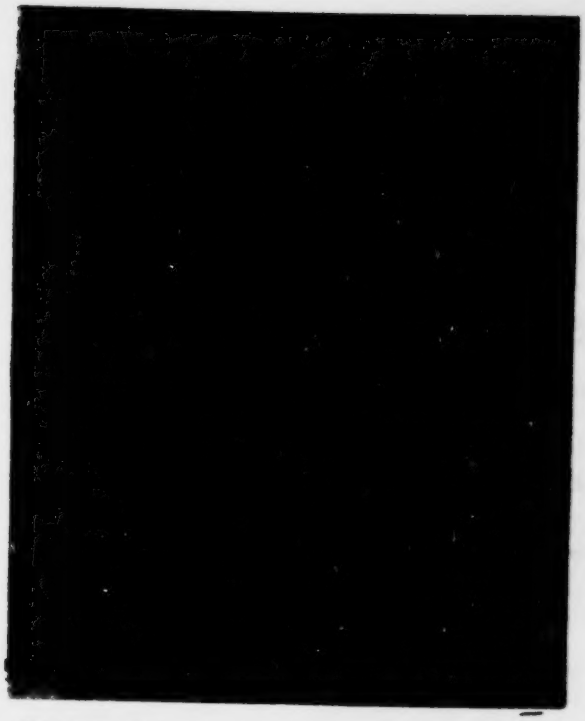

FIGURE 6b: General aspect of the miniprobe after use (X6).

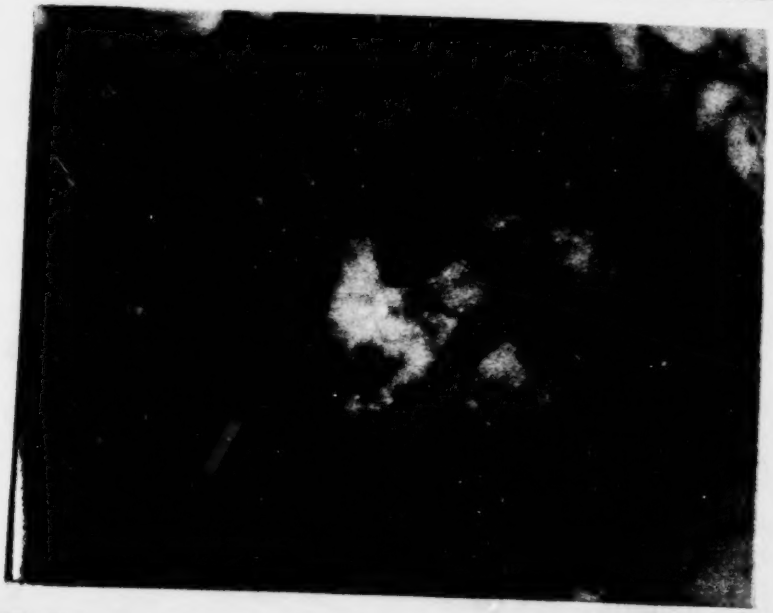

FIGURE 6c: General aspect of the miniprobe after use (X20).

Since the external oxygen pressure is fixed by a continuous flow of reaction gas, the only possible source of error is the instability of the internal oxygen pressure.

The cement was developed and tested for applications in non sulfurizing atmospheres and proved to be non reactive. The addition of sulfur to the reaction gases can lead to the formation of liquid sulfide phases especially with the compounds CaO, Na_2O and K_2O resulting in the degradation of the cement.

An indirect method was then used to verify that the gas compositions introduced represented the desired oxygen and sulfur pressures. Since NiO transforms from the oxide to the sulfide at the conditions required for this study, ultra-pure NiO (Johnson-Matthey) was placed in a crucible normally used for sulfurizing Cr_2O_3.

A gas mixture of $CO-CO_2-SO_2$ representing $Po_2 = 10^{-11}$ atm and $Ps_2 = 10^{-2}$ atm was passed through the reaction chamber. After 24 hours, the oxide has completely reacted and transformed to a liquid sulfide. The liquid sulfide consequently reacted with the platinum crucible which was shown to be highly reactive to liquid sulfides (58). The predominance area diagram of Figure 7 confirms the stability of Ni_3S_2 at these conditions. This test is therefore a confirmation that equilibrium of reaction gas within the reaction chamber is attained.

II.4 METHODS OF SULFUR ANALYSIS

The choice of a method of analysis for sulfur depends on the amount of sulfur in the sample, the precision necessary and the chemical nature of the sample. The methods range from classical wet chemical analysis to sophisticated instrumental techniques for special cases (60).

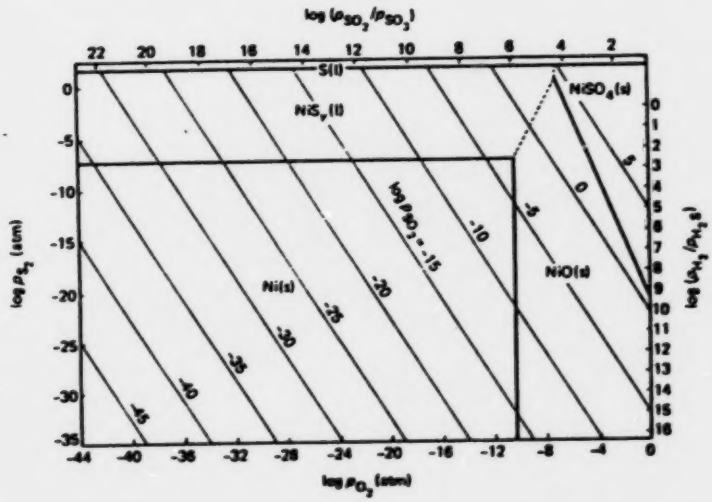

FIGURE 7: Condensed phase equilibria for the Ni-O-S system at 1250K (70)

The classical method normally used necessitates the dissolution of the sample in acid solution followed by precipitation of sulfur as $BaSO_4$. When the sample is not soluble and for sulfur contents below 0.1% this method becomes imprecise. Other difficulties with this method are that the precipitates often adsorb other ions, particularly iron. Other complexing reactions with molybdates, tungstates and chromates can also interfere. The complete dissolution of sulfur in the solution is the key factor in all aqueous methods.

Iodometric titration can also be used in some cases but has the same type of limitations as the gravimetric method, even though it is much more rapid. For special cases colorimetric, potentiometric and turpidimetric methods are also described by Charbot (60).

It can generally be concluded that all chemical methods lack precesion when sulfur contents less than 100 ppm are analysed. Instrumental methods such as atomic adsorption, X ray spectrometry infrared spectrometry, and neutron activation are possible for the sulfur contents of the Cr_2O_3 samples of this study. Among these only three instrumental methods were used:

(1) Infrared spectrometry (LECO)
(2) Neutron activation
(3) Proton induced X ray emission (PIXE).

The facilities of the Department of Metallurgical Engineering of École Polytechnique proved to be inadequate and it was subsequently necessary to explore other methods and to develop specific techniques for the low sulfur contents that were encountered. A high sensitivity LECO infrared sulfur analyser was first used in collaboration with the Sidbec-Dosco facilities at Contrecoeur. The results tested the lower

limits of the apparatus and proved to be inadequate in discriminating the small differences in our samples. The proton induced X ray emission (PIXÉ) method (Nuclear physics department, at University of Montreal) was then used but also proved to be unsuccessful. Finally, a neutron activation technique (Energy Engineering Institute, École Polytechnique) was finally adopted and proved to be accurate within ± 4 ppm.

Each of these methods will be briefly described in the next sections.

II.4.1 LECO infrared analysis

These analyses were carried out at the Sidbec-Dosco, Contrecoeur laboratories, using the LECO CS144 infrared analyser. This instrument is especially adapted for rapid and continuous sulfur analysis of steel samples, but has also been successfully used for analysis of sulfur in brasses, steel slags, iron ores and pellets as well as metallurgical dusts (61).

The analyser consists of three essential components: (a) an electronic balance; (b) an induction furnace for combustion of the sample and (c) a measuring cell.

In addition, a microprocessor is coupled with the analyser to fully automate the procedure. The operating principle of the instrument is based on the measurement of the infrared spectrum of the SO_2 produced by the combustion of the sample with pure excess oxygen in a ceramic crucible (sulfur free) heated by an induction furnace. The gases are then filtered to remove solid particles and are subsequently passed through the infrared cell.

Ten calibrations of samples were first carried out at a level of 70 ppm in order to check the reproducibility and sensitivity of the analyser. Different types of fluxes were also used to accelerate the fusion in the induction furnace (see appendix A). Since these accelerators can also contain traces of sulfur, this has to be taken into consideration during the calibration. After choosing one specific accelerator, the microprocessor compensated for this value in the analysis of all subsequent samples. The standard error of the analyser was also determined by analysing ten samples of pure Cr_2O_3 with the specific accelerator that was chosen.

II.4.2 Analysis by proton induced X-ray emission (PIXE)

Elemental analysis by the PIXE method has been successfully used for a number of varied materials. Even though the sensitivity is not the same for all the elements, the method is precise and rapid for many different trace elements in different matrices (62,63). This is a highly specialized and elaborate analytic equipment, normally associated with fundamental work on nuclear physics. The analysis of each different element requires special specific considerations and design of the procedures.

The limitations of this method are closely linked to the preparation of the targets containing the samples that are subsequently bombarded by protons. Greatest reproducibility is obtained when the sample target has a uniform sample concentration of about 1 mg/cm^2 and does not deteriorate from the proton bombardment.

Only recently, a new technique was developed by Houdayer et al. (63) for powdered solid samples of oxides. Using this method, a uniform deposit of a suspension of the powdered particles in a collo-

dion solution was deposited on a mylar film by centrifuging. Since it was difficult to control the amount of sample deposited within the required range of 1 to 2 mg/cm^2, each reaction product was deposited on four sample targets in order to obtain a representative average value.

In an analogous manner, a calibration for the detector, as well as for the blank samples were carefully carried out. The efficiency of the detector was tested with a sample containing a specific amount of $Cr_2 (SO_4)_3$ K_2SO_4, and blank tests were done on target samples consisting of only the mylar film as well as mylar and collodion only, in order to verify their sulfur content.

The targets were then bombarded with a proton beam of 1 M.E.V., an energy level which normally makes this method more sensitive for the analysis of elements of low atomic number.

It should be noted here that the equipment used for this analysis is located in the Nuclear Physics department of the University of Montreal. Collaboration was established between the two groups in order to adapt their method to the analysis that we required. This is a major piece of equipment used by a number of scientists at U. of M. for fundamental physics experimentation and for analysis that cannot be done by conventional means. Preparation for this type of analysis is very lengthy and requires great care. Once the beam is "on" it is used continuously for a period of about one week by different groups for their specific experiments. This procedure is repeated at a frequency of not less than every two months, and requires all preparatory work for samples as well as the proton accelerator to be brought up to operating conditions.

II.4.3 Analysis of sulfur by neutron activation

The equipment for this type of analysis is located in the Energy Engineering Institute at École Polytechnique making use of the SLOWPOKE nuclear reactor facilities. It is primarily due to the accurate analysis of trace elements that this method has proved to be the most successful. Its application to minor element determination as well as for extremely small sample masses have made the analysis of biological samples, biopsies, corrosion studies and art sampling possible.

This method is based on irradiating the sample at a preselected level followed by the determination of the activity of desired element. The radioactivity of the element is determined by counting the specific β and γ disintegrations, taking into consideration the half-life of the element. This is a very selective and precise method that can detect amounts down to 10^{-12}g of the element with a suitable detector, and with a precision of 2-10% (64). In addition, this method is very fast and the most error free of the three methods used, and has proven to be the most successful for the application of this study.

The solubility of sulfur in Cr_2O_3 was determined by measuring the β radiation of the previously irradiated sample at a neutron flux level of 0.2×10^{12} neutrons $cm^{-2}s^{-1}$ for a period of 2 hours. The reaction product samples as well as pure Cr_2O_3 were simultaneously irradiated, producing the exchange reaction of $^{32}S \rightarrow {}^{32}P$. The number of ^{32}P atoms is proportional to the ^{32}S atoms in the oxide and the β radiation emitted by the ^{32}P atom is therefore a measure of the sulfur content. A spectrometer for β radiation was used one week after the irradiation procedure, in order to eliminate any interference from other elements in the sample that have a very short half life.

A counting time of 15 minutes was used and the number of β disintegrations in a range from 900 to 1700 KEV was recorded and stored on magnetic tape for further data processing. The measurement was repeated for each sample and the arithmetic mean value was reported in the results. Also, a repeat irradiation and counting was carried out where necessary for samples which showed some discrepancy between the first two results.

III. RESULTS

III.1 Calculation of Chemical Equilibrium of the Reaction Gases

The kinetics and reaction mechanism of a gas mixture in contact with a metallic or oxide phase can be characterized only after establishing the chemical potential of the reacting species at the desired temperature. There chemical potentials are usually determined by evaluating the relative stability of each gaseous constituent of the mixture by means of their thermodynamic properties.

These calculations should take into consideration all the chemical equilibria among all the chemical species of the gaseous phase. The solutions of these equilibria are complex and require numerical methods which only recently have led to coherent results.

Gas equilibration studies are prone to different sources of error. The gas mixture introduced can give values of chemical potential that are different from the predicted thermodynamic calculations due to a possible continuous reaction with the solid material (generation or condensation of gaseous species), to systematic errors in the flow meters as well as from the impure nature of the gas. For example, a purified argon bottle of 10 ppm O_2 actually represents an oxygen potential of 10^{-5} atm.

Small fluctuations of flow rates can sometimes result in considerable variation in chemical potential of certain chemical species and are closely related to the choice of gas mixtures initially used. In other words, the choice of the gas mixture used to establish specific partial pressures needs to be based on the a buffering effect when small deviations in either flow rate or gas purity cannot be

CDT
Centre de
Développement
Technologique
École Polytechnique
de Montréal

controlled. This phenomenon can best be illustrated on a ternary isobaric diagrams (Figure 8) for the system H-O-C at 1000K ant 1 atm, taken from the calculations by Melançon (66). The oxygen isobars are indicated by dotted lines and the isoactivity values of carbon are given as solid lines. For example, a point of composition "D" represents a carbon activity of 0.10 and $P_{O_2} = 10^{-20}$ atm. From the figure it is possible to achieve this equilibrium using a mixture of $CO-CH_4$ and CO_2, or a mixture of $CO-CO_2$ and H_2O. This point is in a zone which is very well "buffered" as is indicated by the spacing between the isobar and isoactivity lines. It can be seen that along the CO_2-H_2O line on the diagram, the gaseous mixture is poorly buffered and the overall composition can change from 10^{-2} to 10^{-17} atm for P_{O_2} and for a_C from 10^{-3} to 10^{-19} for a very small change in the CO_2-H_2O ratio.

The influence of the oxygen content in the H-O-C system is clearly shown in Figure 9 where the oxygen pressure is plotted as a function of the oxygen content in the O_2-CH_4 mixture. The flat regions are buffered composition regions, whereas the zone of 67% O_2 is the non-buffered region, corresponding to the ratio of $2H_2O/CO_2$ on the H-O-C diagram.

A similar calculation was carried out for the S-O-C system to determine the P_{S_2} and P_{O_2} isobars. Similar steep gradients of oxygen and sulfur partial pressure are determined as shown in Figure 10 but they are not as drastic as for the case of the H-O-C system. Nevertheless, it is preferable to use the same buffered solution concept.

The gas compositions of this study lie within the SO_2-CO_2-CO triangle and for certain cases, mixtures of CO/CO_2 and SO_2/Ar give compositions which are not well buffered. As a result, it is probable that sharp variations of P_{S_2} and P_{O_2} can occur when small changes in flow rates of input gases, or when impure gases are used while working within the SO^2-CO^2-CO composition triangle.

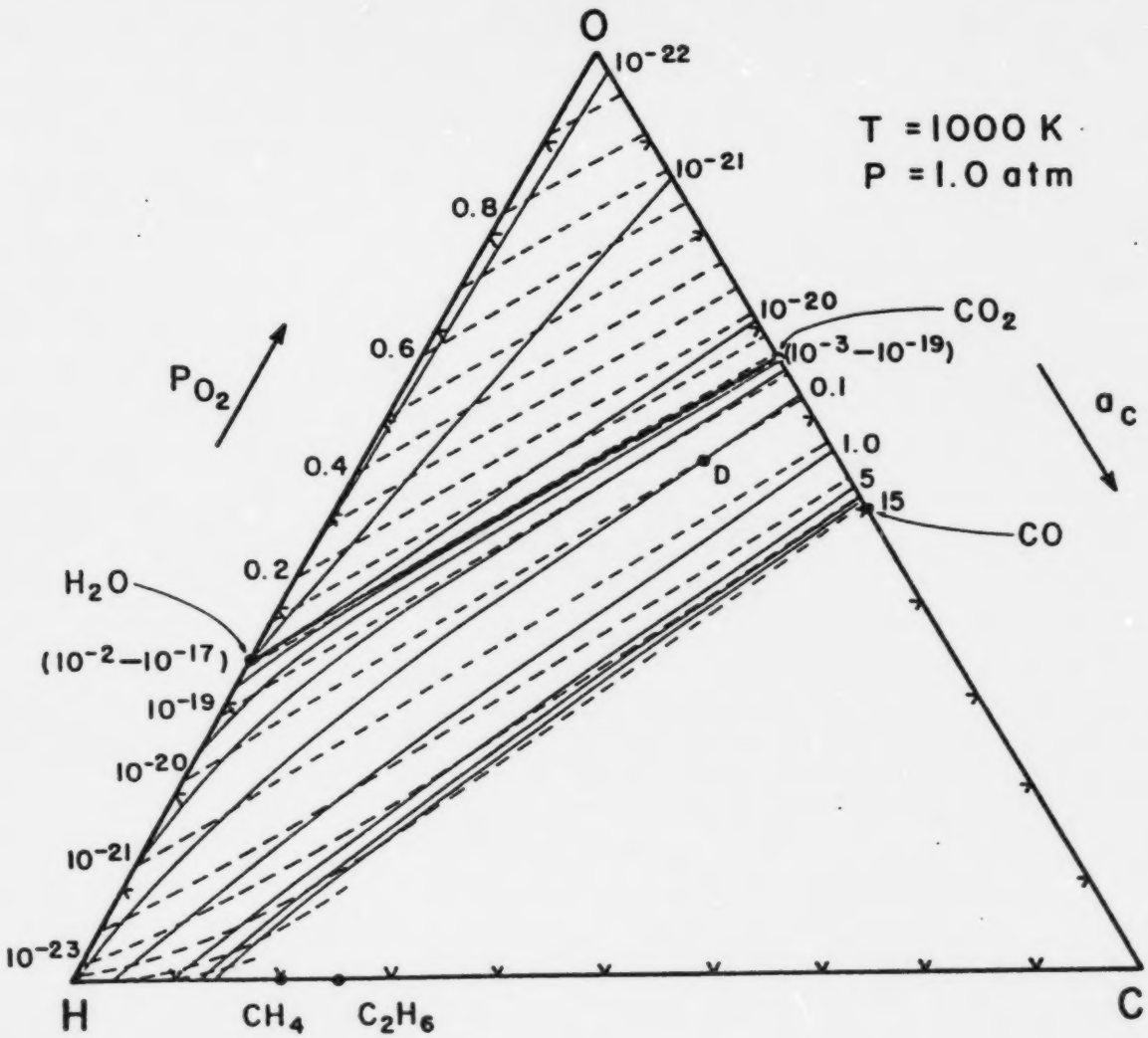

FIGURE 8: Oxygen isobars (---) and isoactivity of carbon (—) for the H-O-C system at 1000K and 1.0 atmosphere.

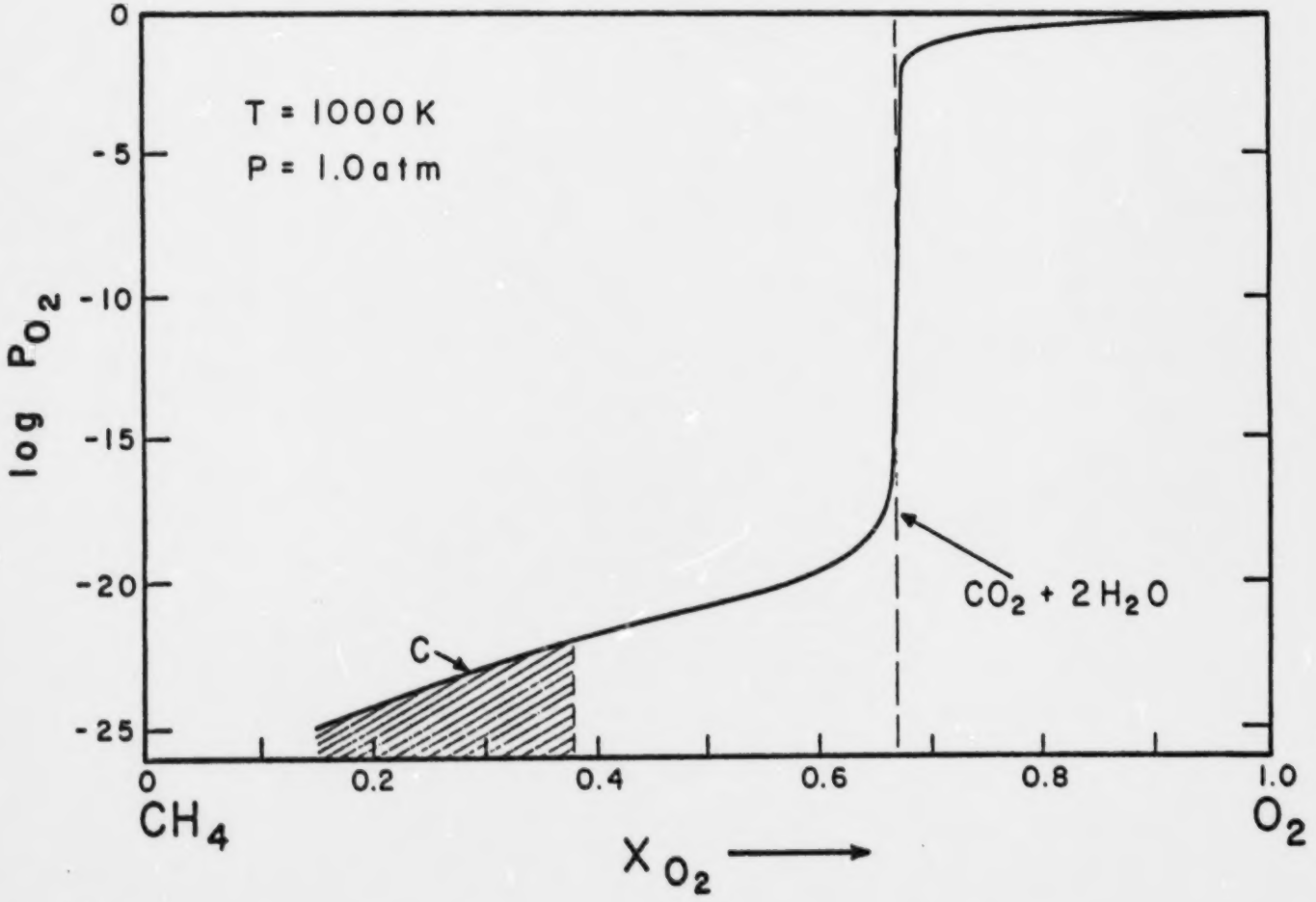

FIGURE 9: Oxygen partial pressure for the CH_4-O_2 system at 1000K and 1.0 atmosphere.

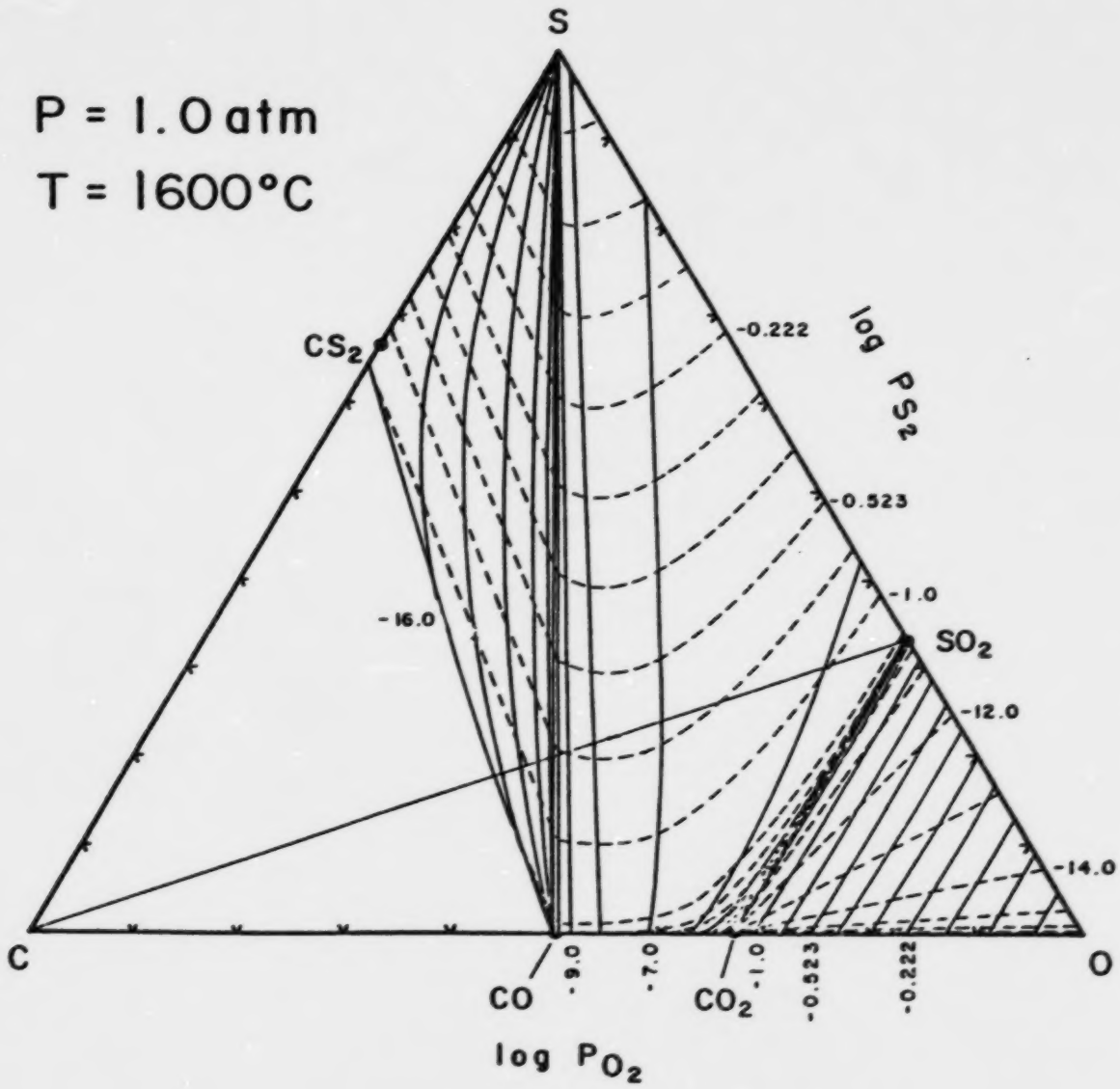

FIGURE 10: Oxygen isobars (---) and isoactivity of carbon (—) for the S-O-C system at 1873K and 1.0 atmosphere.

The variation of the P_{S_2} and P_{O_2} pressures as well as the carbon activity was calculated for varying CO/CO_2 and SO_2/Ar ratios at 1273K using the standard free energy of formation of the various stable species as listed in Table III.1 and taken from the data of Kubaschewski and Alcock (57). Some modifications were necessary in order to adapt the algorithm of Melançon et al. (65) in order to calculate these equilibria, and show a slight difference from the values originally calculated in the first report (67).

The partial pressures P_{O_2}, P_{S_2} and P_{SO_2} calculated from this data are given in Table III.2 For each specific gas mixture the P_{O_2}, P_{S_2} and a_C were also plotted in a series of graphs shown in Figures 11-26 together with the chemical potentials of all the gaseous species when the volume ratio of each gas mixture is 50-50.

A number of significant results can be observed from these figures. When the ratio of CO/CO_2 is 10^{-4} (Figures 11-14), the values of P_{O_2} and a_C are relatively stable for all SO_2/Ar ratio used. This is however not the case for the variation in P_{S_2} where this gas mixture becomes non buffered (for P_{S_2}). On the other hand, the variation of P_{S_2} becomes less pronounced when the SO_2/Ar tends to very high values.

The Figures 15 to 22 show that gas mixtures of CO/CO_2 between 10^{-3} and 10^{-2} are very well buffered for P_{O_2}, P_{S_2} and for a_C, no matter what SO_2/Ar ratios are used.

The partial pressure of sulfur is practically insensitive to variations in a gas mixture of $CO/CO_2 = 10^{-1}$ mixed with different SO_2/Ar ratios as seen in Figures 23 to 26. In addition, the partial pressure of oxygen does not vary greatly, but the activity of carbon is much more affected.

TABLE III.1: CHEMICALS REACTION IN "SO-C" SYSTEM

CHEMICALS REACTION	STANDARD FREE ENERGY (Cal)	TEMP RANGE (°C)
$CO \rightleftarrows [C] + \frac{1}{2} O_2$	27340 - 20.50T	500-2000
$CO_2 \rightleftarrows [C] + \frac{1}{2} O_2$	94490 - 0.13T	500-2000
$COS \rightleftarrows [C] + \frac{1}{2} O_2 + \frac{1}{2} S_2$	48470 - 2.38T	500-2000
$CS \rightleftarrows [C] + \frac{1}{2} S_2$	-39000 - 21.0T	25-2000
$CS_2 \rightleftarrows [C] + S_2$	2730 - 1.55T	25-2000
$S_2 \rightleftarrows 2(S)$	112170 + 38.55T	25-1700
$S_4 \rightleftarrows 2S_2$	15000 + 27.6T	25-1700
$S_6 \rightleftarrows 3S_2$	66000 + 72.9T	25-1700
$S_8 \rightleftarrows 4S_2$	95000 +107.1T	25-1700
$SO \rightleftarrows \frac{1}{2} S_2 + \frac{1}{2} O_2$	13810 - 1.19T	445-2000
$SO_2 \rightleftarrows \frac{1}{2} S_2 + O_2$	86440 + 17.37T	445-2000
$SO_3 \rightleftarrows \frac{1}{2} S_2 + 3/2\ O_2$	109440 + 39.04T	445-2000

TABLE III.2: CALCULATED VALUES OF LOG (P_{O_2}, P_{S_2}, P_{SO_2}) in "S-O-C-Ar" GAS MIXTURE

GAS MIXTURES		CALCULATED PARTIAL PRESSURES		
CO/CO_2 + SO_2/Ar		Log P_{O_2}	Log P_{S_2}	Log P_{SO_2}
10^{-4}	pure SO_2	-6.64	-9.43	-0.3
	10^{-1}	-6.36	-11.74	-1.19
	10^{-2}	-6.22	-13.91	-2.13
	10^{-3}	-6.20	-15.94	-3.13
10^{-3}	pure SO_2	-8.12	-6.44	-0.3
	10^{-1}	-8.14	-8.17	-1.18
	10^{-2}	-8.13	-10.05	-2.13
	10^{-3}	-8.15	-12.03	-3.12
10^{-2}	pure SO_2	-9.68	-3.33	-0.3
	10^{-1}	-10.07	-4.32	-1.18
	10^{-2}	-10.15	-6.05	-2.13
	10^{-3}	-10.10	-8.03	-3.13
10^{-1}	pure SO_2	-10.36	-2.01	-0.32
	10^{-1}	-11.11	-2.37	-1.25
	10^{-2}	-11.9	-2.93	-2.33
	10^{-3}	-12.13	-4.31	-3.25

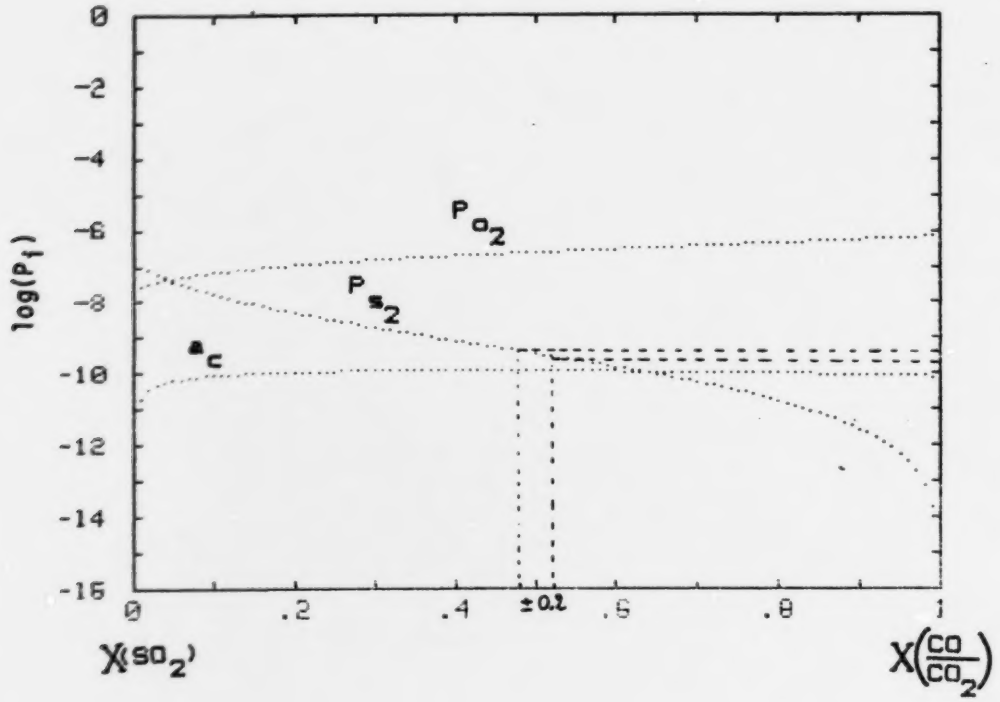

Compose	Press. part. equilibre
S*O2	4.9994788E-001
C*O2	4.9992203E-001
C*O	8.6184959E-005
S*O3	3.9692425E-005
S*O	3.9727482E-006
O2	2.3668153E-007
C*O*S	7.6559727E-010
S2	3.6486775E-010
S	7.3280262E-011
C*S	1.7765596E-017
C*S2	2.7800129E-019
S4	4.6512672E-023
S6	1.2165993E-033
S8	1.4179811E-045

FIGURE 11: Evolution of P_{O_2}, P_{S_2} and a_C with varying volume fraction of CO/CO_2 and SO_2 at 1273K (case of $CO/CO_2 = 10^{-4}$ and pure SO_2).

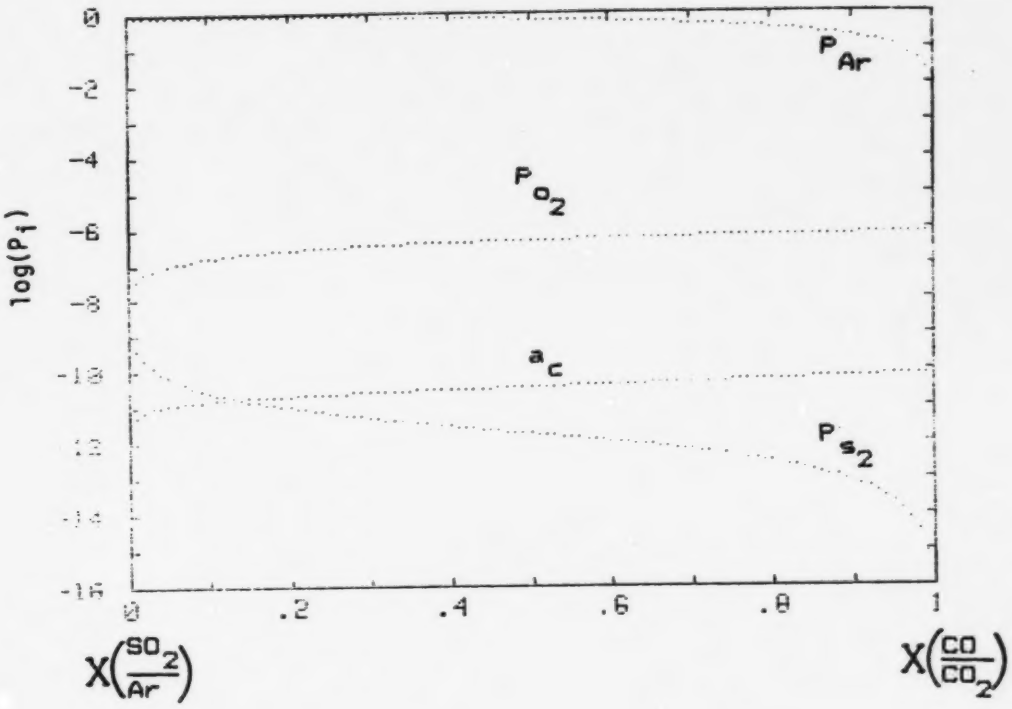

Compose	Press. part. equilibre
AR	6.5216748E-001
C*O2	2.8257953E-001
S*O2	6.5209323E-002
C*O	3.5799472E-005
S*O3	7.0450789E-006
O2	4.3827926E-007
S*O	3.8078753E-007
C*O*S	2.2399789E-011
S	5.1616127E-012
S2	1.8102238E-012
C*S	3.8197069E-019
C*S2	4.2101297E-022
S4	1.1448930E-027
S6	1.4857233E-040
S8	8.5912750E-055

FIGURE 12: Evolution of P_{O_2}, P_{S_2}, P_{Ar} and a_C with varying volume fraction of CO/CO_2 and SO_2/Ar at 1273K (case of $CO/CO_2 = 10^{-4}$ and $SO_2/Ar = 10^{-1}$).

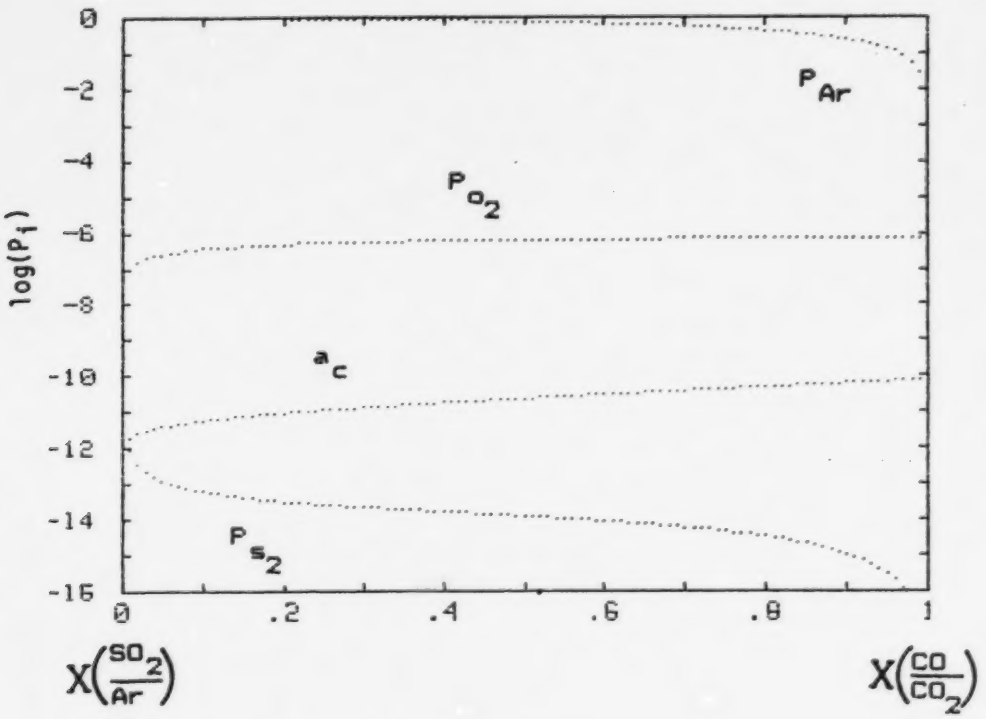

Compose	Press. part. equilibre
AR	7.3890956E-001
C*O2	2.5367327E-001
S*O2	7.3881248E-003
C*O	2.7464840E-005
S*O3	9.3399373E-007
O2	6.0009229E-007
S*O	3.6870047E-008
C*O*S	1.4220072E-012
S	4.2711303E-013
S2	1.2395016E-014
C*S	2.0723082E-020
C*S2	1.8900669E-024
S4	5.3677776E-032
S6	4.7696046E-047
S8	1.8884995E-063

FIGURE 13: Evolution of P_{O_2}, P_{S_2}, P_{Ar} and a_C with varying volume fraction of CO/CO_2 and SO_2/Ar at 1273K (case of $CO/CO_2 = 10^{-4}$ and $SO_2/Ar = 10^{-2}$).

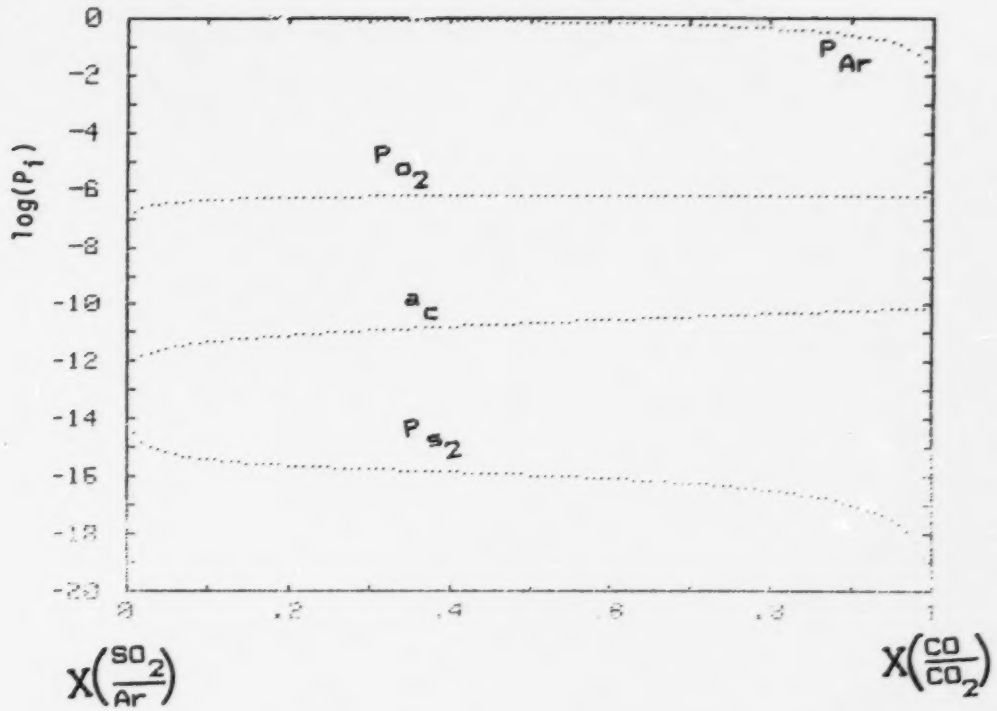

Composé	Press. part. équilibre
AR	7.4866779E-001
C*O2	2.5035414E-001
S*O2	7.4876712E-004
C*O	2.6374802E-005
O2	6.3284231E-007
SAO3	9.7206745E-008
SAO	3.6387202E-009
C*O*S	1.3133466E-013
S	4.1046777E-014
S2	1.1447735E-016
C*S	1.8637737E-021
C*S2	1.6336246E-026
S4	4.5786714E-036
S6	3.7575072E-053
S8	1.3740635E-071

FIGURE 14: Evolution of P_{O_2}, P_{S_2}, P_{Ar} and a_c with varying volume fraction of CO/CO_2 and SO_2/Ar at 1273K (case of $CO/CO_2 = 10^{-4}$ and $SO_2/Ar = 10^{-3}$).

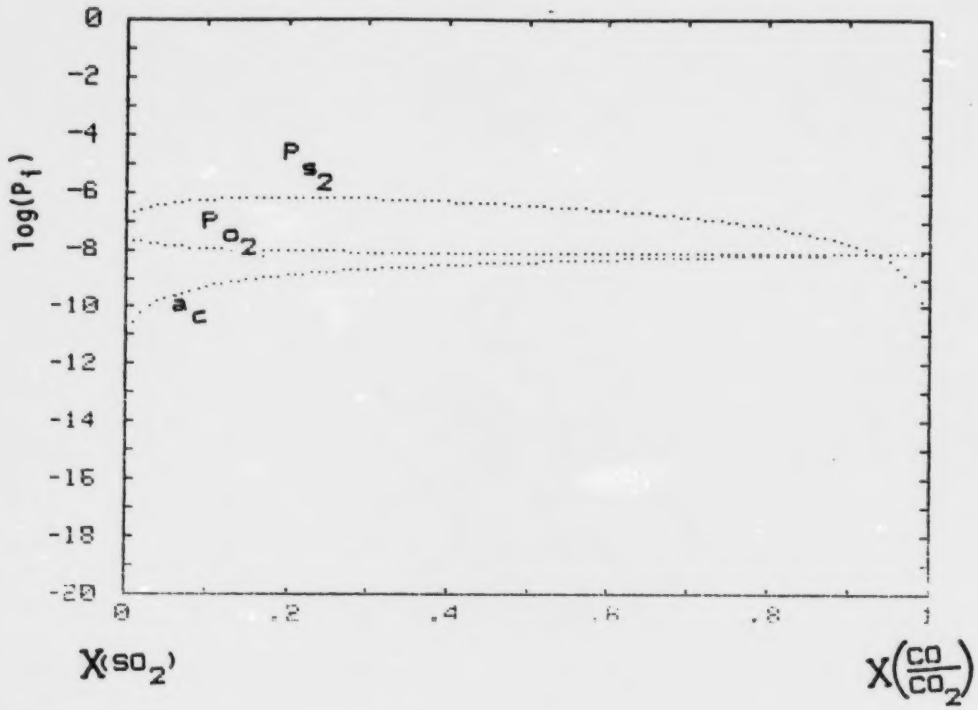

Compose	Press. part. equilibre
S*O2	4.9988678E-001
C*O2	4.9960079E-001
C*O	4.8257968E-004
S*O	2.2256387E-005
S*O3	7.0833361E-006
S2	3.5949773E-007
C*O*S	1.3456071E-007
O2	7.5392987E-009
S	2.3002093E-009
C*S	1.7495017E-014
C*S2	8.5933347E-015
S4	4.5153625E-017
S6	1.1636692E-024
S8	1.3363281E-033

FIGURE 15: Evolution of P_{O_2}, P_{S_2} and a_C with varying volume fraction of CO/CO_2 and SO_2 at 1273K (case of $CO/CO_2 = 10^{-3}$ and pure SO_2).

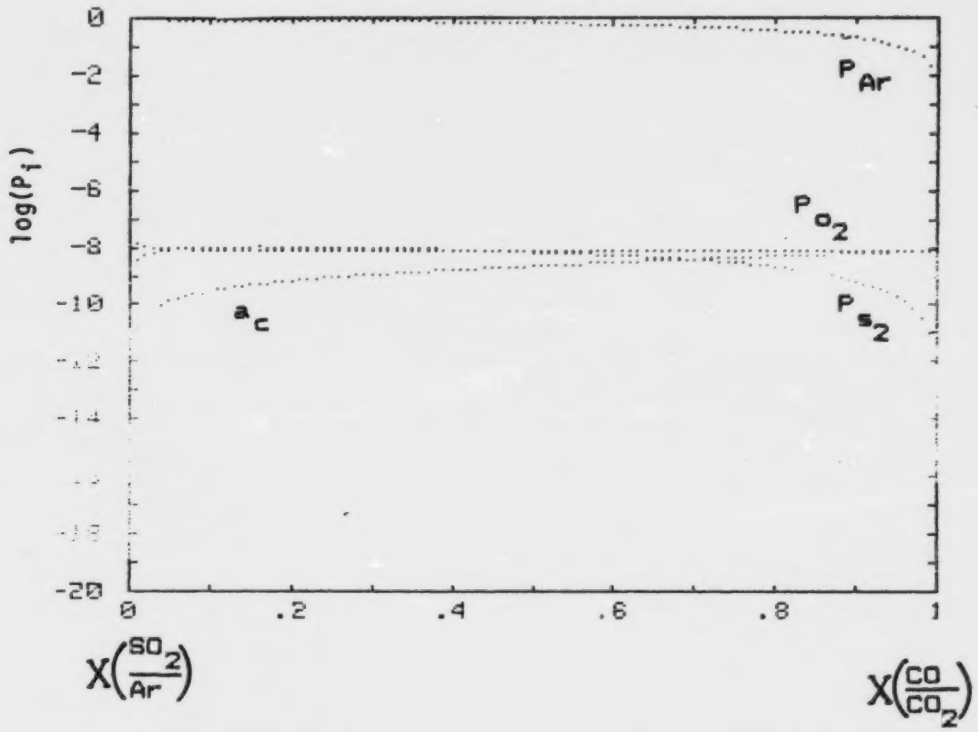

Compose	Press. part. equilibre
AR	6.5211253E-001
C*O2	2.8239595E-001
S*O2	6.5207346E-002
C*O	2.8026429E-004
S*O	2.9829291E-006
S*O3	8.9928909E-007
C*O*S	1.0761397E-008
O2	7.1417422E-009
S2	6.8170966E-009
S	3.1675173E-010
C*S	1.4375672E-015
C*S2	9.7236016E-017
S4	1.6236754E-020
S6	7.9348631E-030
S8	1.7279306E-040

FIGURE 16: Evolution of P_{O_2}, P_{S_2}, P_{Ar} and a_c with varying volume fraction of CO/CO_2 and SO_2/Ar at 1273K (case of $CO/CO_2 = 10^{-3}$ and $SO_2/Ar = 10^{-1}$).

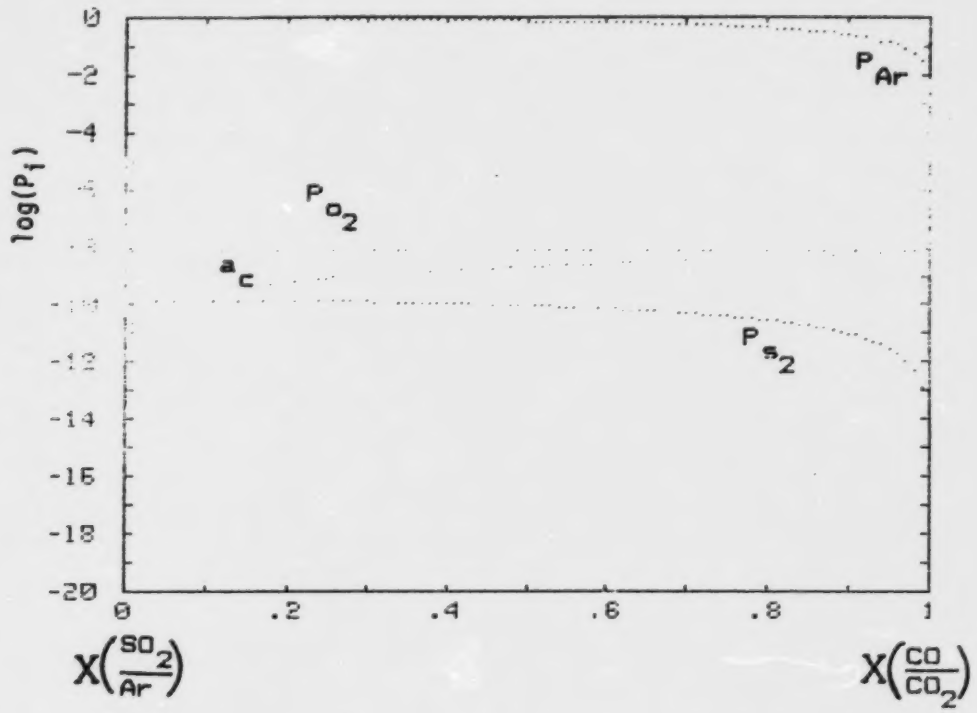

Compose	Press. part. equilibre
AR	7.3885381E-001
C*O2	2.5350437E-001
S*O2	7.3880953E-003
C*O	2.5327543E-004
S*O	3.4023361E-007
S*O3	1.0121316E-007
O2	7.0470530E-009
C*O*S	1.1166744E-009
S2	8.9880329E-011
S	3.6370695E-011
C*S	1.5017041E-016
C*S2	1.1663153E-018
S4	2.8224719E-024
S6	1.8185911E-035
S8	5.2214018E-048

FIGURE 17: Evolution of P_{O_2}, P_{S_2}, P_{Ar} and a_C with varying volume fraction of CO/CO_2 and SO_2/Ar at 1273K (case of $CO/CO_2 = 10^{-3}$ and $SO_2/Ar = 10^{-2}$).

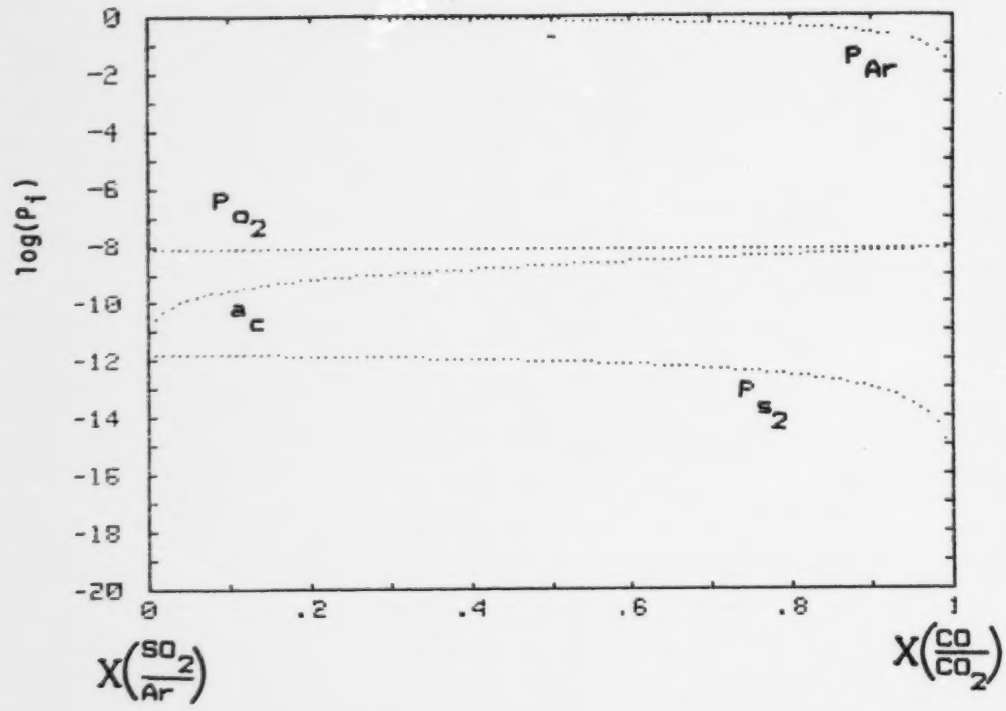

Compose	Press. part. equilibre
AR	7.4881423E-001
C*O2	2.5018678E-001
S*O2	7.4876935E-004
C*O	2.5017623E-004
S*O	3.4511739E-008
S*O3	1.0248929E-008
O2	7.0349238E-009
C*O*S	1.1198071E-010
S	3.6924558E-012
S2	9.2638616E-013
C*S	1.5072146E-017
C*S2	1.1884213E-020
S4	2.9983646E-028
S6	1.9912109E-041
S8	5.8924612E-056

FIGURE 18: Evolution of P_{O_2}, P_{S_2}, P_{Ar} and a_C with varying volume fraction of CO/CO_2 and SO_2/Ar at 1273K (case of $CO/CO_2 = 10^{-3}$ and $SO_2/Ar = 10^{-3}$).

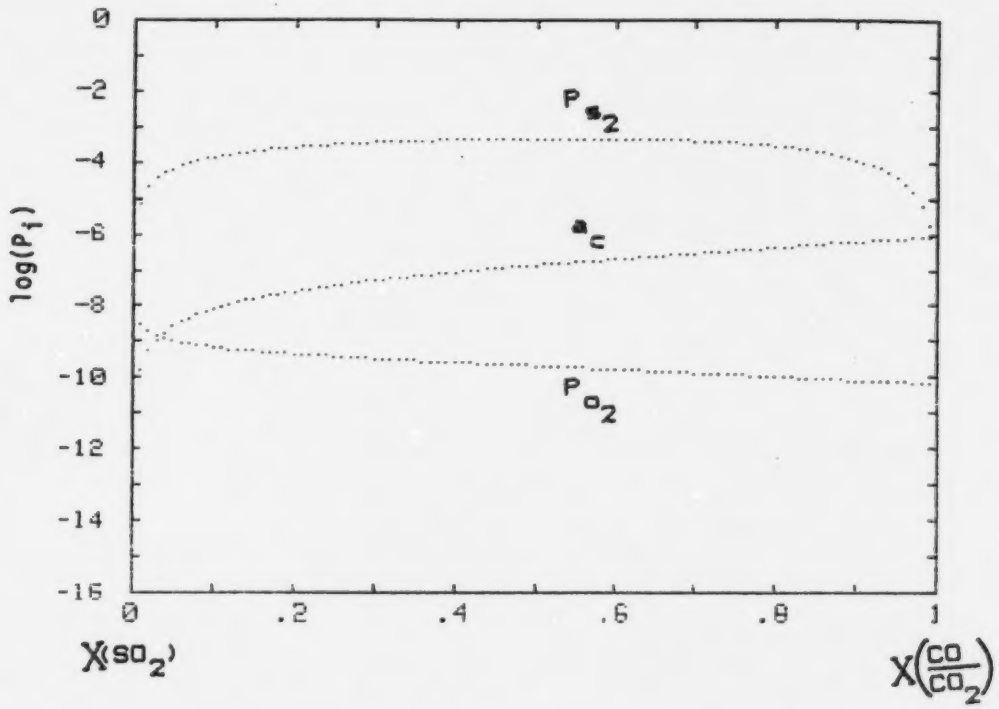

Compose	Press. part. equilibre
S*O2	4.9832892E-001
C*O2	4.9815621E-001
C*O	2.8879671E-003
S2	4.6356238E-004
S*O	1.3316187E-004
C*O*S	2.8916618E-005
S*O3	1.1765259E-006
S	8.2598730E-008
C*S2	3.9799515E-010
O2	2.0930007E-010
S4	7.5078692E-011
C*S	2.2564431E-011
S6	2.4949719E-015
SR	3.6945474E-021

FIGURE 19: Evolution of P_{O_2}, P_{S_2} and a_C with varying volume fraction of CO/CO_2 and SO_2 at 1273K (case of $CO/CO_2 = 10^{-2}$ and pure SO_2).

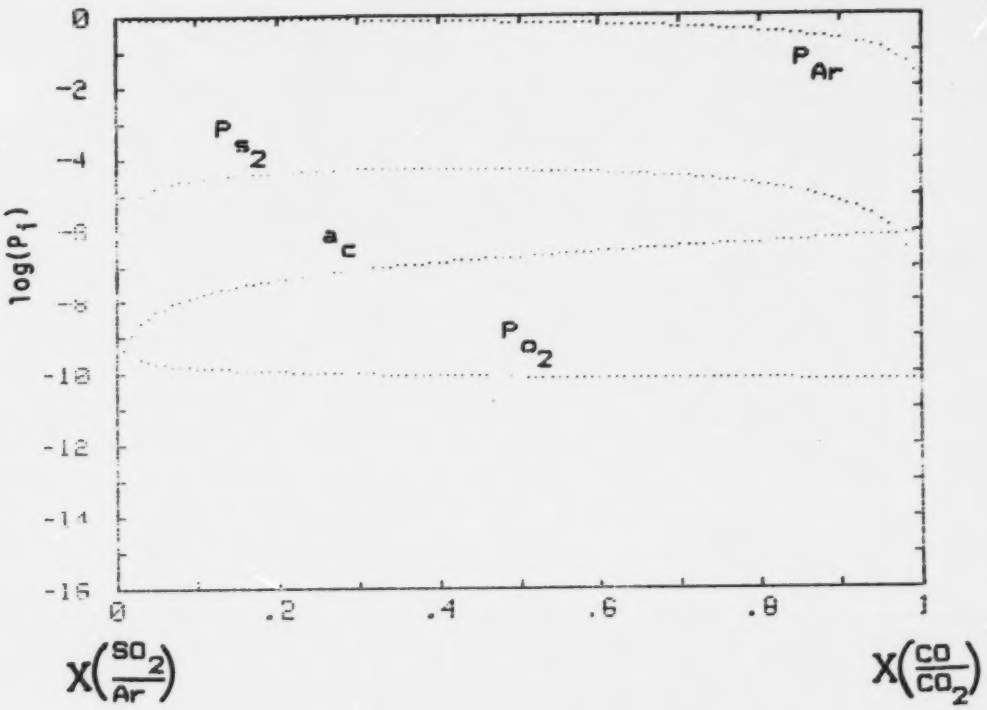

Compose	Press. part. equilibre
AR	6.5160104E-001
C*O2	2.8072754E-001
S*O2	6.5027784E-002
C*O	2.5596128E-003
S2	4.8297444E-005
S*O	2.7329099E-005
C*O*S	8.2725140E-006
S*O3	9.7616176E-008
S	2.6661302E-008
O2	8.4614394E-011
C*S2	5.7801396E-011
C*S	1.0152593E-011
S4	8.1498314E-013
S6	2.8217176E-018
S8	4.3533652E-025

FIGURE 20: Evolution of P_{O_2}, P_{S_2}, P_{Ar} and a_C with varying volume fraction of CO/CO_2 and SO_2/Ar at 1273K (case of $CO/CO_2 = 10^{-2}$ and $SO_2/Ar = 10^{-1}$).

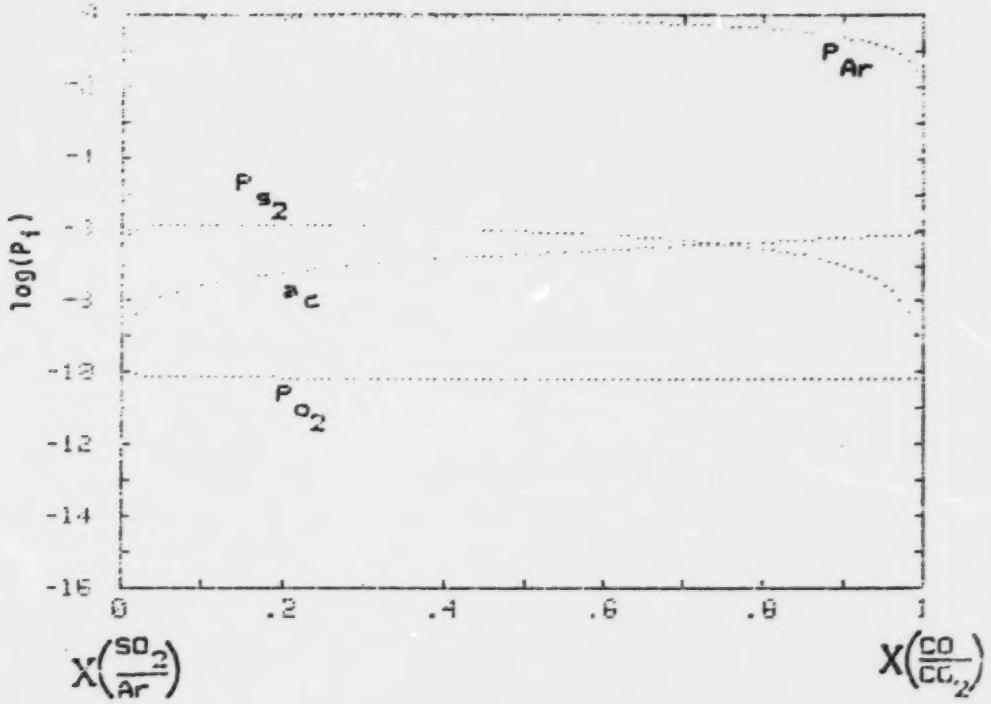

Compose	Press. part. equilibre
AR	7.3829751E-001
C*O2	2.5181237E-001
S*O2	7.3767089E-003
C*O	2.5078219E-003
S*O	3.3862501E-006
C*O*S	1.0967420E-006
S2	6.8465033E-007
S*O3	1.0138074E-008
S	3.6083204E-009
O2	7.0922526E-011
C*S	1.4704598E-012
C*S2	1.1330218E-012
S4	2.7342839E-016
S6	1.7340277E-023
S8	4.9002143E-032

FIGURE 21: Evolution of P_{O_2}, P_{S_2}, P_{Ar} and a_C with varying volume fraction of CO/CO_2 and SO_2/Ar at 1273K (case of $CO/CO_2 = 10^{-2}$ and $SO_2/Ar = 10^{-2}$).

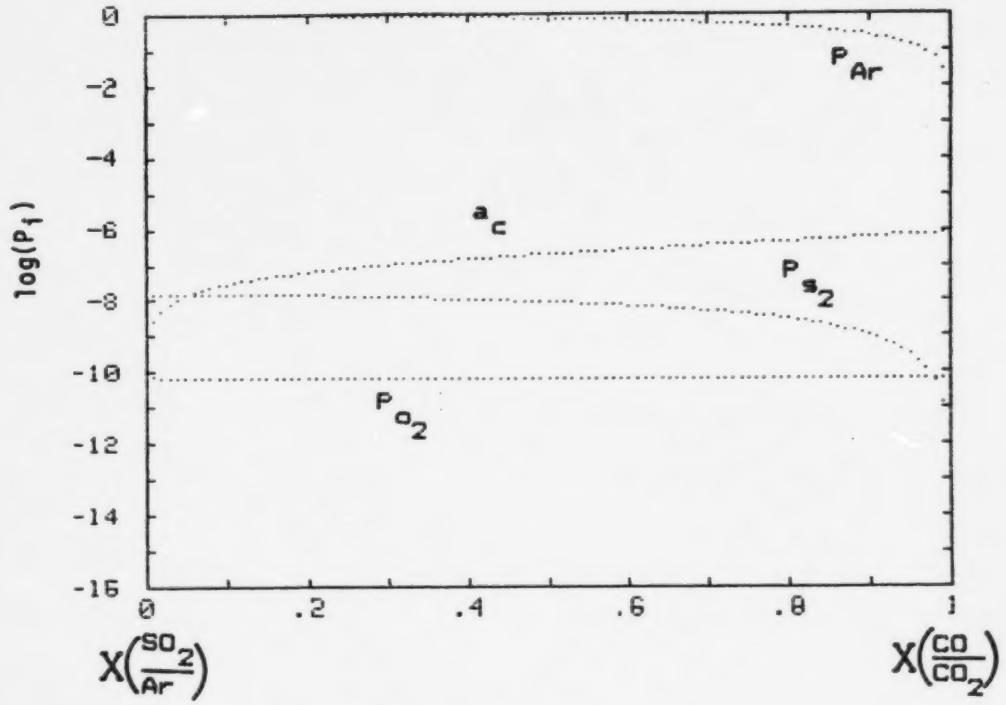

Compose	Press. part. equilibre
AR	7.4825643E-001
C*O2	2.4851093E-001
C*O	2.4843892E-003
S*O2	7.4778100E-004
S*O	3.4457651E-007
C*O*S	1.1100131E-007
S2	9.2302741E-009
S*O3	1.0237936E-009
S	3.6857559E-010
O2	7.0384089E-011
C*S	1.4936623E-013
C*S2	1.1755985E-014
S4	2.9766620E-020
S6	1.9696311E-029
S8	5.8074690E-040

FIGURE 22: Evolution of P_{O_2}, P_{S_2}, P_{Ar} and a_C with varying volume fraction of CO/CO_2 and SO_2/Ar at 1273K (case of $CO/CO_2 = 10^{-2}$ and $SO_2/Ar = 10^{-3}$).

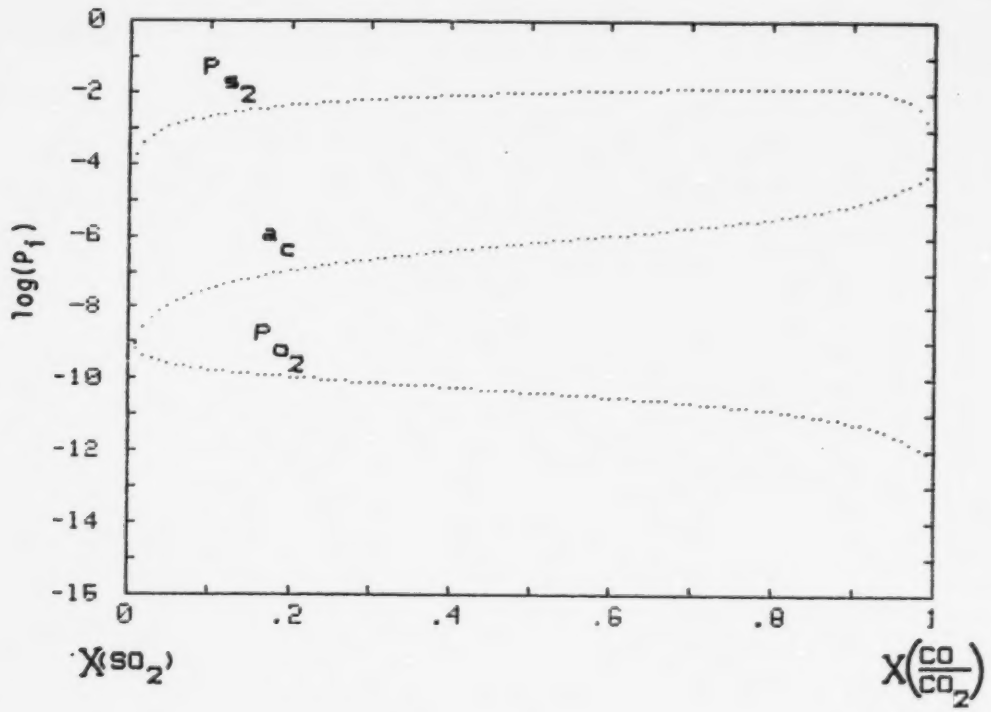

Compose	Press. part. equilibre
C*O2	5.0607891E-001
S*O2	4.7716618E-001
S2	9.7576975E-003
C*O	6.4221131E-003
C*O*S	2.9502090E-004
S*O	2.7910426E-004
S*O3	5.1466194E-007
S	3.7895963E-007
C*S2	4.0778913E-008
S4	3.3265574E-008
C*S	5.0392126E-010
O2	4.3682084E-011
S6	2.3269291E-011
S8	7.2530036E-016

FIGURE 23: Evolution of P_{O_2}, P_{S_2} and a_C with varying volume fraction of CO/CO_2 and SO_2 at 1273K (case of $CO/CO_2 = 10^{-1}$ and pure SO_2).

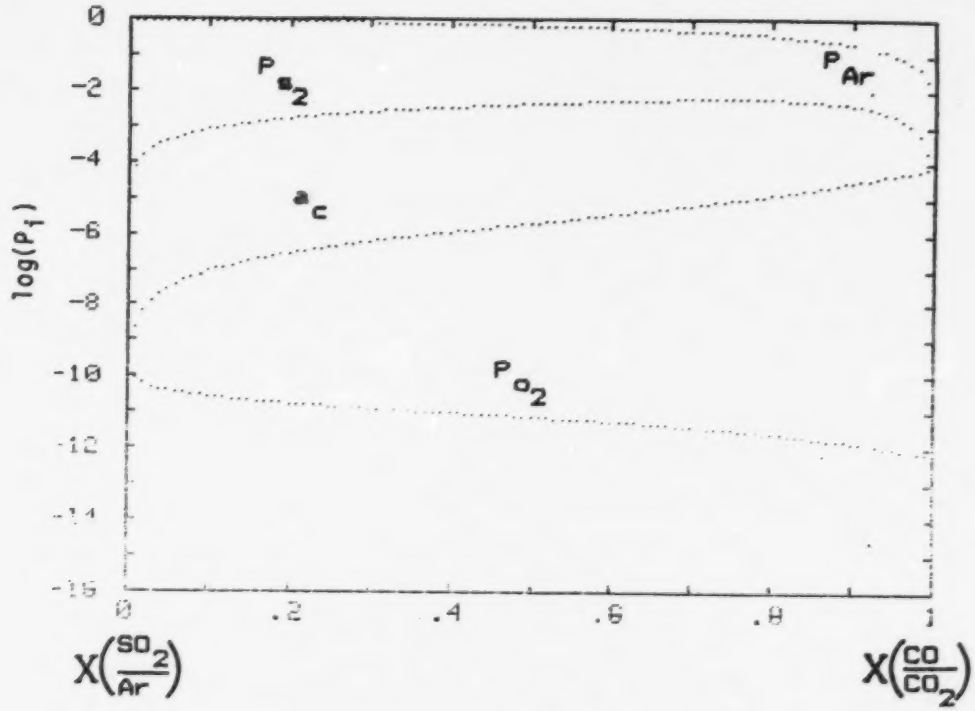

Compose	Press. part. equilibre
AR	6.4938808E-001
C*02	2.8146611E-001
S*02	5.6073796E-002
C*0	8.4718329E-003
S2	4.2647558E-003
C*0*S	2.5729161E-004
S*0	7.7794398E-005
S	2.5053382E-007
C*S2	5.5766209E-008
S*03	2.5498862E-008
S4	6.3546065E-009
C*S	1.0423824E-009
02	7.7646206E-012
S5	1.9427799E-012
S6	2.6467028E-017

FIGURE 24: Evolution of P_{O_2}, P_{S_2}, P_{Ar} and a_C with varying volume fraction of CO/CO_2 and SO_2/Ar at 1273K (case of $CO/CO_2 = 10^{-1}$ and $SO_2/Ar = 10^{-1}$).

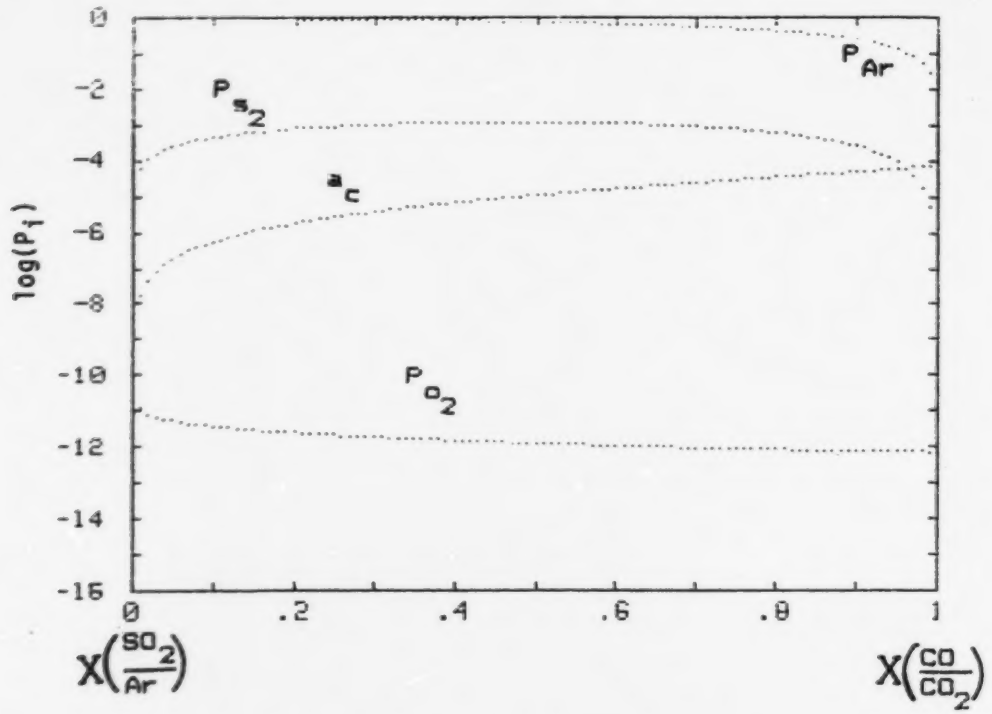

Compose	Press. part. equilibre
AR	7.3416593E-001
C*O2	2.4154488E-001
C*O	1.8108699E-002
S*O2	4.7159395E-003
S2	1.1610830E-003
C*O*S	2.8695913E-004
S*O	1.6296515E-005
S	1.3072267E-007
C*S2	8.0833349E-008
C*S	2.8957405E-009
S*O3	8.6097576E-010
S4	4.7100648E-010
O2	1.2515378E-012
S6	3.9204050E-014
S8	1.4540576E-019

FIGURE 25: Evolution of P_{O_2}, P_{S_2}, P_{Ar} and a_C with varying volume fraction of CO/CO_2 and SO_2/Ar at 1273K (case of $CO/CO_2 = 10^{-1}$ and $SO_2/Ar = 10^{-2}$).

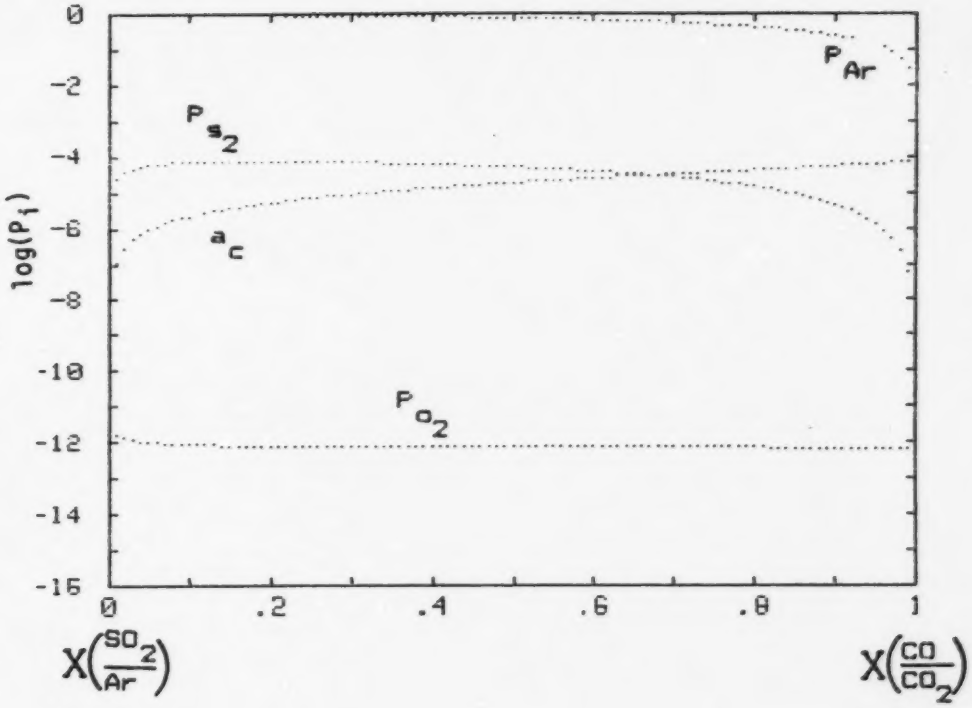

Compose	Press. part. equilibre
AR	7.4315479E-001
C*O2	2.3328113E-001
C*O	2.2870108E-002
S*O2	5.6759821E-004
C*O*S	7.4588554E-005
S2	4.9181936E-005
S*O	2.5648780E-006
S	2.6904324E-008
C*S2	5.6547457E-009
C*S	9.8426259E-010
S*O3	7.9243658E-011
S4	8.4510674E-013
O2	7.3188960E-013
S6	2.9796000E-018
S8	4.6811331E-025

FIGURE 26: Evolution of P_{O_2}, P_{S_2}, P_{Ar} and a_C with varying volume fraction of CO/CO_2 and SO_2/Ar at 1273K (case of $CO/CO_2 = 10^{-1}$ and $SO_2/Ar = 10^{-3}$).

In all cases, since the gases used are ultra pure and the rate of dissolution of sulfur in Cr_2O_3 is very small compared to the gas throughput of the system, the only error that can arise is due to the error of the volumetric flow rate of each gas admitted to the reaction clamber. This was determined to be only about 2% with the type of flowmeter used. Thus for the worse possible conditions when CO/CO_2 = 10^{-4} with pure SO_2, the value of P_{S_2} changes only by about 20%. We did not use any gas composition ratios that would find us in the non-buffered zone shown in Figure 9.

III.2 Determination of Sulfur Solubility in Cr_2O_3

III.2.1 Solubility of sulfur using LECO infrared analysis

Calibration of the apparatus was carried out in order to determine the standard error and the limit of detection. Ten samples of pure Cr_2O_3 with the accelerator (tungsten or tungsten-tin) were analysed successively and the results are shown in Table III.3.

TABLE III.3: CALIBRATION OF THE LECO-IR ANALYSER

N°	1	2	3	4	5	6	7	8	9	10
ppm detected	5.1	6.7	6.7	6.9	5.5	3.3	0.2	1.8	2.8	8.2

The arithmetic mean of these results is 4.72 with a variance σ of 2.6 ppm. The detection limit can therefore be said to be around 5 ppm ($\simeq 2\sigma$). Even though this seems quite acceptable, the results of the reaction product analyses proved to be unsatisfactory.

Table III.4 presents the oxygen and sulfur partial pressures of a series of equilibration experiments and the sulfur analysis using the LECO-IR analyser. Results were repeated and averages are indicated in the table III.4.

The results in the table show the poor reproducibility even for identical samples which can vary up to 100% as is the case of $CO/CO_2 = 10^{-2}$ with 48 h reaction time. The inhomogeneity of the samples cannot be the source of these differences since neutron activation results of the same samples proved to be much more consistent.

TABLE III.4: SULFUR ANALYSIS BY LECO-IR

CO/CO_2	SO_2/Ar	log P_{O_2}	log P_{S_2}	Reaction time (h)	Sulfur Content		Average (ppm)
					Test 1 (ppm)	Test 2 (ppm)	
10^{-4}	pure SO_2	-6.62	-9.43	24	7	12	9.5 ± 3.5
10^{-4}	pure SO_2	-6.62	-9.43	48	7	15	11 ± 5.6
10^{-4}	pure SO_2	-6.62	-9.43	72	7	9	8 ± 1.4
10^{-3}	pure SO_2	-8.12	-6.44	24	28	43	33.5 ± 10.6
10^{-3}	pure SO_2	-8.12	-6.44	48	33	26	29.5 ± 4.9
10^{-3}	pure SO_2	-8.12	-6.44	72	7	8	7.5 ± 0.7
10^{-2}	pure SO_2	-9.68	-3.33	24	39	35	37 ± 2.8
10^{-2}	pure SO_2	-9.68	-3.33	48	36	13	24.5 ± 16.3
10^{-2}	pure SO_2	-9.68	-3.33	72	15	18	16.5 ± 2.1
10^{-2}	10^{-1}	-10.10	-4.40	2 weeks	40	31	35.5 ± 6.3

Normally the solubility of sulfur in the samples increases with increasing reaction time, as would be expected in a saturation process. The results of the LECO-IR analysis show the opposite phenomena, which is highly unlikely.

Various alternative procedures were attempted in order to obtain reproducible results (Appendix A) but no improvement was observed. In discussions of this problem with LECO personnel, the only possible improvement would be to design a more sensitive spectrometer for the detection of sulfur levels below 100 ppm. At present this type of detector is not available on the market.

Ravaine (61) has shown that the use of IR spectrometry is not reliable for values below 0.005% (50 ppm). This was particularly true for "insulating" type materials such as refractories and ceramics where considerable errors were reported for sulfur contents even up to 0.1%.

III.2.2 Sulfur analysis using the PIXÉ method

Figure 27 shows the X ray spectrum of the samples containing pure Cr_2O_3. It can be seen that the predominant peaks are the K_α and K_β of chromium. Other peaks identified as those pertaining to Si, P, Ca, and Cl are attributed to the mylar film sample target.

After exposure to different sulfur and oxygen atmospheres, the samples indicated that a certain amount of sulfur had been dissolved in the Cr_2O_3, as shown in the X ray spectra of figures 28 to 31. The sulfur peaks are small and are difficult to differentiate from the background energy distribution function. This problem was complicated by the fact that the results on the blank tests using only

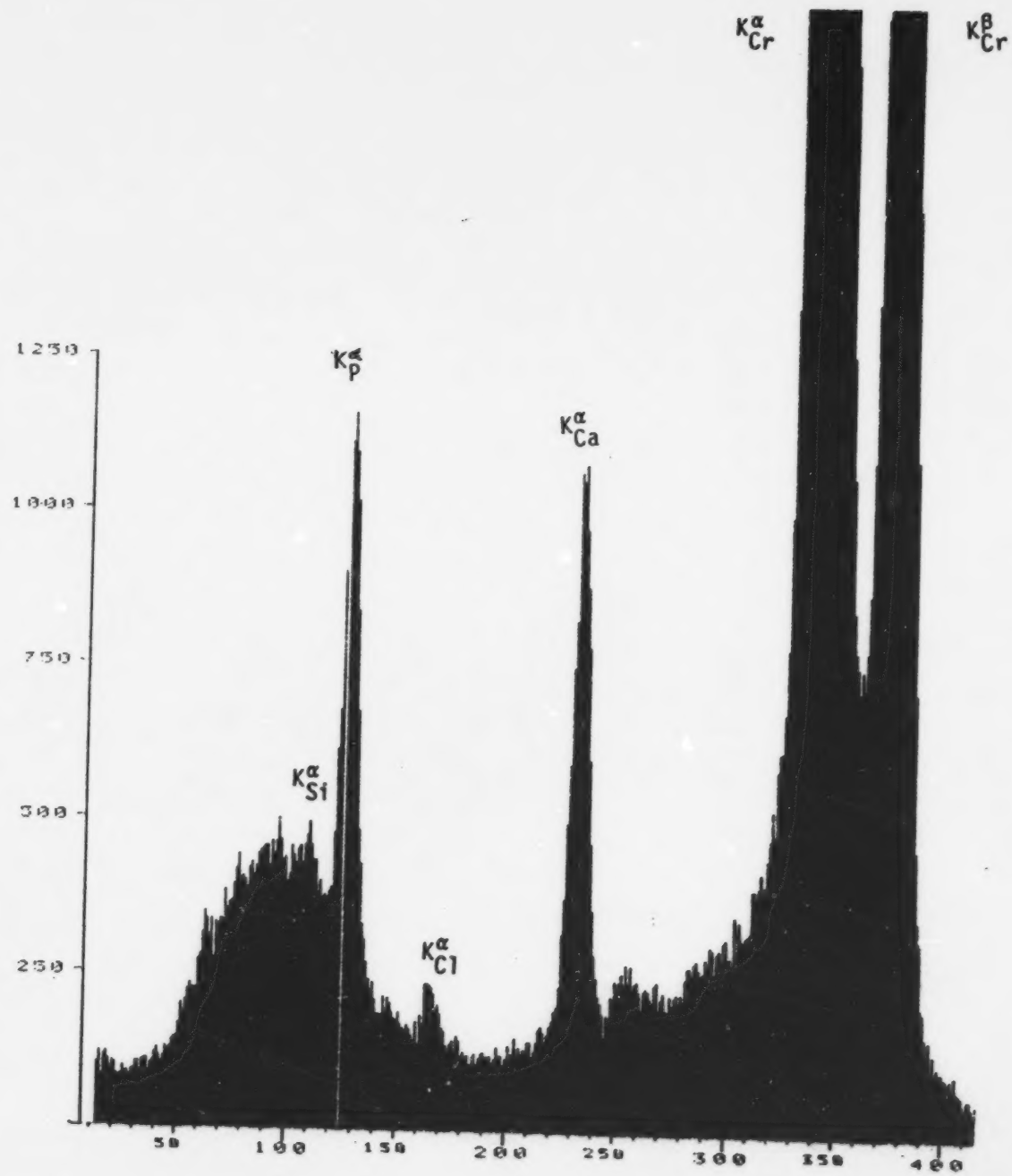

FIGURE 27: X-Ray spectrum of pure Cr_2O_3.

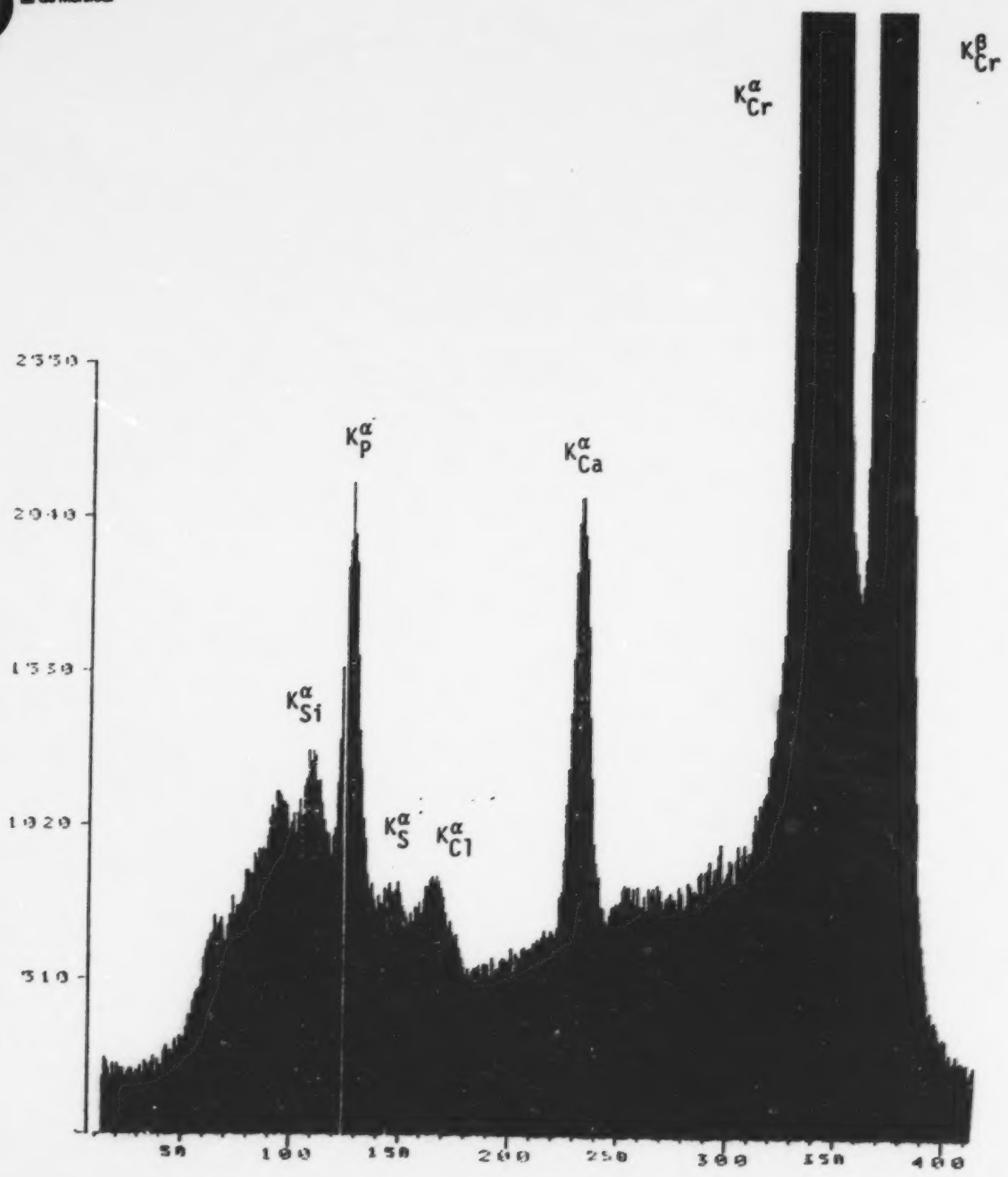

FIGURE 28: X-Ray spectrum of reaction product in $CO/CO_2 = 10^{-4}$ and pure SO_2 mixture for a reaction time of 72 h.

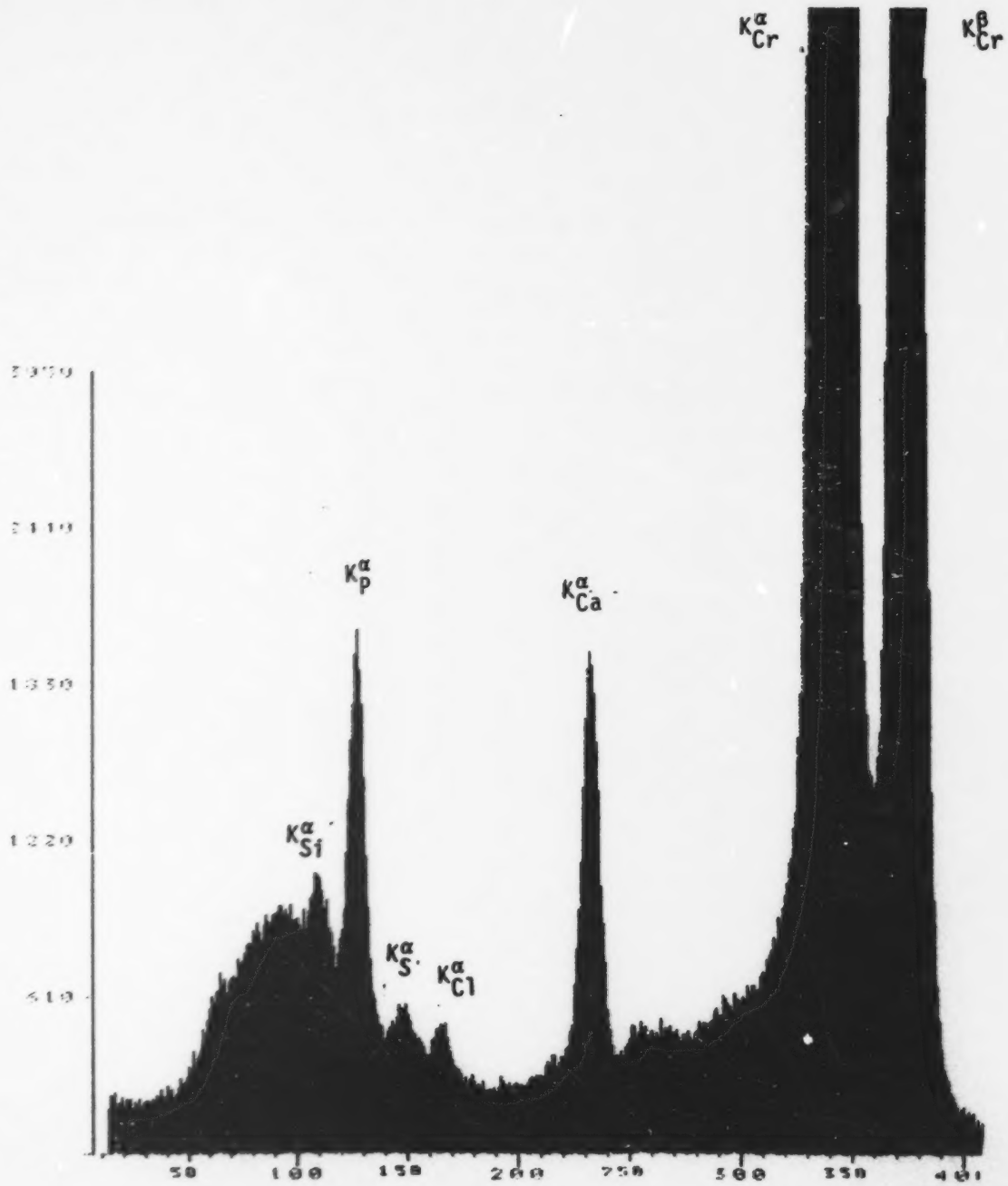

FIGURE 29: X-Ray spectrum of reaction product in CO/CO_2 = 10^{-3} and pure SO_2 mixture for a reaction time of 48 h.

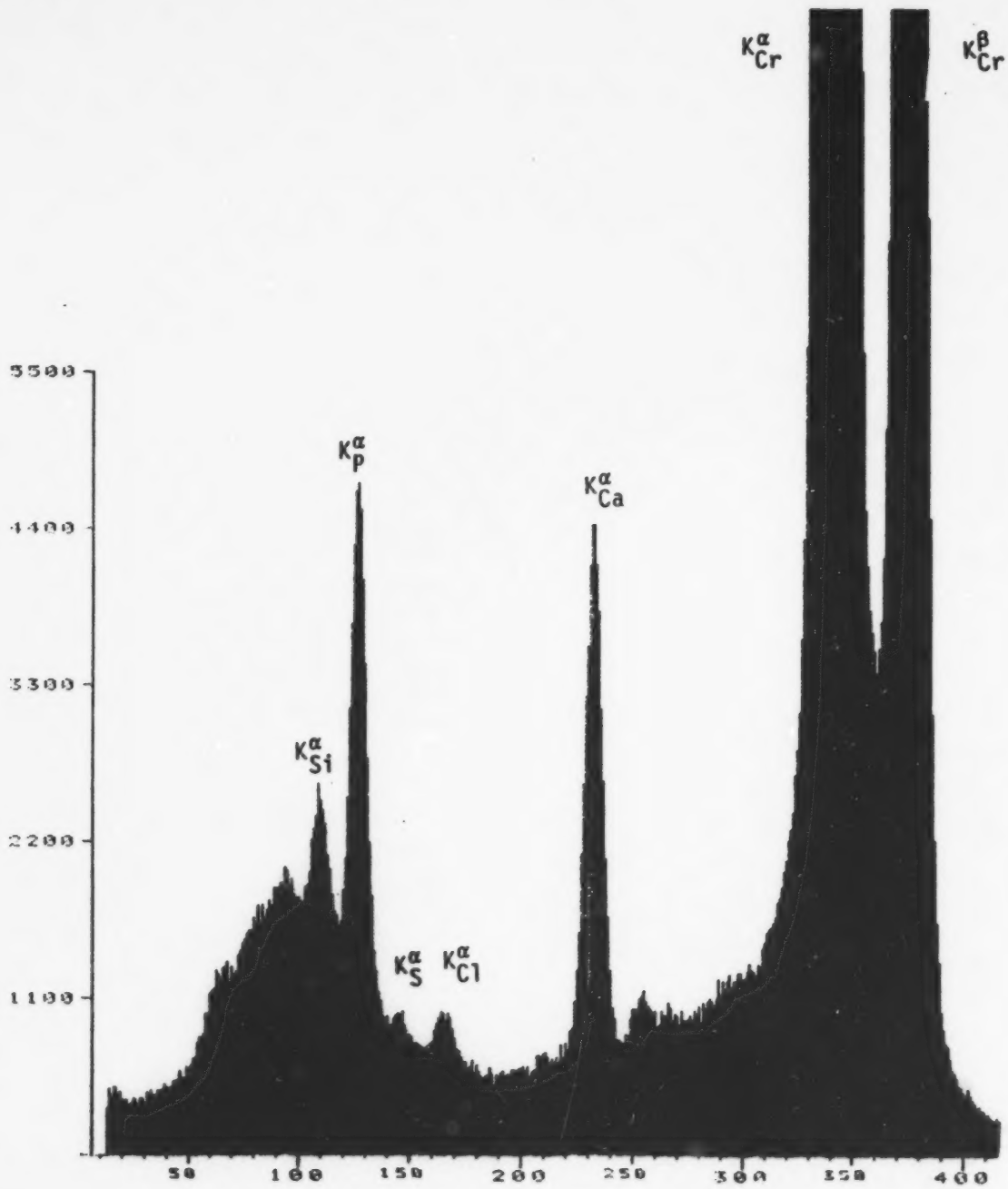

FIGURE 30: X-Ray spectrum of reaction product in CO/CO_2 = 10^{-2} and pure SO_2 mixture for a reaction time of 72 h.

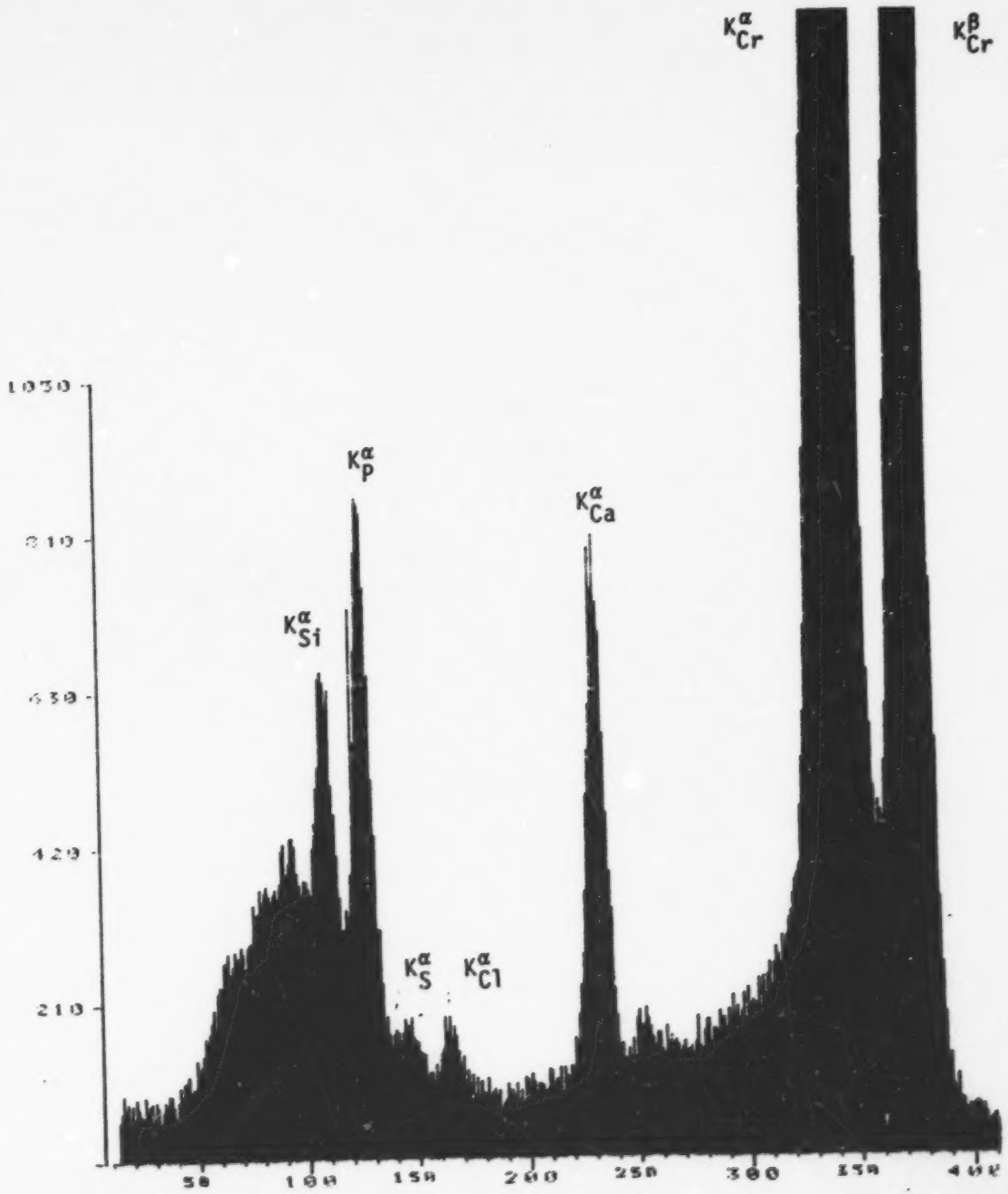

FIGURE 31: X-Ray spectrum of reaction product in CO/CO_2 = 10^{-2} and SO_2/Ar = 10^{-1} mixture for a reaction time of two weeks.

the mylar film, and also for mylar with the collodion solution, also showed small amounts of sulfur in the collodion solution. The sample deposition technique of centrifuging leaves an indeterminable amount of collodion on the mylar film which can vary from sample to sample. Since these intensities are so small with respect to the other peaks, a statistical analysis is also prone to considerable error.

In conclusion, it was shown taht the PIXE method with the present sample preparation technique could not be used successfully, even though it has proven to be a reliable method for tracer levels of elements of large atomic number. It has severe limitations for cases of $Z < 20$.

III.2.3 Results of sulfur analysis by neutron activation

This method has proved to be successful in terms of the determination of the solubility of sulfur in Cr_2O_3 for the entire range of oxygen and sulfur pressures required for this study, and in the reproducibility of results.

Table III.5 shows the values of the solubilities obtained for different reaction times and for different ratios of CO/CO_2 and SO_2/Ar at 1273K. Repeat measurements show good reproducibility. In comparing these results with those of the LECO-IR method, it can be seen that the largest difference between a pair of samples is about 23% for the case of $CO/CO_2 = 10^{-3}$, pure SO_2 reaction atmosphere and reaction time of 48 h, whereas a relative difference of about 100% was obtained using the LECO-IR analyser.

TABLE III.5: SULFUR ANALYSIS BY NEUTRAL ACTIVATION

CO/CO_2	SO_2/Ar	log P_{O_2}	log P_{S_2}	Reaction time (h)	Sulfur Content		Average (ppm)	Repeated Analysis
					Test 1 (ppm)	Test 2 (ppm)		
10^{-4}	SO_2 pur	-6.62	-9.43	24	36	40	38 ± 2.8	
	SO_2 pur	-6.62	-9.43	48	46	40	43 ± 2.2	
	SO_2 pur	-6.62	-9.43	72	43	44	43.5 ± 0.7	
	10^{-1}	-6.36	-11.74	24	11	13	12 ± 1.4	
	10^{-1}	-6.36	-11.74	48	21	23	22 ± 1.4	
	10^{-1}	-6.36	-11.74	72	27	23	25 ± 2.8	
	10^{-2}	-6.22	-13.91	24	22	20	21 ± 1.4	
	10^{-2}	-6.22	-13.91	48	35	28	31.5 ± 4.9	
	10^{-2}	-6.22	-13.91	72	21	22	20.5 ± 0.7	
	10^{-3}	-6.20	-15.94	24	16	19	17.5 ± 2.1	
	10^{-3}	-6.20	-15.94	48	12	17	14.5 ± 3.5	19 ± 2.8
	10^{-3}	-6.20	-15.94	72	14	18	16 ± 2.8	
10^{-3}	SO_2 pur	-8.12	-6.44	24	12	16	14 ± 2.8	22 ± 3.5
	SO_2 pur	-8.12	-6.44	48	49	64	56.5 ± 10.6	
	SO_2 pur	-8.12	-6.44	72	52	58	55 ± 4.2	
	10^{-1}	-8.14	-8.17	24	28	26	27 ± 0.7	
	10^{-1}	-8.14	-8.17	48	26	30	28 ± 2.8	
	10^{-1}	-8.14	-8.17	72	32	33	32.5 ± 0.7	
	10^{-2}	-8.13	-10.05	24	18	19	18.5 ± 0.7	
	10^{-2}	-8.13	-10.05	48	20	24	22 ± 1.4	
	10^{-2}	-8.13	-10.05	72	28	32	30 ± 2.2	32 ± 1.4
	10^{-3}	-8.15	-12.03	24	26	27	26.5 ± 0.7	
	10^{-3}	-8.15	-12.03	48	29	31	30 ± 1.4	
	10^{-3}	-8.15	-12.03	72	27	29	28 ± 1.4	

(Cont'd) -

TABLE III.5

CO/CO_2	SO_2/Ar	log P_{O_2}	log P_{S_2}	Reaction time (h)	Sulfur Content Test 1 (ppm)	Sulfur Content Test 2 (ppm)	Average (ppm)	Repeated Analysis
10^{-2}	SO_2 pur	-9.68	-3.33	24	78	75	76.5 ± 2.1	
	SO_2 pur	-9.68	-3.33	48	75	65	70 ± 7.1	
	SO_2 pur	-9.68	-3.33	72	68	66	67 ± 1.4	
	10^{-1}	-10.07	-4.32	24	64	66	65 ± 1.4	
	10^{-1}	-10.07	-4.32	48	58	62	60 ± 2.8	
	10^{-1}	-10.07	-4.32	72	57	59	58 ± 1.4	
	10^{-2}	-10.15	-6.05	24	33	30	31.5 ± 2.1	
	10^{-2}	-10.15	-6.05	48	29	27	28 ± 1.4	
	10^{-2}	-10.15	-6.05	72	33	31	32 ± 1.4	
	10^{-3}	-10.10	-8.03	24	18	14	16 ± 2.8	
	10^{-3}	-10.10	-8.03	48	31	30	30.5 ± 0.7	
	10^{-3}	-10.10	-8.03	72	30	24	27 ± 2.2	
10^{-1}	SO_2 pur	-10.36	-2.01	24	137	153	145 ± 11.3	
	SO_2 pur	-10.36	-2.01	48	82	86	84 ± 1.4	
	SO_2 pur	-10.36	-2.01	72	96	90	93 ± 2.2	
	10^{-1}	-11.11	-2.37	24	58	59	58.5 ± 0.7	
	10^{-1}	-11.11	-2.73	48	69	70	69.5 ± 0.7	
	10^{-1}	-11.11	-2.37	72	75	84	79.5 ± 6.4	
	10^{-2}	-11.90	-2.93	24	101	102	101.5 ± 0.7	
	10^{-2}	-11.90	-2.93	48	68	67	67.5 ± 0.7	
	10^{-2}	-11.90	-2.93	72	70	71	70.5 ± 0.7	
	10^{-3}	-12.13	-4.31	24	67	64	65.5 ± 2.1	
	10^{-3}	-12.13	-4.31	48	75	85	80 ± 7.1	
	10^{-3}	-12.13	-4.31	72	58	62	60 ± 2.8	68.5 ± 2.1

The homogeneity of the reaction product and the reproducibility of the method was checked by repeating a series of selected samples of highest and lowest sulfur contents. The irradiation and counting was repeated about one month after the original series of analyses. These results are shown in column 8 of Table III.5 and compare very well with the first series of results.

IV. DISCUSSION

IV.1 INTRODUCTION

It was shown that the solubility limit of sulfur varies according to the combined effect of the sulfur and oxygen pressure from the lowest determined value of 16 ppm for $CO/CO_2 = 10^{-4}$ ($P_{O_2} = 10^{-6.36}$) and $SO_2/Ar = 10^{-1}$ ($P_{S_2} = 10^{-11.24}$) to 93 ppm for $CO/CO_2 = 10^{-2}$ ($P_{O_2} = 10^{-10.36}$) and pure SO_2 ($P_{S_2} = 10^{-2.01}$). Also, for a given constant oxygen pressure, the solubility of sulfur in Cr_2O_3 increases as the sulfur pressure increases. When the oxygen pressure decreases, the sulfur content seems to increase. However, it is very difficult to separate the effects of simultaneous changes in oxygen and sulfur pressure, which can only be quantified by a methematical analysis of the different possible methods of incorporating sulfur in the oxide matrix.

The mobility of sulfur in Cr_2O_3 strongly depends on its ionic radius. Sulfur can have several ionic states, each with different ionic radii and can thus migrate through an oxide structure with varying degrees of difficulty in order to reach various levels of saturation. The ionic radius of sulfur in an oxide structure is not well known. It depends on the coordination sphere of sulfur in the lattice and changes with the valence state of the sulfur ion. The different ionic forms of sulfur and the most commonly accepted (56) ionic radii are indicated in Table IV.1.

TABLE IV.1: IONIC RADII OF SULFUR

Valence state	S^{-2}	S^{-}	S°	S^{+}	S^{+2}
Ionic radius Å	1.84	1.19	1.04	0.64	0.50

CDT
Centre de Développement Technologique
École Polytechnique de Montréal

From size consideration only, the incorporation of sulfur in the Cr_2O_3 lattice can take place according to three different structural positions.

(1) Cationic site, in the form of S^{+} or S^{+2}
(2) Anionic site, in the form of S°, S^{-} or S^{-2}
(3) Interstitial site, in the form of S_i^{-}, S_i°, S_i^{+}.

For relatively low oxygen pressures and for temperatures below 1473K, Crawford and Vest (16) have proposed a defect equation for Cr_2O_3 in terms of chromium vacancies V_{cr}''' and election holes, $h^{\cdot}$

$$3/2\ O_2 \overset{K_1}{\ddagger} 3O_o + 2V_{cr}''' + 6h^{\cdot} \qquad \text{(IV.1)}$$

where O_o represents the oxygen anion or its anionic site.

The following development of different reaction and substitution mechanisms are based on the above equation considering that Cr_2O_3 is a "p-type" semi-conductor. It is assumed that this property is not greatly affected by the small amounts of dissolved sulfur that were experimentally determined in this study.

If the equilibrium constant for equation (IV.1) is given as K_1, a mass balance results in

$$[V_{cr}''']^2 = P_{O_2}^{3/2} \cdot [h^{\cdot}]^{-6} \cdot K_1 \qquad \text{(IV.2)}$$

and a charge balance relates the concentration of the chromium vacancies and the electron holes by:

$$3[V_{cr}'''] = [h^{\cdot}] \qquad \text{(IV.3)}$$

also, $e^{-} + h^{\cdot} \ddagger 0$

where $K_e = [e^{-}]\,[h^{\cdot}]$
$= n.p$

CDT
Centre de
Développement
Technologique
École Polytechnique
de Montréal

IV.2 SUBSTITUTION ON AN ANIONIC SITE

IV.2.1 Sulfur in the form of S^{-2}

When S^{-2} is substituted on the oxygen anionic site the equation can be written as

$$\tfrac{1}{2} S_2 + O_2 \overset{K_4}{\rightleftharpoons} S_O + \tfrac{1}{2} O_2 \qquad (IV.4)$$

The sulfur concentration is then related to the oxygen and sulfur pressure by the equilibrium constant K_4 so that:

$$[S_O] = P_{S_2}^{\frac{1}{2}} P_{O_2}^{-\frac{1}{2}} K_4 \qquad (IV.5)$$

IV.2.2 Sulfur in the form of S^-

When sulfur in the form of S^- substitutes on the oxygen anionic site, however, the equation is written as

$$\tfrac{1}{2} S_2 + O_O \overset{K_6}{\rightleftharpoons} S_O^{\bullet} + \tfrac{1}{2} O_2 + e^- \qquad (IV.6)$$

and, from the mass balance

$$[S_O^{\bullet}] = P_{S_2}^{\frac{1}{2}} P_{O_2}^{-\frac{1}{2}} K_6' [e^-]^{-1} \qquad (IV.7)$$

In considering that $[h^{\bullet}] [e^-] = K_e$, equation IV.7 becomes

$$[S_O^{\bullet}] = P_{S_2}^{\frac{1}{2}} P_{O_2}^{-\frac{1}{2}} [h^{\bullet}] K_6' \qquad (IV.8)$$

where $K_6' = K_6 \cdot K_e$

and $\quad 3[V'''_{Cr}] + [e^-] = [S^{\cdot}_0] + [h^{\cdot}]$

for a p-type semi conductor $[h] >> [e^-]$.

Therefore $3[V'''_{Cr}] - [S^{\cdot}_0] = [h^{\cdot}]$ (IV.9)

Combining equations (IV.9), (IV.8) and (IV.2) we obtain

$$[h^{\cdot}] = [3\, K_1^{\frac{1}{2}}\, P_{O_2}^{3/4}\, [h^{\cdot}]^{-3}] - [P_{S_2}^{\frac{1}{2}}\, P_{O_2}^{-\frac{1}{2}}\, [h^{\cdot}]\, K_6'] \qquad \text{(IV.10)}$$

or $$[h^{\cdot}] = \left[\frac{3\, K_1^{\frac{1}{2}}\, P_{O_2}^{3/4}}{1 + K_6'(P_{S_2}/P_{O_2})^{\frac{1}{2}}}\right] \qquad \text{(IV.11)}$$

In a similar fashion, from equations (IV.11) and (IV.8) we obtain

$$[S^{\cdot}_0] = K_6'(P_{S_2}/P_{O_2})^{\frac{1}{2}} \left[\frac{3\, K_1^{\frac{1}{2}}\, P_{O_2}^{3/4}}{1 + K_6'(P_{S_2}/P_{O_2})^{\frac{1}{2}}}\right] \qquad \text{(IV.12)}$$

The interpretation of equations (IV.11) and (IV.12) are not simple. To estimate the evolution of the concentration of $[S^{\cdot}_0]$ as a function of P_{S_2} and P_{O_2}, two limiting cases can be considered.

When the solubility is small, such that $[S^{\cdot}_0] << [h^{\cdot}]$, we obtain from equation (IV.8)

$$K_6'(P_{S_2}/P_{O_2}) << 1 \qquad \text{(IV.13)}$$

Combining this result with equations (IV.11) and (IV.12)

$$[h^{\cdot}] \simeq (3\,K_1^{\frac{1}{2}})^{\frac{1}{4}}\,(P_{O_2})^{3/16} \qquad \text{(IV.14)}$$

and

$$[S_O^{\cdot}] \simeq K_6' \cdot (3K_1)^{1/8}\,P_{S_2}^{\frac{1}{2}}\,P_{O_2}^{-5/16} \qquad \text{(IV.15)}$$

If the solubility is very large, such that

$[S_O^{\cdot}] \gg [h^{\cdot}]$, we obtain from equation (IV.8):

$$K_6'(P_{S_2}/P_{O_2}) \gg 1 \qquad \text{(IV.16)}$$

In a similar manner, we can therefore write

$$[h^{\cdot}] = \left(\frac{3K_1^{\frac{1}{2}}}{K_6'}\right)^{\frac{1}{4}}\,P_{S_2}^{-1/8}\,P_{O_2}^{+5/16} \qquad \text{(IV.17)}$$

and

$$[S_O^{\cdot}] = K_6'^{3/4}(3K_1)^{1/8}\,P_{S_2}^{3/8}\,P_{O_2}^{-3/16} \qquad \text{(IV.18)}$$

IV.2.3 Sulfur in the form S°

Substitution of neutral sulfur on an anionic site can be written as

$$\tfrac{1}{2}\,S_2 + O_O \underset{\leftarrow}{\overset{K_{19}}{\rightarrow}} S_O^{\cdot\cdot} + \tfrac{1}{2}\,O_2 + 2\,e^- \qquad \text{(IV.19)}$$

The $[S_O^{\cdot\cdot}]$ concentration can then be related to the equilibrium constant K_{19} by

$$[S_O^{\cdot\cdot}] = K_{19}'\,[h^{\cdot}]^2\,(P_{S_2}/P_{O_2})^{\frac{1}{2}} \qquad \text{(IV.20)}$$

where $K_{19}' = K_{19} \times K_e$

Again considering $[h^\cdot] \ll [e^-]$, we can write

$$[h^\cdot] = 3[V'''_{cr}] - 2[S''_0] \qquad \text{(IV.21)}$$

From equation (IV.20), (IV.21) and (IV.22) we can obtain:

$$[h^\cdot] = [3K_1^{\frac{1}{2}} P_{O_2}^{3/4} [h^\cdot]^{-3}] - [2K'_{19} P^2 (P_{S_2}/P_{O_2})^{\frac{1}{2}}] \qquad \text{(IV.22)}$$

that is

$$[h^\cdot]^4 [1 + 2K'_{19} [h^\cdot] (P_{S_2}/P_{O_2})^{\frac{1}{2}}] = 3K_1^{\frac{1}{2}} P_{O_2}^{3/4} \qquad \text{(IV.23)}$$

In addition, from equation (IV.20) we also have

$$[h^\cdot] = \frac{[S''_0]^{\frac{1}{2}}}{(K'_{19})^{\frac{1}{2}}} (P_{S_2}/P_{O_2})^{\frac{1}{4}} \qquad \text{(IV.24)}$$

Regrouping equations (IV.21), (IV.24) and (IV.2) we can now write

$$2[S''_0] = \frac{3K_1^{\frac{1}{2}} (K_{19})^{3/2} P_{S_2}^{3/4}}{[S''_0]^{3/2}} - \frac{[S''_0]^{\frac{1}{2}}}{(K'_{19})^{\frac{1}{2}}} (P_{S_2}/P_{O_2})^{\frac{1}{4}}$$

which gives

$$[S''_0]^{5/2} \left[1 + \frac{1}{2(K'_{19})^{\frac{1}{2}} [S''_0]^{\frac{1}{2}}} (P_{O_2}/P_{S_2})^{\frac{1}{4}}\right]$$

$$= 3/2\, K_1^{\frac{1}{2}} (K'_{19})^{3/2} P_{S_2}^{3/4} \qquad \text{(IV.25)}$$

Again, two limiting cases can be considered. If the dissolved sulfur is small, so that $[S_O^{\cdot\cdot}] \ll [h^{\cdot}]$

$$K'_{19} \left(P_{S_2}/P_{O_2}\right)^{\frac{1}{2}} [h^{\cdot}] \ll 1 \qquad \text{(IV.26)}$$

and, from equations (IV.26) and (IV.23) we have

$$[h^{\cdot}] = (3K^{\frac{1}{2}})^{\frac{1}{4}} P_{O_2}^{3/16} \qquad \text{(IV.27)}$$

Similarly, from equations (IV.25) and (IV.26) and taking into consideration equation (IV.20), we have:

$$[S_O^{\cdot\cdot}] = (3)^{\frac{1}{2}} K_1^{\frac{1}{4}} K'_{19} P_{S_2} P_{O_2}^{-1/8} \qquad \text{(IV.28)}$$

where $\frac{1}{2}(K'_{19})^{\frac{1}{2}} (S_O^{\cdot\cdot})^{\frac{1}{2}} (P_{O_2}/P_{S_2})^{\frac{1}{4}} = \frac{1}{2} K'_{19}[h^{\cdot}] (P_{O_2}/P_{S_2})^{\frac{1}{2}}$

If, however, the sulfur solubility is high and $[S_O^{\cdot\cdot}] \gg [h^{\cdot}]$

then $$K'_{19}(P_{S_2}/P_{O_2})^{\frac{1}{2}} [h^{\cdot}] \gg 1 \qquad \text{(IV.29)}$$

From equations (IV.29) and (IV.23), therefore

$$[h^{\cdot}] = \left(\frac{3}{2} \frac{K_1^{\frac{1}{2}}}{K'_{19}}\right)^{1/5} P_{O_2}^{\frac{1}{4}} P_{S_2}^{-1/10} \qquad \text{(IV.30)}$$

Combining equations (IV.29) and (IV.25) we obtain

$$[S_O^{\cdot\cdot}] = (3/2\, K_1^{\frac{1}{2}} (K'_{19})^{3/2})^{2/5} P_{S_2}^{3/10} \qquad \text{(IV.31)}$$

IV.3 SUBSTITUTION ON AN INTERSTITIAL SITE

IV.3.1 Sulfur in the form S_i°

When a neutral sulfur atom occupies an interstitial site, we have a simple equation

$$\tfrac{1}{2} S_2 \underset{\leftarrow}{\overset{K_{32}}{\rightarrow}} S_i^\circ \qquad \text{(IV.32)}$$

and

$$[S_i^\circ] = K_{32}(P_{S_2}^{\frac{1}{2}}) \qquad \text{(IV.33)}$$

IV.3.2 Sulfur in the form S_i^+

When the sulfur atom in the interstitial site is positively charged as S^+, we can write

$$\tfrac{1}{2} S_2 \underset{\leftarrow}{\overset{K_{34}}{\rightarrow}} S_i^+ + e^- \qquad \text{(IV.34)}$$

Using the relation of mass conservation and charge balance

$$[S_i^+] = K'_{34}\, P_{S_2}^{\frac{1}{2}}\, [h^\cdot] \qquad \text{(IV.35)}$$

where $K'_{34} = K_{34} \times K_e$

Considering that $[h^\cdot] \gg [e^-]$, we have

$$3[V_{Cr}'''] = [h^\cdot] + [S_i^+] \qquad \text{(IV.36)}$$

and, combined with equations (IV.36), (IV.35) and (IV.2)

$$[h^\cdot] = [3K_i^{\frac{1}{2}}\, P_{O_2}^{3/4}\, [h^\cdot]^{-3}] - [K'_{34}\, P_{S_2}^{\frac{1}{2}}\, [h^\cdot]]$$

where $$[h^{\cdot}] = \left(\frac{3K_1^{\frac{1}{2}} P_{O_2}^{3/4}}{1 + K'_{34} P_{S_2}^{\frac{1}{2}}}\right)^{\frac{1}{4}} \qquad \text{(IV.37)}$$

Similarly, from equations (IV.37) and (IV.35) we arrive at

$$[S_i^{+}] = K'_{34} P_{S_2}^{\frac{1}{2}} \left(\frac{3K_1^{\frac{1}{2}} P_{O_2}^{3/4}}{1 + K'_{34} P_{S_2}^{\frac{1}{2}}}\right)^{\frac{1}{4}} \qquad \text{(IV.38)}$$

Using a development analogous to the previous case for substitution on anionic sites, we can consider two limiting cases: first, when the sulfur solubility is low such that:

$$[S_i^{+}] \ll [h^{\cdot}]$$

So that $K'_{34} P_{S_2}^{\frac{1}{2}} \ll 1$

which gives $$[h^{\cdot}] = \left(\frac{3K_1^{\frac{1}{2}} P_{O_2}^{3/4}}{K'_{34} P_{S_2}^{\frac{1}{2}}}\right)^{\frac{1}{4}} \qquad \text{(IV.39)}$$

and $$[S_i^{+}] = (3K'_{34} K_1^{\frac{1}{2}})^{\frac{1}{4}} P_{O_2}^{3/16} P_{S_2}^{3/8} \qquad \text{(IV.40)}$$

When the solubility is high such that:

$$[S_i^{+}] \gg [h^{\cdot}]$$

so that $K'_{34} P_{S_2}^{\frac{1}{2}} \gg 1$

which results in

$$[h^{\cdot}] = (3K_1^{\frac{1}{2}})^{\frac{1}{4}} P_{O_2}^{3/16} \qquad \text{(IV.41)}$$

and thus, $$[S_i^{+}] = K'_{34} (3K_1^{\frac{1}{2}})^{\frac{1}{4}} P_{O_2}^{3/16} P_{S_2}^{\frac{1}{2}} \qquad \text{(IV.42)}$$

IV.3.3 Sulfur in the form S^{+2}

When sulfur takes the interstitial location as S^{+2}, the dissociation equation is given as

$$\tfrac{1}{2} S_2 \overset{K_{43}}{\rightleftharpoons} S_i^{+2} + 2 e^{-} \qquad \text{(IV.43)}$$

Using the mass balance form

$$[S_i^{+}] = K'_{43} P_{S_2}^{\frac{1}{2}} [h^{\cdot}]^2 \qquad \text{(IV.44)}$$

where $K'_{43} = K_{43} \times K_e$

Again, since $[h^{\cdot}] \gg [e^{-}]$

$$3[V_{cr}^{'''}] = 2[S_i^{+2}] + [h^{\cdot}] \qquad \text{(IV.45)}$$

The same development used for the substitution of sulfur as a neutral atom can be used to arrive at equation (IV.46).

$$[S_i^{+2}]^{5/2} \left[1 + \frac{P_{S_2}^{-\frac{1}{4}}}{2(K'_{43})^{\frac{1}{2}} [S_i^{+2}]^{\frac{1}{2}}}\right] = \frac{3}{2} K_1^{\frac{1}{2}} (K'_{43})^{3/2} P_{O_2}^{3/4} P_{S_2}^{3/4} \qquad \text{(IV.46)}$$

when the solubility is low, such that:

$$[S_i^{+2}] \ll [h^\cdot]$$

and thus, $[h^\cdot] = (3K_1^{\frac{1}{2}})^{\frac{1}{4}} P_{O_2}^{3/16}$ (IV.47)

and $[S_i^{+2}] = 3^{\frac{1}{2}} K_1^{\frac{1}{4}} K'_{43} P_{S_2} P_{O_2}^{3/8}$ (IV.48)

and, when the solubility is high, such that: $[S_i^{+2}] \gg [h^\cdot]$

we have

$$[h^\cdot] = \left(\frac{3}{2} \frac{K_1^{\frac{1}{2}}}{K'_{43}}\right)^{1/5} P_{S_2}^{-1/6} P_{O_2}^{3/20} \quad \text{(IV.49)}$$

and

$$[S_i^{+2}] = \left(\frac{3}{2} K_1^{\frac{1}{2}} K_{43}'^{3/2}\right)^{2/5} (P_{O_2} P_{S_2})^{3/10} \quad \text{(IV.50)}$$

IV.4 SUBSTITUTION IN A CATIONIC VACANCY

IV.4.1 Sulfur in the form of S^{+2}

The exchange equation can be written as

$$\tfrac{1}{2} S_2 + V_{cr}''' \overset{K_{51}}{\rightleftharpoons} S'_{cr} + 2\, e^- \quad \text{(IV.51)}$$

Using mass and charge balance equations

$$[S'_{cr}] = K'_{51} P_{S_2}^{\frac{1}{2}} [V_{cr}'''] [h^\cdot]^2 \quad \text{(IV.52)}$$

where $K'_{51} = K_{51} \times K_e$

and $$3[V'''_{cr}] + [S'_{cr}] = [h^{\cdot}] \qquad (IV.53)$$

Again, combining (IV.53), (IV.52) and equation (IV.2)

$$[h^{\cdot}] = [3K_1^{\frac{1}{2}} P_{O_2}^{3/4} [h^{\cdot}]^{-3}] + [K'_{51} P_{S_2}^{\frac{1}{2}} K_1^{\frac{1}{2}} P_{O_2}^{3/4} [h^{\cdot}]^{-1}]$$

which is equivalent to

$$[h^{\cdot}]^4 \left[1 - \frac{K'_{51} K_1^{\frac{1}{2}} P_{S_2}^{\frac{1}{2}} P_{O_2}^{3/4}}{[h^{\cdot}]^2}\right] = 3K_1^{\frac{1}{2}} P_{O_2}^{3/4} \qquad (IV.54)$$

Solving for $[h^{\cdot}]$ gives

$$[h^{\cdot}] = \frac{K'_{51} K_1^{\frac{1}{2}} P_{S_2}^{\frac{1}{2}} P_{O_2}^{3/4}}{[S'_{cr}]}$$

and from equation (IV.53)

$$[S'_{cr}] = \frac{K_{51} K_1^{\frac{1}{2}} P_{S_2}^{\frac{1}{2}} P_{O_2}^{3/4}}{[S'_{cr}]} - \frac{3K_1^{\frac{1}{2}} P_{O_2}^{3/4}}{[S'_{cr}]^{-3}} (K'_{51})^{-3} K_1^{-3/2} P_{S_2}^{-3/2} P_{O_2}^{-9/4}$$

or $$[S'_{cr}]^2 \left[1 + \frac{3[S'_{cr}]^2}{K_1 (K'_{51})^3 P_{S_2}^{3/2} P_{O_2}^{3/2}}\right] = K'_{51} K_1^{\frac{1}{2}} P_{S_2}^{\frac{1}{2}} P_{O_2}^{3/4} \qquad (IV.55)$$

Again, considering the two limiting cases of low and high solubilities of sulfur:

for $[S'_{cr}] \ll [h^{\cdot}]$

$$[h^{\cdot}] = (3K_1^{\frac{1}{2}} \cdot P_{O_2}^{3/4})^{\frac{1}{4}}$$

and $$[S'_{cr}] = 3^{-\frac{1}{4}} K'_{51} K_1^{3/16} P_{O_2}^{9/16} P_{S_2}^{\frac{1}{2}} \qquad (IV.56)$$

if $$[S'_{cr}] \gg [h^\cdot]$$

i.e. $$K_1^{\frac{1}{2}} K'_{51} P_{S_2}^{\frac{1}{2}} P_{O_2}^{3/4} [h^\cdot]^2 \gg 1$$

we obtain from equation (IV.54)

$$[h^\cdot] = -3^{\frac{1}{2}}/(K'_{51})^{-\frac{1}{2}} P_{S_2}^{-\frac{1}{4}}$$

which is an unrealistic solution.

IV.4.2 Sulfur in the form S^+

Sulfur substituted on a cation vacancy in the form of S^+ in expressed by the exchange equation:

$$\tfrac{1}{2} S_2 + V'''_{cr} \overset{K_{57}}{\rightleftharpoons} S''_{cr} + e^- \qquad (IV.57)$$

again $$[S''_{cr}] = K'_{57} P_{S_2}^{\frac{1}{2}} [V'''_{cr}] [h^\cdot] \qquad (IV.58)$$

where $$K'_{57} = K_{57} \times K_e$$

by electroneutrality

$$3[V'''_{cr}] + 2[S''_{cr}] = [h^\cdot] \qquad (IV.59)$$

from equations (IV.59), (IV.58) and (IV.2)

$$[h^\cdot] = [3K_1^{\frac{1}{2}} P_{O_2}^{3/4} [h^\cdot]^{-3} + K'_{57} K_1^{\frac{1}{2}} P_{O_2}^{3/4} P_{S_2}^{\frac{1}{2}} [h^\cdot]^{-2}]$$

which can also be given as

$$[h^{\cdot}]^4 \left[1 + \frac{K'_{57}\, K_1^{\frac{1}{2}}}{[h^{\cdot}]^3}\, P_{O_2}^{3/4}\, P_{S_2}^{\frac{1}{2}}\right] = 3K_1^{\frac{1}{2}}\, P_{O_2}^{3/4} \qquad \text{(IV.60)}$$

Combining equations (IV.58) and (IV.2) we can solve for

$$[h^{\cdot}] = \frac{(K'_{57})^{\frac{1}{2}}\, K_1^{\frac{1}{4}}\, P_{O_2}^{3/8}\, P_{S_2}^{\frac{1}{4}}}{[S''_{cr}]^{\frac{1}{2}}} \qquad \text{(IV.61)}$$

from equations (IV.59), (IV.61) and (IV.2)

$$2[S''_{cr}] = \frac{(K'_{57})^{\frac{1}{2}}\, K_1^{\frac{1}{4}}\, P_{O_2}^{3/8}\, P_{S_2}^{\frac{1}{4}}}{[S''_{cr}]^{\frac{1}{2}}} - \frac{3K_1^{\frac{1}{2}}\, P_{O_2}^{3/4}\, [S''_{cr}]^{3/2}}{(K'_{57})^{3/2}\, K_1^{3/4}\, P_{O_2}^{9/8}\, P_{S_2}^{3/4}}$$

or

$$2[S''_{cr}]^{3/2}\left[1 + \frac{3[S''_{cr}]^{\frac{1}{2}}}{K_1^{\frac{1}{4}}\, K_{57}^{3/2}\, P_{O_2}^{9/8}\, P_{S_2}^{3/4}}\right]$$

$$= (K'_{57})^{\frac{1}{2}}\, K_1^{\frac{1}{4}}\, P_{O_2}^{3/8}\, P_{S_2}^{\frac{1}{4}} \qquad \text{(IV.62)}$$

Considering the cases of low and high sulfur solubility,

for $[S''_{cr}] \ll [h^{\cdot}]$

$$K_1^{\frac{1}{2}}\, K'_{57}\, P_{S_2}^{\frac{1}{2}}\, P_{O_2}^{3/4}\, [h^{\cdot}]^{-3} \ll 1$$

and thus $P << 0$, which is unrealistic

for $[S''_{Cr}] >> [h^{\cdot}]$

$$[h^{\cdot}] = (3K_1^{\frac{1}{2}} P_{O_2}^{3/4})^{\frac{1}{4}}$$

and thus $[S''_{Cr}] = K'_{57} K_1^{\frac{1}{4}} P_{O_2}^{3/8} P_{S_2}^{\frac{1}{2}}$

IV.5 CHOICE OF THE MECHANISM OF SULFUR DISSOLUTION

The choice of a specific model for sulfur dissolution in the Cr_2O_3 matrix is based on the comparison of the experimental values obtained in this study with the calculated values using the analytic formulation for the different methods of sulfur dissolution as summarized in Table IV.2.

In view of the non-linearity of most of the derived equations, this comparison can only be done by a mathematical treatment of these equations which can only be solved once all equilibrium constants are known.

In order to determine the equilibrium constants these equations were linearized as shown in Table IV.3 and then fitted to the experimental values by using a least squares method.

The values of the fitted parameters are then used in the basic equations presented in Table IV.2, which are then solved by a non-linear least squares regression as described by the Marquardt (69) method.

TABLE IV.2: ANALYTICAL EXPRESSIONS FOR DIFFERENT MODES OF SULFUR DISSOLUTION IN Cr_2O_3

POSITION AND VALENCE STATE	REACTION MECHANISMS	TYPE	ANALYTICAL EQUATION
S^{-2} on anionic site	$\frac{1}{2} S_2 + O_O \overset{K_{A_1}}{\rightleftharpoons} S_O + \frac{1}{2} O_2$	(A_1)	$[S_O] = K_{A_1} \left(\frac{P_{S_2}}{P_{O_2}}\right)^{\frac{1}{2}}$
S^{-1} on anionic site	$\frac{1}{2} S_2 + O_O \overset{K_{A_2}}{\rightleftharpoons} S_O^{\cdot} + \frac{1}{2} O_2 + e^-$	(A_2)	$[S_O^{\cdot}] = K_{A_2} \left(\frac{P_{S_2}}{P_{O_2}}\right)^{\frac{1}{2}} \cdot \left(\frac{3K_1^{\frac{1}{2}} \cdot P_{O_2}^{3/4}}{1 + K_{A_2} (P_{S_2}/P_{O_2})^{\frac{1}{2}}}\right)^{\frac{1}{4}}$
S_o on anionic site	$\frac{1}{2} S_2 + O_O \overset{K_{A_3}}{\rightleftharpoons} S_O^{\cdot\cdot} + \frac{1}{2} O_2 + 2e^-$	(A_3)	$[S_O^{\cdot\cdot}]^{5/2} \left(1 + \frac{1}{2K_{A_3}^{\frac{1}{2}} [S_O^{\cdot\cdot}]^{\frac{1}{2}}} \cdot (P_{O_2}/P_{S_2})^{\frac{1}{4}}\right) = 3/2\ K_1^{\frac{1}{2}} \cdot K_{A_3}^{3/2} \cdot P_{S_2}^{3/4}$
S^{+2} on interstitial site	$\frac{1}{2} S_2 \overset{K_{I_1}}{\rightleftharpoons} S_i^{2+} + 2e^-$	(I_1)	$[S_i^{2+}]^{5/2} \left[1 + \frac{P_{S_2}^{-\frac{1}{4}}}{2K_{I_3}^{\frac{1}{2}} \cdot [S_i^{2+}]^{\frac{1}{2}}}\right] = 3/2\ K_1^{\frac{1}{2}} \cdot K_{I_3}^{3/2} \cdot P_{O_2}^{3/4} \cdot P_{S_2}^{3/4}$
S^{+} on interstitial site	$\frac{1}{2} S_2 \overset{K_{I_2}}{\rightleftharpoons} S_i^{+} + e^-$	(I_2)	$[S_i^{+}] = K_{I_2} P_{S_2}^{\frac{1}{2}} \left(\frac{3K_1^{\frac{1}{2}} \cdot P_{O_2}^{3/4}}{1 + K_{I_2} P_{S_2}^{\frac{1}{2}}}\right)^{\frac{1}{4}}$
S° on interstitial site	$\frac{1}{2} S_2 \overset{K_{I_3}}{\rightleftharpoons} S_i$	(I_3)	$[S_i] = K_{I_3} P_{S_2}^{\frac{1}{2}}$
S^{+2} on cationic site	$\frac{1}{2} S_2 + V_{Cr}^{'''} \overset{K_{L_1}}{\rightleftharpoons} S_{Cr}^{'} + 2e^-$	(L_1)	$[S_{Cr}^{'}]^2 \left[1 + \frac{3[S_{Cr}^{'}]^2}{K_1 \cdot K_{L_1}^3 \cdot P_{S_2}^{3/2} \cdot P_{O_2}^{3/2}}\right] = K_{L_1} \cdot K_1^{\frac{1}{2}} \cdot P_{S_2}^{\frac{1}{2}} \cdot P_{O_2}^{3/4}$
S^{+1} on cationic site	$S_2 + V_{Cr}^{'''} \overset{K_{L_2}}{\rightleftharpoons} S_{Cr}^{''} + e^-$	(L_2)	$[S_{Cr}^{''}]^{3/2} \left[1 + \frac{3[S_{Cr}^{''}]^{\frac{1}{2}}}{K_1^{\frac{1}{4}} \cdot K_{L_2}^{3/2} \cdot P_{O_2}^{3/8} \cdot P_{S_2}^{3/4}}\right] = \frac{1}{2} K_{L_2}^{\frac{1}{2}} \cdot K_1^{\frac{1}{4}} \cdot P_{O_2}^{3/8} \cdot P_{S_2}^{\frac{1}{2}}$

TABLE IV.3: LINEARIZED EQUATIONS

TYPE	FORM OF EQUATION
A_1	$\text{Log}\,[S_o] = \frac{1}{2}\,\text{Log}\,(P_{s_2}/P_{o_2}) + \text{Log}\,K_{A_1}$
A_2	$P_{o_2}^{3/4}\,(P_{s_2}/P_{o_2})^2 \cdot \frac{1}{[S_o^{\cdot}]^4} = \frac{1}{K_{A_2}^4} \cdot \frac{1}{3K_I^{\frac{1}{2}}} + \frac{1}{3K_I^{\frac{1}{2}} \cdot K_{A_2}^3}\,(P_{s_2}/P_{o_2})^{\frac{1}{2}}$
A_3	$P_{s_2}^{3/4} \cdot [S_o^{\cdot\cdot}]^{-5/2} = \frac{1}{3K_{A_3}^2 \cdot K_I^{\frac{1}{2}}}\,[P_{o_2}/P_{s_2}]^{\frac{1}{4}} \cdot [S_o^{\cdot\cdot}]^{-\frac{1}{2}} + \frac{2}{3}\,\frac{1}{K_I^{\frac{1}{2}} \cdot K_{A_3}^{3/2}}$
I_1	$P_{o_2}^{3/4} \cdot P_{s_2}^{3/4}\,[S_i^{2+}]^{-5/2} = \frac{2}{3K_I^{\frac{1}{2}} \cdot K_{I_1}^{3/2}} + \frac{P_{s_2}^{-\frac{1}{4}}\,[S_i^{2+}]^{-\frac{1}{2}}}{3K_I^{\frac{1}{2}} \cdot K_{I_1}^2}$
I_2	$P_{o_2}^{3/4} \cdot \frac{P_{s_2}^2}{[S_i^{+}]^4} = \frac{1}{3K_{I_2}^4 \cdot K_I^{\frac{1}{2}}} + \frac{1}{3K_I^{\frac{1}{2}} \cdot K_{I_2}^3} \cdot P_{s_2}^{\frac{1}{2}}$
I_3	$\text{Log}\,[S_i] = \frac{1}{2}\,\text{Log}\,P_{s_2} + \text{Log}\,K_{I_3}$
L_1	$[S_{cr}^{\prime}]^{-4} \cdot P_{s_2}^2 \cdot P_{o_2}^{9/4} = \frac{3}{K_1^{3/2} \cdot K_{L_1}^4} + \frac{1}{K_I^{\frac{1}{2}} \cdot K_{L_1}}\,P_{s_2}^{3/2} \cdot P_{o_2}^{3/2} \cdot [S_{cr}^{\prime}]^{-2}$
L_2	$P_{o_2}^{3/4} \cdot P_{s_2} \cdot [S_{cr}^{\prime\prime}]^{-2} = \frac{3}{\frac{1}{2}K_{L_2}^2\,K_I^{\frac{1}{2}}} + \frac{P_{o_2}^{3/8} \cdot P_{s_2}^{3/4} \cdot [S_{cr}^{\prime\prime}]^{-\frac{1}{2}}}{\frac{1}{3}K_{L_2}^{\frac{1}{2}}\,K_I^{\frac{1}{2}}}$

The most likely form of sulfur dissolution is then determined by the comparison of the sum of the squares of the residues for the different models tested. The model with the smallest sum $\sum(S_{model}-S_{exp})^2$ is then selected as the predominant mechanism of sulfur dissolution.

The mathematical treatment of this minimization procedure has presented a considerable degree of difficulty and has not yet been completely resolved. In fact, for a specific model, the sum of the squares of the residues can present several minima and depend on the values of the predetermined parameters. If the initial values of these parameters are very different from those that minimize the sum of the squares of the residues, a relative minimum can result but may not be an absolute minimum. This phenomenon commonly occurs for such unstable functions.

The Marquardt (69) is very sensitive to the initial values of the estimated parameters, and it is not uncommon that convergence problems are encountered in this type of analysis.

The complete mathematical analysis for the solution of these equations requires considerable computation time. For the purposes of this report the method of resolving the equations only is presented. Numerical techniques using sophisticated mathematical software have been applied. Due to time and computer constraints, a definitive choice of the model of sulfur dissolution based on the experimental results of this study has not yet been presented.

V. STUDIES UNDER INVESTIGATION

Following the completion of the sulfur solubility experiments and exploring the various methods of analysis of trace amounts of sulfur, the second stage of the project deals with the measurement of the diffusivity of sulfur in Cr_2O_3 in polycrystalline and monocrystal form.

The method used for determining the diffusion coefficient consists essentially of exposing a sample of monocrystalline or polycrystalline Cr_2O_3 to an atmosphere containing sulfur. Once the dissolution mechanism of sulfur is established, the migration of sulfur into the solid sample under a sulfur atmosphere will result in a specific concentration profile. A solution of Fick's law for the transient state needs to be applied, using the appropriate boundary conditions, in order to obtain the values of the diffusion coefficient.

In this study, conventional methods of analysis of the concentration profile such as by electron microprobe, or chemical analysis are not applicable due to the extremely low sulfur solubilities. The only method that can be successfully used is the radiotracer method which has been used in many diffusion problems, since isotopes of nearly all the elements are possible with an experimentelly convenient half-life, and since the chemical and physical characteristics of the isotopes are essentially identical to the elements in their natural state.

The isotope ^{35}S was chosen as the radiotracer for this study and will be deposited on the solid sample surface in solution form as $H_2^{35}SO_4(H_2O)_n$. Evaporation of this solution will leave a small quantity

of ^{35}S on the surface of the sample. In a second step, the sample is then sealed in a quartz ampoule and diffusion was allowed to proceed at a sulfur pressure generated by the evaporated solution for the required period and at constant temperature. The sulfur profile will be analysed using a scintillation counter by sectioning at 10 μ intervals. The new sample surface will be analysed after removing each layer.

This method developed by Gruzin (30) measures the residual activity, and accounts for the selfabsorption of the emitted radiation. The normalized analytic solution for this method is given by Howng and Wagner (46) for the case of ^{35}S diffusion in NiO. The same analysis can be used for Cr_2O_3.

$$\frac{I(b)}{I_0} = \frac{\int_{\infty}^{b} \left[1-\text{erf}\ \frac{x+B}{2\sqrt{Dt}}\right] E_2[-\mu x]dx}{\int_{\infty}^{0} \left[1-\text{erf}\ \frac{x}{2\sqrt{Dt}}\right] E_2[-\mu x]dx}$$

where:
- b is the thickness of the layer removed by abrasion
- $I(b)$ is the radioactivity counted on the surface after each abrasion
- I_0 is the radioacivity before sectioning (x=0)
- $E_2[-\mu x]$ is a parameter accounting for the selfabsorption of β rays
- D is the diffusion coefficient
- t is the diffusion time.

A plot of the experimental values of $I(b)/I_0$ as a function of $b/\sqrt{t}$ results in a series of curves for different values of the diffusion coefficient, which can then be calculated from this relation.

V.1 EXPERIMENTAL PROCEDURE

Polycrystalline Cr_2O_3 samples have been prepared by first pressing the Spec-pure Cr_2O_3 powder (Johnson-Matthey) into 12 mm diameter cyclinders using a hydraulic press. These cylinders were then placed on a layer of loose powdered Cr_2O_3 in an Al_2O_3 crucible and heated for 12 hours in a drying oven at 120°C under a mechanical vacuum. This was done to avoid a solid solution reaction with the crucible. The Al_2O_3 crucible was then covered with an Al_2O_3 disk and introduced into a high temperature furnace (Tungsten resistance).

The literature has indicated (50,51) that the sintering mechanism is largely controlled by the diffusion of oxygen anions within the Cr_2O_3 grains. It is generally concluded that the density of the final product is related to the oxygen pressure used during sintering, and that when this pressure is reduced to the decomposition pressure for Cr/Cr_2O_3, the sample will attain the theoretical density of pure Cr_2O_3. Under these condition Grimeley et al. (68) have shown that the transformation of Cr_2O_3 (solid) $\rightarrow$ CrO_3 (gas) is thermodynamically not favorable, and that for increased oxygen pressures, the volatilisation of CrO_3 prevents densification during sintering at high temperatures.

Similar results were observed in this study when the oxygen pressure was varied. Figures 32 and 33 show the microscopic aspects of the samples sintered at 1873K in air and in purified argon ($P_{O_2} \approx 10^{-6}$ atm) respectively. It can be observed that the product sintered under argon is very near the theoretical polycrystalline density, whereas the sample sintered in air shows considerable porosity.

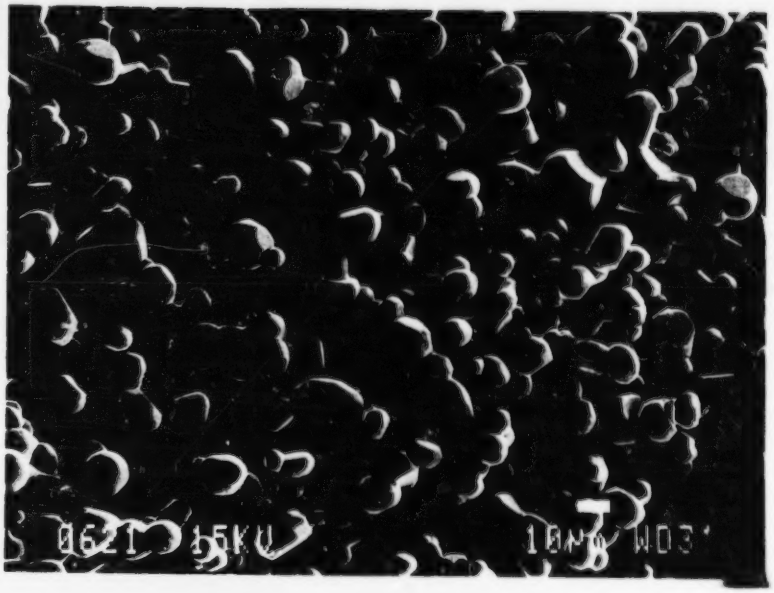

FIGURE 32: Microscopic aspect of Cr_2O_3 sintered in air at 1873K.

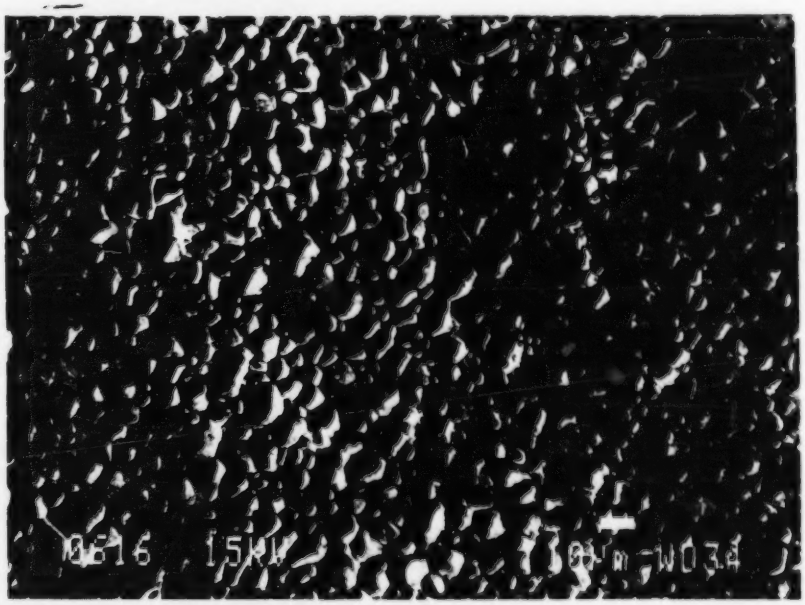

FIGURE 33: Microscopic aspect of Cr_2O_3 in purified argon (P_{O_2} = 10^{-6} atm) at 1873K.

After many attempts in obtaining ideal polycrystalline samples the following procedures proved to be the most successful based on microscopic examination.

Initial compression	:	40 000 psi (275 MN/m^2)
Time under pressure	:	60 s
Temp. of sintering	:	1873K
Atmosphere	:	$P_{O_2} = 10^{-6}$ atm
Sintering time	:	2 hrs.

These cylinders were then sectioned using a diamond micro saw in order to produce parallelpipeds measuring 3 mm × 3 mm × 1.5 mm. The two major faces were then polished down to 1 μ, using diamond paste. The microstructures of the polished sections are shown in Figures 3 4 and 3 5 and clearly indicate the lack of pores or any type of fissurisation.

Before exposing these samples to the sulfur atmosphere for diffusion, they were first washed in an ultrasound bath with acetone, dried, and duplicate samples were heat treated for a period of 2 weeks at temperatures that are to be used for the diffusion experiments (1173, 1223, 1273, 1323 and 1373K). In order to preserve the non porous structure of these samples the heat treatment was carried out by sealing the samples in quartz ampoules.

These samples are presently ready for the diffusion tests which will begin shortly.

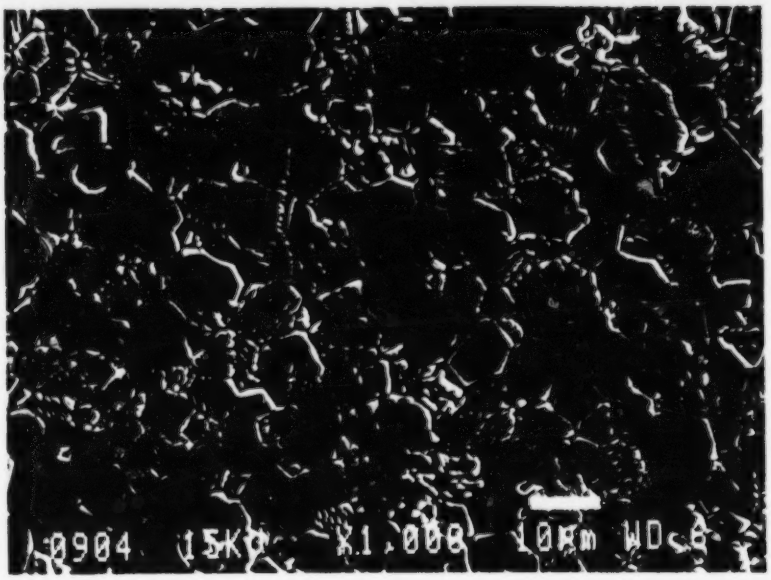

FIGURE 34: Microscopic aspect of polished sample of Cr_2O_3 sintered in purified argon ($P_{O_2} \approx 10^{-6}$ atm) at 1873K.

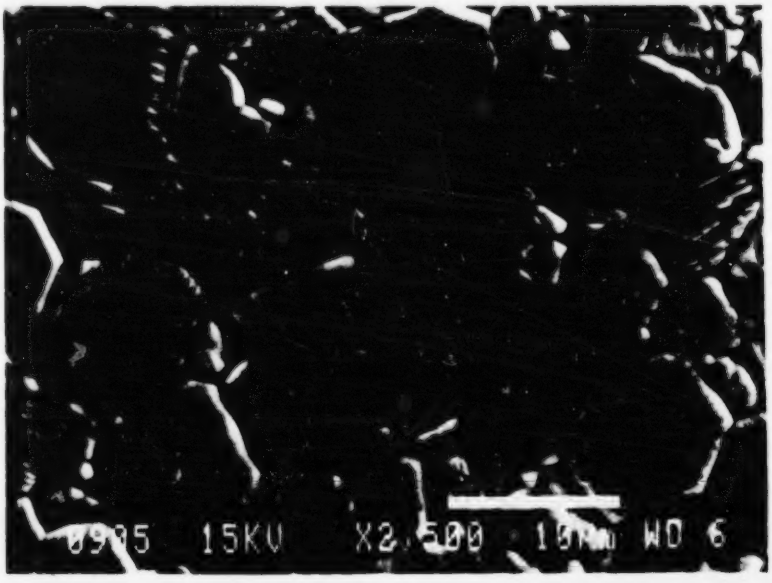

FIGURE 35: Microscopic aspect of polished sample of Cr_2O_3 (high magnification) sintered in purified argon ($P_{O_2} \approx 10^{-6}$ atm) at 1873K.

CONCLUSIONS

A thorough literature review was carried out on the available data and methods of determining the solubility of sulfur in Cr_2O_3 and the results were critically evaluated. No reliable consistent solubility data was found and diffusivity data was virtually inexistent.

Experimental techniques for the equilibration of Cr_2O_3 in controlled reaction gas atmospheres were developed. It was shown that the control of thermodynamic conditions is extremely important for the long duration tests and buffered gas mixture are necessary to maintain stable conditions.

Different analytical techniques for the determination of sulfur are described. Due to the low solubility levels (less than 100 ppm) the number of methods were limited to sophisticated techniques for trace element analysis. LECO infrared analysis, and proton induced X-ray emission (PIXE) were unsuccessful. A neutron activation method was finally adopted which produced reliable, reproducible results.

This analysis showed that the limiting solubility of sulfur in Cr_2O_3 varied between 16 ppm to 93 ppm for the range of oxygen and sulfur pressures used in this study. The solubility was found to vary depending on the combined effect of sulfur and oxygen pressure, and for a given oxygen pressure, the amount dissolved increases with an increase in sulfur pressure.

An analysis of the different modes of sulfur dissolution in Cr_2O_3 is presented in detail. The combined effects of sulfur and oxygen pressure on the sulfur dissolution on anionic, interstitial and

cationic lattice sites was taken into consideration. Valence states of sulfur from S^{+2} to S^{-2} were considered for each case. Analytical equations were developed relating the sulfur content to each type of mechanism and solutions to these equations were proposed which lead to the identification of the most probable mechanism. Eight different modes of dissolution are presented resulting in formulations of varying degrees of complexity. Fitting the experimental data to each of these expressions should lead to the most likely mechanism of dissolution. Due to the complexity of the numerical solution technique involved, a final solution and mechanism cannot be proposed at the present time. The experimental technique for carrying out the diffusion of sulfur in polycrystalline Cr_2O_3 is presented. Polycrystalline samples of Cr_2O_3 were successfully prepared by suitering the compressed pure powder at 1873K for 2 hours. It was found that the porosity of the final product depends on the oxygen pressure used during the sintering process. Microscopic examination has shown that sintering in air produces pores caused by CrO_3 volatilization. Oxygen pressures of the order of 10^{-6} are required to obtain homgeneous, theoretically dense samples at this temperature. A technique was developed to obtain small polished parallelepipeds of the polycrystalline Cr_2O_3 which are then exposed to a sulfur atmosphere containing ^{35}S. These have all been prepared and await the diffusion experiments. A method for the analysis of the sulfur profile data has been proposed from which the diffusion coefficients can be calculated.

REFERENCES

(1) T.C. Tiarney, Jr. and K. Natesan, J. Materials for Energy Systems, Vol. 1, (3) 1980, p. 13.

(2) J. Stringer, Proceeding JIMIS-3 (1983): High Temperature Corrosion Transaction of the Japan Institute of Metals, Supplement, p. 45.

(3) E.A. Gulbaransen and K.F. Andrew, J. Electrochem. Soc., 103 (1956) 429.

(4) W.C. Hagel, Trans. ASM, 43 (1951) 1098.

(5) H. Hindam and D.P. Whittle, J. Electrochem. Soc., 130 (1983) 1519.

(6) B. Kubota, J. Am. Cer. Soc., 44 (1961) 239.

(7) R.K. DiCerbo and A.U. Seybolt, Ibid, 42, [9], (1959) 430.

(8) A. Michel and J. Bénard, Bull. Soc. Chim., 10 (1943) 315.

(9) C. Monty, École d'été "Défauts ponctuels dans les solides", Ed. La revue de physique, Confolent (1977), 345.

(10) K.A. Hay, F.G. Hicks and D.R. Holmes, Werkst. Korros., 21, 917 (1970).

(11) C.S. Tedmon, J. Electrochem. Soc., 113, 766, 1966.

(12) L.N. Cojocaru, Z. Phys. Chem., N.F., (1969) 255.

(13) W.C. Hagel and A.U. Seybolt, J. Electrochem. Soc., 108 (1961) 1146.

(14) K. Hauffe and J. Block, J.Z. Phys. Chem. (Lpz), 198, (1951) 232.

(15) F.G. Hicks, D.R. Holmes and D.B. Meadowcroft, Proceedings of the Fourth International Congress on Metallic Corrosion, Hormane, Hamner, Nace Houston, Texas Editor.

(16) J.A. Crawford and R.W. Vest, J. Appl. Phys., 35 (1964) 2413.

(17) L.C. Walters and R.E. Grace, Ibid., 8 (1965) 2331.

(18) P. Kofstad and K.P. Lillerud, J. Electrochem., 127, (1980) 2397.

(19) W.A. Fisher and G. Lorenz, Z. Phys. Chem., N.F., 5, (1955) 100.

(20) P. Kofstad, "Non stoichiometry, Diffusion, and Electrical Conductivity in Binary Metal Oxides", Wiley-Interscience, New York (1972).

(21) C.A. Phalnikar, E.B. Evans, and W.M. Balwin, Jr., J. Electrochem. Soc., 103 (1956) 429.

(22) W.C. Hagel, Trans. ASM, 56 (1963) 583.

(23) T.F. Kassner, L.C. Walters and R.E. Grace, Proceedings of "Symposium on Thermodynamics with Emphasis on Nuclear Materials and Atomic Transport in Solids", IAEA, Vienna, 1966.

(24) F.A. Kröger, in "Proceedings of NACE Conference on High Temperature Corrosion", San Diego, C.A. (1981).

(25) K.P. Lillerud and P. Kofstad, J. Electrochem. Soc., 127, 11, (1980) 2397.

(26) R.A. Perkins, Annual Report June 1976 - June 1977. Electrical Power Research Institute, Pabo Alto, California, 94304.

(27) C.J. Spengler, Trans. AIME, 3, 1 (1972) 161.

(28) F.S. Petit, Corrosion Sc., 9 (1969) 903.

(29) C.B. Alcock, Ibid, (1969) 111.

(30) Y. Adda and J. Philibert, "La diffusion dans les solides", Institut national des sciences et techniques nucléaires, 1966.

(31) G.R. St-Pierre and J. Chipman, Trans. Am. Inst. Min. Metall. Pet. Eng., 206 (1956) 1474.

(32) R.A. Sharmo and F.D. Richardson, Ibid, 233 (1965) 1586.

(33) G.J.W. Kor and F.D. Richardson, Trans. Inst. Met. 79, C148 (1970).

(34) G.J.W. Kor and E.T. Turkdogen, Met. Trans., 2 (1971) 1571.

(35) G.J.W. Kor, Met. Trans., 3 (1972) 2343.

(36) B.A. Gordon, Oxid. Met., 13, N° 1, 1979.

(37) T. Flatley and N. Birks, J. Iron Steel Inst., 209 (1971) 523.

(38) N. Birks, Corrosion Sc., 12 (1972) 829.

(39) D.R-H. Chang, Ph.D. thesis, Northwestern University, 1973.

(40) M.C. Pope and N. Birks, Oxid. Met., 12, (2) 191, 1978.

(41) C.D. Asmundis, F. Gesmundo and R. Bottino, Oxid. Met., 14 (4) (1980) 351.

(42) V.N. Korev, N.G. Bogacheva and V.I. Arkorov, Viz. Met. Metallowed, 9, (1960) 358.

(43) G. Romeo and H.S. Spacil, "High Temperature Gas-Metal reaction in Mixed Environments", S.A. Joussan and Z.A. Faroulis Ed. TMS-AIME, 299, New York (1983).

(44) W.L. Worrell and E.T. Turkdogan, Trans. AIME, 242 (1968) 1673.

(45) J.L. Domange, "Colloque de physique des surfaces dans les gaz raréfiés", Scalay (1968).

(46) W.Y. Howng and J.B. Wagner, J. Phys. Chem. Solids, 30 (1978) 1019.

(47) W.Y. Howng, Ibid, 41 (1979) 259.

(48) G. Romeo, H.S. Spacil and W.J. Pasko, J. Electrochem. Soc., 122, 10 (1973) 1329.

(49) G. Moulin, Doctorat ès sciences physiques, Université de Paris-sud, Centre d'Orsay, 1981.

(50) W.C. Hagel, P.J. Jorgensen and D.S. Tomalin, J. Am. Cer. Soc., 49, 1 (1966) 23.

(51) P.D. Ownby and G.E. Juncquist, Ibid, 55, 9 (1972) 433.

(52) C. Deportes, M. Henault, F. Tasset and G. Vitter, "Jauge électrochimique à oxygène", Brevet Français N° 7332 671 du 11-09-1973.

(53) G. Vitter, Thèse de doctorat de 3^{e} cycle, Université scientifique et médicale de Grenoble, 1980.

(54) M. Gantès, Thèse de doctorat de 3^{e} cycle, Ibid, 1980.

(55) M. Rivier and A.D. Pelton, Ceram. Bull., 57 (1978) 183.

(56) P. Pascal, "Nouveau traité de chimie minérale", Masson, Paris 1960.

(57) O. Kubaschewski and C.B. Alcock, "Metallurgical Thermochemistry", Fifth edition, Pergamon Press, Toronto (1979).

(58) M. Benlyamani, M.Sc.A. thesis, École Polytechnique de Montréal (1984).

(59) N. Birks and N. Tattam, Corros. Sci., 10 (1970) 857.

(60) G. Charlot, "Les méthodes de la chimie analytique", 4e édition, Paris, Masson, 1961.

(61) D. Ravaine, Revue de métallurgie - CIT, Août-Septembre (1980) 725.

(62) S. Monaro and R. Lecomte, Int. J. Nucl. Med. and Biol., 8 (1981) 1.

(63) A.J. Houdayer, P. Beaudoin and L. Lessard, Nucl. Instr. and Meth., 202 (1982) 487.

(64) E. Roth, Chimie nucléaire appliquée, 1968, Masson et Cie Editeurs Paris.

(65) J. Melançon, Y. Blanchette and Christopher W. Bale, Met. Trans. 16B, 11 (1985) 793.

(66) J. Melançon, M.Sc.A. Thesis, École Polytechnique de Montréal (1981).

(67) Progress report, September 1985.

(68) R.T. Grimeley, R.P. Burns, and M.G. Inghram, J. Chem. Phys., 34 (1961) 664.

(69) K.L. Nielsen, McMillan Corporation, NY, Second edition, 1964.

(70) N. Birks and G.H. Meier, "Introduction to High Temperature Oxidation of Metals" by Edward Arnold (Publishers) Ltd., London, 1983.

APPENDIX A

SIDBEC–DOSCO - Complexe de Contrecoeur

1900 Montée de la Pomme d'Or, C.P. 1000, Contrecoeur, P.Q., J0L 1C0
Tél. (514) 587-2091 Telex 05-25498

Contrecoeur, le 1er avril 1986

Mohamed Benlyamani
Département de Métallurgie
Ecole polytechnique
Campus Université de Montréal
C.P. 6079
Succursale A
Montréal, P.Q.
H3C 3A7

Le travail de recherche de M. Benlyawani exigeait l'analyse du soufre dans de l'oxyde de chrome par une méthode infrarouge pour confirmer ses résultats. L'analyseur "LECO CS 144" semblait être une alternative acceptable. Le fabricant donnait une précision de 5% de la lecture avec une limite de détection de .0050%. L'accélérateur utilisé est du tungstène avec un four à induction d'une fréquence de 18 Mhz et d'une puissance de 2.2 kilowatts. Le système de détection est par absorption infrarouge. Le standard le plus bas disponible était de .0070% de soufre. Pour une teneur inférieure à 0.35% de soufre, le poids suggéré est de 1 gramme.

L'oxyde de chrome ayant un point de fusion très élevé, il est très difficile d'avoir une excellente reproductibilité des analyses. Plusieurs alternatives ont été essayées, soit:

1. 1 gramme de tungstène
2. 1 gramme de tungstène et 0.5 gramme d'étain
3. 1 gramme de tungstène et 1 gramme de fer pur métallisé
4. 1 gramme de tungstène et 0.5 gramme de cuivre
5. 1 gramme de tungstène + 1 capsule d'étain
6. Calciner les creusets avant l'analyse
7. Purger le système avant chaque analyse

.../2

Les résultats n'ont pas été satisfaisants dû à plusieurs facteurs, entre autre au poids de l'échantillon disponible, à la nature et à la granulométrie du matériel ainsi que la limite de détection de l'analyseur.

Jean-Yves Beaudoin
Laboratoire de chimie

/lb

APPENDIX B

Sulfur Determination by Instrumental Neutron Activation Analysis

Gregory Kennedy
Energy Engineering Institute
Ecole Polytechnique of Montreal

Sulfur concentrations in the Cr_2O_3 samples were determined by neutron activation followed by beta ray spectroscopy.

When a substance containing sulfur is placed in the neutron flux near the core of a nuclear reactor, the high energy neutrons can induce nuclear reactions which change sulfur-32 atoms to phosphorus-32. The number of ^{32}P atoms produced is proportional to the number of sulfur atoms in the sample. After the sample is removed from the reactor the radioactive ^{32}P emits beta rays which can be detected in order to determine the sulfur concentration.

Because of the low sulfur concentrations encountered in this work, less than 100 ppm, steps were taken to improve the detection of the beta rays emitted by ^{32}P produced from the sulfur in the sample in the presence of several interferences.

Samples of Cr_2O_3 powder of approximate weight 200 mg were sealed in small polyethylene bags and ten of these at a time were placed inside a cadmium cylinder with wall thickness 0.5 mm. With a pneumatic transfer system they were sent to an irradiation site near the core of the SLOWPOKE reactor of the Ecole Polytechnique. The samples were thus irradiated for 2 hours in a fast neutron flux of 0.21×10^{12} neutrons $cm^{-2}s^{-1}$. The purpose of the cadmium cylinder was to reduce the flux of low energy neutrons which bombard the samples. Low energy neutrons would produce large amounts of radioactive chromium and they may also produce some ^{32}P from phosphorus impurities in the samples.

After removal from the reactor and before measurement of the ^{32}P, the samples were left for seven days in order to eliminate any radioactivity due to impurities with short half-lives. ^{32}P has a half-life of 14 days and emits beta rays with energies from 0 to 1710 keV. Each sample was weighed, formed into a thin disk, and attached to a card for beta spectroscopy. They were placed at a distance of 1 cm from a beta ray spectrometer consisting of a 6 mm thick plastic scintillator coupled to a photomultiplier tube whose output was amplified and sent to a multichannel analyser. This spectrometer produces a voltage pulse proportional to the energy of each beta ray detected. It also produces voltage pulses for a small fraction of the gamma rays emitted from the sample such as those from ^{51}Cr which have an energy of 320 keV.

With the multichannel analyser a spectrum was accumulated for 15 minutes and the number of betas detected in the energy range 900 to 1700 keV was recorded. For each sample two beta measurements were averaged and the result used to calculate the sulfur concentration. The relation between the number of betas detected and the amount of sulfur was determined from standards prepared by mixing known amounts of sulfur with Cr_2O_3.

It was found that even a few ppm antimony in the samples would produce a significant amount of beta rays which could not be resolved from those of ^{32}P. This problem was solved by using pure Cr_2O_3 containing less than 0.1 ppm antimony. Gamma ray spectroscopy with a germanium detector was used to verify that no other interfering activities besides ^{51}Cr were present.

With this method the sulfur concentrations in Cr_2O_3 samples containing between 10 and 200 ppm sulfur were determined with a precision of 4 ppm.